

FINAL
CONTRACT REPORT

**CORROSION PROTECTION
PERFORMANCE EVALUATION
OF LOW PERMEABLE CONCRETES
IN EXPOSURE SPECIMENS**

JERZY ZEMAJTIS
Research Associate
Virginia Polytechnic Institute
and State University

RICHARD E. WEYERS
Professor
Virginia Polytechnic Institute
and State University

MICHAEL M. SPRINKEL
Research Manager
Virginia Transportation Research Council



Standard Title Page - Report on State Project

Report No. VTRC 99-CR5	Report Date January , 1999	No. Pages 142	Type Report: Final Contract Report Period Covered:	Project No.: 9812-010-940
				Contract No.
Title and Subtitle: Contract Report: Performance Evaluation of Low Permeability Concretes in Exposure Specimens				Key Words: Epoxy-coated reinforcement, corrosion, bridge decks, piles, low permeability concrete, silica fume, fly ash, slag
Authors: Mr. Jerzy Zemajtis, Dr. Richard E. Weyers, Mr. Michael Sprinkel				
Performing Organization Name and Address: Virginia Transportation Research Council 530 Edgemont Road Charlottesville, VA 22903				
Sponsoring Agencies' Name and Address Virginia Department of Transportation 1401 E. Broad Street Richmond, VA 23219				
Supplementary Notes				
<p>Abstract</p> <p>The application of a mineral admixture or a combination of a mineral admixture with corrosion inhibitor are the methods used for the corrosion protection for reinforced concrete bridges. The results of a 1.5-year study on evaluation of three concretes with fly ash, slag cement (SC), and silica fume (SF) and one concrete with silica fume and a corrosion inhibitor (SFD) are presented. The specimens were built to simulate four exposure conditions typical for concrete bridges located in the coastal region or inland where deicing salts are used. The exposure conditions were horizontal, vertical, tidal, and immersed zones. The specimens were kept inside the laboratory and were exposed to weekly ponding cycles of 6% sodium chloride solution by weight. In addition, cover depth measurements from 21 bridge decks and chloride data from 3 bridge decks were used, together with laboratory data, in modeling the service lives of investigated corrosion protection methods.</p> <p>The methods used to assess the condition of the specimens included chloride concentration measurements, corrosion potentials, and corrosion rates (3LP). Additionally, visual observations were performed for identification of rust stains and cracking on concrete surfaces.</p> <p>The results of chloride testing indicate that the amount of chlorides present at the bar level is more than sufficient to initiate corrosion. Chloride and rapid permeability data demonstrate that for low permeable (LP) concretes there appears to be significant difference both in a rate of chloride ingress and in the diffusion coefficients in comparison to the controls. Corrosion potentials agree with corrosion rates and suggest the possibility of an active corrosion process development on control specimens during indoor exposure.</p> <p>The structural cracks that were observed in some specimens appeared to have no influence on the corrosion development on the bars in the vicinity of the these cracks. It was concluded that the silicone and duct tape protection was adequate. The cracking, other than structural, appeared to be related to the reinforcing steel corrosion, except the cracks in the horizontal zone of the specimen with slag cement which were probably caused by the subsidence cracking. The least number of cracks was observed on the SF and SFD specimens.</p> <p>Modeling the time as a function of probability of the end of functional service life (EFSL) was presented. It has been shown that the distributions of surface concentrations of chloride ions (C_0) and diffusion constants (D_C) are key elements in the model. Model predictions show that the LP concretes provide much better level of protection against moisture and chlorides than the A4 concrete alone. Application of a corrosion inhibitor causes an elevation of the chloride threshold resulting in an additional increase in time to EFSL.</p> <p>Recommendations are to continue monitoring until cracking has occurred in all specimens to a greater extent to better estimate the service lives of LP concretes than is presently known in the construction of concrete bridge components in Virginia. The specimens with LP concretes and one control (continuous reinforcement in the legs) should be taken to the Hampton Road North Tunnel Island and placed in the brackish water to a depth of the immersed zone at low tide for further exposure to chloride. The the other control (non-continuous reinforcement in the legs) should remain in an outdoor exposure in Southwest Virginia like the Civil Engineering Materials Research Laboratory in Blacksburg, Virginia. Also more field studies are needed to better estimate distributions of surface chloride concentration and diffusion coefficient of Virginia bridge decks, and to confirm predicted times to EFSL for LP concretes.</p>				

Final Contract Report

**Corrosion Protection Performance Evaluation of Low Permeable Concretes
in Exposure Specimens**

**Jerzy Żemajtis, Research Associate
Charles E. Via Department of Civil Engineering
Virginia Polytechnic Institute and State University**

**Richard E. Weyers, Professor
Charles E. Via Department of Civil Engineering
Virginia Polytechnic Institute and State University**

**Michael M. Sprinkel, Research Manager
Virginia Transportation Research Council**

(The opinions, findings, and conclusions expressed in this report are those of the authors and not necessarily those of the sponsoring agencies.)

Project Monitors

Michael M. Sprinkel, Virginia Transportation Research Council

Contract Research Sponsored by
Virginia Transportation Research Council

Virginia Transportation Research Council
(A Cooperative Organization Sponsored Jointly by the
Virginia Department of Transportation and
the University of Virginia.)

Charlottesville, Virginia

January, 1999
VTRC 99 - CR5

NOTICE

The project that is the subject of this report was done under contract for the Virginia Department of Transportation, Virginia Transportation Research Council. The opinions and conclusions expressed or implied are those of the contractors, and although they have been accepted as appropriate by the project monitors, they are not necessarily those of the Virginia Transportation Research Council or the Virginia Department of Transportation.

Each contract report is peer reviewed and accepted for publication by Research Council staff with expertise in related technical areas. Final editing and proofreading of the report are performed by the contractor.

Table of Contents

ABSTRACT	1
INTRODUCTION	3
PURPOSE & SCOPE	4
METHODS & MATERIALS	4
Specimen Design	4
Experimental Plan	6
Evaluation Methods	6
Chlorides	7
Rapid concrete chloride permeability	7
Corrosion Potentials	8
Corrosion Rates	8
Materials	8
Reinforcing Steel	8
Concrete	8
RESULTS	9
Corrosion Potentials	9
Corrosion Rates	9
Chlorides	10
Rapid Concrete Chloride Permeability	10
Visual Observations	10
DISCUSSION	10
Corrosion Potentials	10
Corrosion Rates	12
Chlorides	13
Rapid Concrete Chloride Permeability	14
Visual Observations	14
Discussion Summary	15
SERVICE LIFE ESTIMATES	16
CONCLUSIONS	20
RECOMMENDATIONS	20
REFERENCES	21

List of Tables:

TABLE 1.	Specimen Configuration
TABLE 2.	Recommended Action for Chloride Content Measurements
TABLE 3.	ASTM C-876 Interpretation of Potential Readings
TABLE 4.	Manufacturer's Data Interpretation for 3LP Device
TABLE 5.	Physical and Chemical Properties of Bare Steel
TABLE 6.	Concrete Mixture Proportions
TABLE 7.	Cement Properties (as Provided by the Manufacturer)
TABLE 8.	Fresh Concrete Properties
TABLE 9.	Compressive Strengths
TABLE 10.	Rapid Concrete Chloride Permeability
TABLE 11.	Diffusion Coefficients

List of Figures:

FIGURE 1.	Specimen Configuration
FIGURE 2.	Measurement Plan
FIGURE 3.	Corrosion Potentials in the Horizontal Zone, BS-1 Specimen (Control 1)
FIGURE 4.	Corrosion Potentials in the Horizontal Zone, BS-2 Specimen (Control 2)
FIGURE 5.	Corrosion Potentials in the Horizontal Zone, FA Specimen
FIGURE 6.	Corrosion Potentials in the Horizontal Zone, SC Specimen
FIGURE 7.	Corrosion Potentials in the Horizontal Zone, SF Specimen
FIGURE 8.	Corrosion Potentials in the Horizontal Zone, SFD Specimen
FIGURE 9.	Corrosion Potentials in the Vertical Zone, Left Leg, BS-1 Specimen (Control 1)
FIGURE 10.	Corrosion Potentials in the Vertical Zone, Right Leg, BS-1 Specimen (Control 1)
FIGURE 11.	Corrosion Potentials in the Vertical Zone, Left Leg, BS-2 Specimen (Control 2)
FIGURE 12.	Corrosion Potentials in the Vertical Zone, Right Leg, BS-2 Specimen (Control 2)
FIGURE 13.	Corrosion Potentials in the Vertical Zone, Left Leg, FA Specimen
FIGURE 14.	Corrosion Potentials in the Vertical Zone, Right Leg, FA Specimen
FIGURE 15.	Corrosion Potentials in the Vertical Zone, Left Leg, SC Specimen
FIGURE 16.	Corrosion Potentials in the Vertical Zone, Right Leg, SC Specimen
FIGURE 17.	Corrosion Potentials in the Vertical Zone, Left Leg, SF Specimen
FIGURE 18.	Corrosion Potentials in the Vertical Zone, Right Leg, SF Specimen
FIGURE 19.	Corrosion Potentials in the Vertical Zone, Left Leg, SFD Specimen
FIGURE 20.	Corrosion Potentials in the Vertical Zone, Right Leg, SFD Specimen
FIGURE 21.	Corrosion Potentials in the Tidal Zone, Left and Right Legs, BS-1 and BS-2 Specimens
FIGURE 22.	Corrosion Potentials in the Immersed Zone, Left and Right Legs, BS-1 and BS-2 Specimens

- FIGURE 23. Corrosion Potentials in the Tidal Zone, Left and Right Legs, FA Specimen
- FIGURE 24. Corrosion Potentials in the Immersed Zone, Left and Right Legs, FA Specimen
- FIGURE 25. Corrosion Potentials in the Tidal Zone, Left and Right Legs, SC Specimen
- FIGURE 26. Corrosion Potentials in the Immersed Zone, Left and Right Legs, SC Specimen
- FIGURE 27. Corrosion Potentials in the Tidal Zone, Left and Right Legs, SF Specimen
- FIGURE 28. Corrosion Potentials in the Immersed Zone, Left and Right Legs, SF Specimen
- FIGURE 29. Corrosion Potentials in the Tidal Zone, Left and Right Legs, SFD Specimens
- FIGURE 30. Corrosion Potentials in the Immersed Zone, Left and Right Legs, SFD Specimens
- FIGURE 31. Corrosion Rates in the Horizontal Zone, BS-1 Specimen
- FIGURE 32. Corrosion Rates in the Horizontal Zone, BS-2 Specimen
- FIGURE 33. Corrosion Rates in the Vertical Zone, Left Leg, BS-1 Specimen
- FIGURE 34. Corrosion Rates in the Vertical Zone, Right Leg, BS-1 Specimen
- FIGURE 35. Corrosion Rates in the Vertical Zone, Left Leg, BS-2 Specimen
- FIGURE 36. Corrosion Rates in the Vertical Zone, Right Leg, BS-2 Specimen
- FIGURE 37. Corrosion Rates in the Tidal Zone, Left Leg, BS-1 Specimen
- FIGURE 38. Corrosion Rates in the Tidal Zone, Right Leg, BS-1 Specimen
- FIGURE 39. Corrosion Rates in the Tidal Zone, Left Leg, BS-2 Specimen
- FIGURE 40. Corrosion Rates in the Tidal Zone, Right Leg, BS-2 Specimen
- FIGURE 41. Corrosion Rates in the Immersed Zone, Left Leg, BS-1 Specimen
- FIGURE 42. Corrosion Rates in the Immersed Zone, Right Leg, BS-1 Specimen
- FIGURE 43. Corrosion Rates in the Immersed Zone, Left Leg, BS-2 Specimen
- FIGURE 44. Corrosion Rates in the Immersed Zone, Right Leg, BS-2 Specimen
- FIGURE 45. Corrosion Rates in the Horizontal Zone, FA Specimen
- FIGURE 46. Corrosion Rates in the Horizontal Zone, SC Specimen
- FIGURE 47. Corrosion Rates in the Horizontal Zone, SF Specimen
- FIGURE 48. Corrosion Rates in the Horizontal Zone, SFD Specimen
- FIGURE 49. Corrosion Rates in the Vertical Zone, Left Leg, FA Specimen
- FIGURE 50. Corrosion Rates in the Vertical Zone, Left Leg, SC Specimen
- FIGURE 51. Corrosion Rates in the Vertical Zone, Left Leg, SF Specimen
- FIGURE 52. Corrosion Rates in the Vertical Zone, Left Leg, SFD Specimen
- FIGURE 53. Corrosion Rates in the Vertical Zone, Right Leg, FA Specimen
- FIGURE 54. Corrosion Rates in the Vertical Zone, Right Leg, SC Specimen
- FIGURE 55. Corrosion Rates in the Vertical Zone, Right Leg, SF Specimen
- FIGURE 56. Corrosion Rates in the Vertical Zone, Right Leg, SFD Specimen
- FIGURE 57. Corrosion Rates in the Tidal Zone, Left Leg, FA Specimen

- FIGURE 58. Corrosion Rates in the Tidal Zone, Left Leg, SC Specimen
- FIGURE 59. Corrosion Rates in the Tidal Zone, Left Leg, SF Specimen
- FIGURE 60. Corrosion Rates in the Tidal Zone, Left Leg, SFD Specimen
- FIGURE 61. Corrosion Rates in the Tidal Zone, Right Leg, FA Specimen
- FIGURE 62. Corrosion Rates in the Tidal Zone, Right Leg, SC Specimen
- FIGURE 63. Corrosion Rates in the Tidal Zone, Right Leg, SF Specimen
- FIGURE 64. Corrosion Rates in the Tidal Zone, Right Leg, SFD Specimen
- FIGURE 65. Corrosion Rates in the Immersed Zone, Left Leg, FA Specimen
- FIGURE 66. Corrosion Rates in the Immersed Zone, Left Leg, SC Specimen
- FIGURE 67. Corrosion Rates in the Immersed Zone, Left Leg, SF Specimen
- FIGURE 68. Corrosion Rates in the Immersed Zone, Left Leg, SFD Specimen
- FIGURE 69. Corrosion Rates in the Immersed Zone, Right Leg, FA Specimen
- FIGURE 70. Corrosion Rates in the Immersed Zone, Right Leg, SC Specimen
- FIGURE 71. Corrosion Rates in the Immersed Zone, Right Leg, SF Specimen
- FIGURE 72. Corrosion Rates in the Immersed Zone, Right Leg, SFD Specimen
- FIGURE 73. Chloride Concentrations at 33 Weeks, Tidal Zone
- FIGURE 74. Chloride Concentrations at 33 Weeks, Immersed Zone
- FIGURE 75. Chloride Concentrations at 1 Year, Tidal Zone
- FIGURE 76. Chloride Concentrations at 1 Year, Immersed Zone
- FIGURE 77. Chloride Concentrations at 1.5 Year, Horizontal Zone
- FIGURE 78. Chloride Concentrations at 1.5 Year, Vertical Zone
- FIGURE 79. Chloride Concentrations at 1.5 Year, Tidal Zone
- FIGURE 80. Chloride Concentrations at 1.5 Year, Immersed Zone
- FIGURE 81. Electrical Indication of Concrete's Ability to Resist Chloride Ion Penetration @ 28 days and @ 1 year
- FIGURE 82. Visual Observations: October 1996. Cracking and Rust Spots in the BS-1 Specimen
- FIGURE 83. Visual Observations: October 1996. Cracking and Rust Spots in the BS-2 Specimen
- FIGURE 84. Visual Observations: October 1996. Cracking and Rust Spots in the FA Specimen
- FIGURE 85. Visual Observations: October 1996. Cracking and Rust Spots in the SC Specimen
- FIGURE 86. Visual Observations: October 1996. Cracking and Rust Spots in the SF Specimen
- FIGURE 87. Visual Observations: October 1996. Cracking and Rust Spots in the SFD Specimen
- FIGURE 88. Cumulative Distribution Function (CDF) of Surface Chloride Concentration, Gamma Distribution, ($\alpha = 3.56$, $\beta = 1.25$)
- FIGURE 89. Cumulative Distribution Function (CDF) of Diffusion Coefficient, Gamma Distribution, ($\alpha = 1.42$, $\beta = 27.1$)
- FIGURE 90. Predicted Time to Corrosion Initiation for A4 Concrete, w/c = 0.45, Chloride Threshold = 0.89 kg/m³

- FIGURE 91. Predicted Time to Corrosion Initiation for FA Concrete (20/85),
w/cm = 0.45, Chloride Threshold = 0.89 kg/m³
- FIGURE 92. Predicted Time to Corrosion Initiation for SC Concrete (40/60),
w/cm = 0.45, Chloride Threshold = 0.89 kg/m³
- FIGURE 93. Predicted Time to Corrosion Initiation for SF Concrete (7/93),
w/cm = 0.45, Chloride Threshold = 0.89 kg/m³
- FIGURE 94. Predicted Time to Corrosion Initiation for SFD Concrete (7/93),
w/cm = 0.45, Chloride Threshold = 1.78 kg/m³
- FIGURE 95. Probability of End of Functional Service Life for A4 Concrete:
Comparison Between Field Performance (SHRP) and Predictions
from Field Data (A-4)
- FIGURE 96. Probability of End of Functional Service Life for LP Concretes versus
A4 Concrete: Predictions from Laboratory and Field Data
- APPENDIX. Average Corrosion Potentials for the Deck and Left and Right Legs of
Specimens
- FIGURE A1. Average Potentials for BS-1 Specimen
- FIGURE A2. Average Potentials for BS-2 Specimen
- FIGURE A3. Average Potentials for BS-3 Specimen
- FIGURE A4. Average Potentials for BS-4 Specimen
- FIGURE A5. Average Potentials for BS-5 Specimen
- FIGURE A6. Average Potentials for BS-7 Specimen

ABSTRACT

The application of a mineral admixture or a combination of a mineral admixture with corrosion inhibitor are the methods used for the corrosion protection for reinforced concrete bridges. The results of a 1.5-year study on evaluation of three concretes with fly ash, slag cement (SC), and silica fume (SF) and one concrete with silica fume and a corrosion inhibitor (SFD) are presented. The specimens were built to simulate four exposure conditions typical for concrete bridges located in the coastal region or inland where deicing salts are used. The exposure conditions were horizontal, vertical, tidal, and immersed zones. The specimens were kept inside the laboratory and were exposed to weekly ponding cycles of 6% sodium chloride solution by weight. In addition, cover depth measurements from 21 bridge decks and chloride data from 3 bridge decks were used, together with laboratory data, in modeling the service lives of investigated corrosion protection methods.

The methods used to assess the condition of the specimens included chloride concentration measurements, corrosion potentials, and corrosion rates (3LP). Additionally, visual observations were performed for identification of rust stains and cracking on concrete surfaces.

The results of chloride testing indicate that the amount of chlorides present at the bar level is more than sufficient to initiate corrosion. Chloride and rapid permeability data demonstrate that for low permeable (LP) concretes there appears to be significant difference both in a rate of chloride ingress and in the diffusion coefficients in comparison to the controls. Corrosion potentials agree with corrosion rates and suggest the possibility of an active corrosion process development on control specimens during indoor exposure.

The structural cracks that were observed in some specimens appeared to have no influence on the corrosion development on the bars in the vicinity of the these cracks. It was concluded that the silicone and duct tape protection was adequate. The cracking, other than structural, appeared to be related to the reinforcing steel corrosion, except the cracks in the horizontal zone of the specimen with slag cement which were probably caused by the subsidence cracking. The least number of cracks was observed on the SF and SFD specimens.

Modeling the time as a function of probability of the end of functional service life (EFSL) was presented. It has been shown that the distributions of surface concentrations of chloride ions (C_0) and diffusion constants (D_c) are key elements in the model. Model predictions show that the LP concretes provide much better level of protection against moisture and chlorides than the A4 concrete alone. Application of a corrosion inhibitor causes an elevation of the chloride threshold resulting in an additional increase in time to EFSL.

Recommendations are to continue monitoring until cracking has occurred in all specimens to a greater extent to better estimate the service lives of LP concretes than is presently known in the construction of concrete bridge components in Virginia. The specimens with LP concretes and one control (continuous reinforcement in the legs) should be taken to the Hampton Road North

Tunnel Island and placed in the brackish water to a depth of the immersed zone at low tide for further exposure to chloride. The the other control (non-continuous reinforcement in the legs) should remain in an outdoor exposure in Southwest Virginia like the Civil Engineering Materials Research Laboratory in Blacksburg, Virginia. Also more field studies are needed to better estimate distributions of surface chloride concentration and diffusion coefficient of Virginia bridge decks, and to confirm predicted times to EFSL for LP concretes.

Final Contract Report

**Corrosion Protection Performance Evaluation of Low Permeable Concretes
in Exposure Specimens**

by

Jerzy Żemajtis, Research Associate
Charles E. Via Department of Civil Engineering
Virginia Polytechnic Institute and State University

Richard E. Weyers, Professor
Charles E. Via Department of Civil Engineering
Virginia Polytechnic Institute and State University

Michael M. Sprinkel, Research Manager
Virginia Transportation Research Council

INTRODUCTION

Presently, the extent of the rapid deterioration of reinforced concrete bridges from chloride ion induced corrosion is well known. During the early recognition stages of the cause, process and severity of the concrete bridge deterioration problem in the United States, a multitude of corrosion abatement techniques were developed for existing and newly constructed bridges. Epoxy-coated reinforcing steel (ECR) and corrosion inhibiting admixtures (CIA) are two techniques developed to extend the service life of newly constructed concrete bridge components. ECR, presently, is the most used corrosion protection method for concrete bridges in the United States. CIA have been used for over 20 years but significantly less frequent than ECR and in Virginia primarily in precast-prestressed members.

Until 1986 when Florida reported that the Long Key Bridge showed signs of corrosion only 6 years after construction, the corrosion protection effectiveness of ECR remained unquestioned. Since the Florida reported findings, 12 field studies have been conducted on the corrosion protection effectiveness of ECR.¹ Conclusions have been mixed, from satisfactory corrosion protection performance to date for bridge decks to poor performance in substructures with predictions that ECR will not provide long-term (50 years) of corrosion protection performance for substructures or decks.¹ The reason for the mixed conclusions of the performance of ECR include limited or inappropriate evaluation methods which always accompany a lack of knowledge of the cause(s) of failure and subjectively defined failure criteria. From studies where care and appropriate evaluation methods and failure criteria have been employed, the conclusions are that ECR will not provide 50 years of corrosion free protection for steel in concrete bridge

components.^{2,3} More recent studies, including one in Virginia, support the earlier conclusions that ECR will not provide long term corrosion protection performance.^{4,5} As a result of these recent findings on the limited effectiveness of ECR, more interest has been developed in the effectiveness of low permeability (LP) concretes and CIA.

Thus, the Virginia Department of Transportation initiated an evaluation of ECR and alternative corrosion protection systems for use in the construction of new concrete structures. Evaluation of the corrosion protection effectiveness was assessed in both a simulated concrete pore water solution and in concrete. The performance of ECR in 21 bridge decks and 3 bridge substructures was also included. The protection systems evaluated are ECR (present and new coatings), galvanized reinforcing steel, three commercial CIA, LP concretes, and two dual corrosion protection systems (CIA and ECR in the simulated concrete pore water solution and CIA and LP concrete). The field study bridges were 3, 8 year old substructures in a marine environment and 21 bridge decks ranging in age from 2 to 20 years in a deicer salt environment. This report presents the results of the evaluation of exposure specimens made with LP concrete and CIA and LP concrete.

PURPOSE & SCOPE

The purpose of this study was threefold:

1. To evaluate the short term laboratory corrosion protection performance of LP concretes and bare steel (BS).
2. To develop a methodology for predicting the field corrosion protection effectiveness of LP concrete based on short term laboratory testing.
3. To provide well characterized specimens for long term corrosion protection performance evaluation of LP concretes and BS.

The study was limited to present Virginia Department of Transportation mixture specifications of a maximum water-to-cementitious material ratio (w/cm) of 0.45 and practices in the use of fly ash (FA), slag cement (SC), and silica fume (SF) mineral admixtures.

METHODS & MATERIALS

Specimen Design

To assess the performance of the BS in LP concretes, four specimens with FA, SC, SF, and SF with DCI-S CIA (SFD), and two control specimens, with neither mineral admixtures nor CIA, were cast. The constant design parameters for these specimens were a 0.45 water to cementitious

material ratio, slump, and air content. All specimens had 25 mm reinforcing cover depth and had been exposed to a 6%, by weight, sodium chloride wetting solution. Each specimen, as shown in Figure 1, was 1.72 m high, had horizontal dimensions of 1.12 m by 1.12 m, and was designed to simulate four exposure conditions: wetted deck surface (horizontal zone), wetted vertical surfaces of bridge members (vertical zone), tidal zone, and immersed zone. The immersed zone covered an area from the bottom of specimens' legs to the height of 305 mm. The tidal zone was 305 mm to 610 mm from the bottom of specimens' legs. A vertical surface area above 610 mm from the bottom of a specimen corresponded to the vertical zone, and the horizontal zone was the top surface area of the specimen.

The specimens differed by the following parameters (see Table 1):

- configuration of the BS in specimen's legs:
 - type I - BS electrically disconnected in both legs,
 - type II - BS electrically connected in both legs (same bars for vertical, tidal, and immersed zones),
 - type III- BS electrically disconnected in the right leg and BS electrically connected in the left leg (same bars for vertical, tidal, and immersed zones)

- concrete type:
 - Virginia Department of Transportation (A4) concrete - control specimens,
 - A4 concrete with FA (removal of 15% portland cement and replacement with 20% FA by weight) - FA specimen,
 - A4 concrete with SC (40% portland cement replacement with SC by weight) - SC specimen,
 - A4 concrete with SF (7% portland cement replacement with SF by weight) - SF specimen, and
 - A4 concrete with DCI-S CIA and SF (7% portland cement replacement with SF by weight) - SFD specimen.

Specimens were cast in steel forms, which were carefully cleaned and oiled with a form release agent before each concrete placement. Specimens were wet cured in the forms for seven days. After removing the specimens from the forms, the specimens were wrapped with wet burlap and covered with plastic for additional 21 days of wet curing. After 28 days of wet curing, specimens were air-dried in the laboratory for a minimum of 30 days. During that time the specimens were prepared for wet-dry cycles. All bar ends protruding from specimen legs in the lower part of the legs (0.61 m from the bottom) were protected with plastic tubing, stoppers, and silicone rubber against contact with wetting solution. Then plexiglass dikes were assembled on the specimen's top surface so that the NaCl solution would wet the horizontal zone and uniformly wet the legs. Each specimen was placed into a 0.71 m deep high-density polyethylene (HDPE) tank and exposed to wet-dry cycles.

During specimens' removal from the steel forms, a few structural cracks developed on some

specimens. Before exposure to sodium chloride solution, all structural cracks were filled with silicone rubber and a duct tape was applied over the crack to minimize the influence of these cracks to corrosion development.

Experimental Plan

Specimens were exposed indoors to wet-dry ponding.

Each cycle was one week in duration and was divided into two stages. In the first stage the wetting solution was at high tide level (610 mm from the bottom of a specimen), thus the tidal zone and the immersed zone areas were covered with NaCl solution, and the horizontal and vertical zones of the specimen were allowed to air dry. In the second stage the wetting solution, while at low tide level (water level at 305 mm from the bottom of a specimen), was pumped to the top of a specimen, thus wetting specimen surfaces in the horizontal and vertical zones. At the same time surfaces in the tidal zone were allowed to air dry. Horizontal, vertical, and tidal zones were subjected to wetting for an average of 3.5 days a week and to air drying also for an average of 3.5 days a week. Immersed zone was constantly submerged in the NaCl solution. The wetting solution used in the study was 6% sodium chloride by weight.

After approximately 1.5 years of wet-dry cycles, the specimens were removed from the tanks and moved outdoors for long term monitoring.

Evaluation Methods

Methods used to assess specimen performance included the rate of chloride ingress, rapid chloride permeability, corrosion potential, and corrosion rate measurements. Additionally, visual observations were performed for identification of rust stains and cracking on concrete surfaces.

Chloride ingress was monitored by collecting concrete powder samples at three depths: 13 mm, 25 mm, and 38 mm after 33 weeks, one year, and 1.5 years of ponding. In order not to significantly damage specimens, samples collected at 33 weeks and 1 year, were obtained from small concrete blocks, 300 mm by 300 mm by 130 mm, placed in the tidal and immersed zones. These blocks were cast from the same batch of concrete as the test specimens, cured under the same conditions, and placed into the HDPE tanks at the same time. After 1.5 years of ponding, chloride samples were collected from all four exposure zones of the test specimens. In addition to the chloride samples from the three above mentioned depths, a chloride sample from the depth of 51 mm was collected in the horizontal zone.

Rapid concrete chloride permeability was tested for all concrete types after 28 days and 1 year of moist curing.

Corrosion potential measurements in the horizontal zone were taken on a monthly basis and were recorded at 12 locations: 3 locations each of 4 tested bars. For vertical, tidal, and immersed zones, corrosion potentials were recorded at 9 locations: 3 bars, 3 locations each, for each zone and for each leg of the specimen. Total number of corrosion potential measurement locations was 66: horizontal zone - 12, vertical zone left leg - 9, tidal zone left leg - 9, immersed zone left leg - 9, vertical zone right leg - 9, tidal zone right leg - 9, immersed zone right leg - 9.

Corrosion rates were measured at three locations for each exposure zone and each leg, for a total of 21 different locations per specimen. See Figure 2 for a measurement location plan for horizontal zone and vertical, tidal, and immersed zones on the specimen's right leg. Measurement locations on the specimen's left leg were the same as on the right leg.

Chlorides

Chloride content is considered to be a good indicator of the possibility of corrosion activity. It is generally known that once the concentration of chloride ions reaches the corrosion threshold level, the greater the chloride ion concentration, the greater the probability of active corrosion. Table 2 provides guidelines for interpretation of chloride content measurements.⁶

Samples for chloride concentration were collected as pulverized concrete. The collection apparatus used an impact drill with 29 mm diameter bit, 2.3 times the maximum aggregate size, connected to a vacuum collection unit (7). The concrete powder was collected in the coffee filter, which was then stored in a plastic container until chemical analysis - chloride ion concentration determination was performed. A sample set was taken for each concrete type, and for each exposure condition.

Because of high variability of chloride content close to the surface, powdered concrete samples from the top 6 mm were discarded. Background chloride content measurements were performed by sampling concrete cylinders that were made with the compressive strength cylinders.

Measurements of chloride content were performed in accordance with ASTM C 114 (8). A titration method is used to determine the quantity of acid soluble chlorides in the concrete digestion solution. A simple formula transfers the amount of milliliters of titration solution into chloride ion concentration expressed in kg/m^3 of concrete.

Rapid concrete chloride permeability

An ASTM C-1202 method has shown good correlation with chloride tests (12). That method, often referred to as “rapid permeability”, provides rapid indication of concrete resistance to the penetration of chloride ions. The method relies on the results from a test in which electrical current passes through a concrete sample during six-hour exposure (10). The interpretation is that the larger the Coulomb number, or the charge transferred during the test, the greater the permeability of the sample.

Rapid concrete chloride permeability was tested at the Virginia Transportation Research Council (VTRC), Charlottesville, VA. The rapid permeability was measured on cylinders of all concrete types according to ASTM C-1202 (10).

Corrosion Potentials

Corrosion potentials non-destructively identify the probability of an active corrosion. The method uses a copper-copper sulfate half-cell electrode (CSE) that is connected to the voltmeter and then to the reinforcing steel. According to the standard test method ASTM C 876 the more negative the voltmeter reading, the greater the probability of active corrosion (9). Table 3 presents the relationship of the potential readings versus probability of corrosion for bare reinforcing steel. The locations for potential measurements are shown in Figure 2.

Corrosion Rates

The linear polarization technique is a non-destructive method for assessing the instantaneous corrosion current density. Corrosion current density is directly proportional to the instantaneous rate of metal loss. Often the corrosion current density is referred to as the corrosion rate. Several devices, based on the linear polarization method, presently exist to determine the corrosion current density of steel in concrete. One of the most common is the 3LP device. Corrosion current density measurements are very susceptible to variable field conditions: concrete temperature, moisture, and oxygen content. The manufacturer's interpretation of measured corrosion current density, corrosion rate, is given in Table 4. The locations of 3LP measurements are shown in Figure 2.

Materials

Reinforcing Steel

Bare reinforcing steel was used for fabrication of all tested specimens including controls. All bare steel was #5 (D = 16 mm) bars, Grade 60, and came from one heat. Physical and chemical properties of bare steel, based on mill certificates, are presented in Table 5.

Concrete

Concrete, designated as Virginia Department of Transportation A4, was used for all specimens. The quantities of cement, admixtures, and aggregate used are presented in Table 6.

Type I/II cement was used for all concrete mixtures. Its density was 3.15 g/cm³ and was certified to meet ASTM C-150-92, AASHTO M-85-88, and Federal SS-C-1960 Specifications. Chemical and physical test data is provided in Table 7.

Coarse aggregate used for concrete mixes was #78 stone with unit weight of 96.7. Its density was 2.75 g/cm³ and absorption was measured to be 0.66%. Natural sand, with fineness modulus (FM) of 2.7, 2.66 g/cm³ density, and 0.84% absorption, was used as fine aggregate. Daravair-M air entraining admixture was used for all mixtures. Water reducing admixture, WRDA-19, a high range water reducer, was necessary to keep the water to cementitious material ratio constant and to provide adequate workability during placing of the concrete.

Slump, air content, concrete temperature, and concrete density (unit weight) were recorded before concrete placement. Results of these test and the actual w/cm ratios are presented in Table 8. While placing concrete, several 100 by 200 mm cylinders were made for compressive strength measurements, which were tested after 3, 7, 28, 56 days and 1 year of moist curing. The compression test results are presented in Table 9.

RESULTS

Corrosion Potentials

The potential data collected in the horizontal zone are presented in Figures 3-8, for specimens BS-1, BS-2, FA, SC, SF, and SFD, respectively. Data for the vertical zone are presented separately for the left and right legs in Figures 9-20. The last four readings were taken after the ponding was discontinued and the specimens were moved outdoors. Average values for potentials recorded for the horizontal deck and the left and right legs of the specimens are appended to the report. Overall the potentials are similar for the legs and the deck.

Immediately after the ponding was discontinued, half-cell potential measurements were taken in the immersed and tidal zones on both legs of each specimen (see Figures 21-30).

Each curve, or bar, in Figures 3-30 represents an average of three readings taken from one reinforcing steel bar.

Corrosion Rates

A relationship of corrosion rates (i_{corr}) versus time for the control specimens with bare steel bars is presented in Figures 31 and 32 for the horizontal zone, Figures 33-36 for the vertical zone, Figures 37-40 for the tidal zone, and Figures 41-44 for the immersed zone. Readings collected after 74 and 80 weeks of exposure were made while the specimens were still indoors and the ponding was in progress. Readings after 83 weeks of exposure were made indoors immediately after the ponding was discontinued. Readings at 97th week of exposure and later were taken after the specimens were moved outdoors.

Corrosion rate data for specimens with LP concrete is presented in Figures 45-48 for the horizontal zone, Figures 49-56 for the vertical zone, Figures 57-64 for the tidal zone, and Figures 65-72 for the immersed zone. The first two sets of readings in the horizontal and vertical zones, for all specimens, were collected while the specimens were still indoors and the ponding was in progress. The third set of readings in the horizontal and vertical zones, and the first set of readings in the tidal and immersed zones were collected indoors immediately after the ponding was discontinued. The remaining readings were taken after the specimens were moved outdoors.

Chlorides

Chloride concentrations, for horizontal, vertical, tidal, and immersed zones, versus depth are presented in Figures 73-80.

Rapid Concrete Chloride Permeability

The data from these measurements is presented in Table 10 and Figure 81.

Visual Observations

A crack survey was performed after approximately four months of outdoor exposure. Visually observed cracks and rust stains, in the BS-1, BS-2, FA, SC, SF, and SFD specimens, are presented in Figures 82-87, respectively.

DISCUSSION

Corrosion Potentials

Horizontal Zone

As seen in Figures 3 and 4, a shift towards more negative potentials (higher probability of corrosion herein referred to as increased potential) was observed after about 33 weeks of ponding for all bars in the horizontal zone of both control specimens, BS-1 and BS-2. It is also apparent that the bar No. 4, BS-1 specimen, has a higher potential for active corrosion, with the highest measured potential of -326 mV after 80 weeks of ponding, than any other bar. Corrosion potentials for all other bars of the two control specimens were lower. After a few weeks of outdoor exposure the potential values decreased significantly, especially for all bars in the BS-1 specimen, and their average values after 105 and 106 weeks of exposure were -125 and -219 mV for the BS-1 and BS-2 specimens, respectively. A possible explanation of the low measured

potentials is the fact that the specimens have dried out and the possible active corrosion process taking place has been reduced. Higher potentials at later ages likely indicate the moisture content has increased and the corrosion process is increased.

As seen in Figures 5-8, indoor measurements of corrosion potentials for the FA, SC, SF, and SFD specimens varied. Corrosion potentials observed on the FA specimen were in the uncertain region of corrosion activity and were similar to the controls in the first 54 weeks of ponding, and then, the potentials decreased and were slightly less negative than BS-1 and considerably less negative than BS-2, see Figure 5. Potentials recorded on the SC specimen were significantly more negative than on any other specimen with mineral admixtures. SC potentials were even more negative than the controls in the beginning of ponding, and similar to the controls at the end of indoor exposure, see Figure 6. During the indoor exposure period SC potentials started from the average of -314 mV, stayed in the uncertain region of corrosion activity, and decreased to the average of -233 mV at the end of indoor exposure. Potentials decreased and then increased with outdoor exposure. Both SF and SFD specimens had potentials indicating no corrosion activity, since the values were less negative than -200 mV, see Figures 7 and 8. After the specimens were moved outdoors, potentials decreased even further and then increased.

Vertical Zone

Potentials measured on the left and right legs in the vertical zone of control specimens BS-1 and BS-2 have gradually increased with time. Figure 9-12 indicate a high probability of corrosion in both legs of both specimens at 190 weeks of age.

Potential data recorded in the vertical zone for the left and right legs of the FA, SC, SF, and SFD specimens are presented in Figures 13-14, 15-16, 17-18, and 19-20, respectively. Potentials measured on the FA specimen were very similar to the potentials in the control specimens, see Figures 13 and 14. Potentials measured on both legs of the SC specimen were less negative than the controls and in the uncertain region. Corrosion potentials on the SF specimen were in the uncertain region and the region of 90% probability of no corrosion during the experiment duration, see Figures 17 and 18. Corrosion potentials on the SFD specimen were, as on the SF specimen, in the uncertain region and the region of 90% probability of no corrosion during the experiment duration, see Figures 19 and 20.

Immersed and Tidal Zones

The potential readings in the immersed and tidal zones were collected three times. The first set of readings was collected after the ponding was discontinued and two other ones, after the specimens were moved outdoors. Figures 21 and 22 present potential data for the control specimens, Figures 23 and 24 for the FA specimen, Figures 25 and 26 for the SC specimen, Figures 27 and 28 for the SF specimen, and Figures 29 and 30 for the SFD specimen, in the immersed and tidal zones, respectively.

Potential data for the tidal zone presented in Figure 21 demonstrate no significant difference between specimens BS-1 and BS-2 during the first set of readings. The last two readings, however, show more negative potentials on the BS-2 specimen than on the BS-1 specimen, indicating influence of macrocell corrosion. Similar behavior can be observed in the immersed zone, see Figure 22. In this case, potential data demonstrate no significant difference between the BS-1 and BS-2 specimens during the first two sets of readings. The last reading, however, indicates macrocell action on the BS-2 specimen since potential values on both legs are more negative than the potentials on the BS-1 specimen.

As shown in Figures 23 and 24, potential readings in the tidal and immersed zones of the FA specimen indicate high probability of no active corrosion in the specimen with fly ash. Potentials in the tidal and immersed zones of the SC specimen were more negative on the left leg than on the right leg, indicating some macrocell activity, see Figures 25 and 26. However, the potentials were not very negative, being in either the uncertain range or the range of high probability of no corrosion. Potentials measured on the left and right legs of the SF specimen were similar to those for the SC specimen, see Figures 27 and 28. Potentials recorded on both legs in the tidal and immersed zones of the SFD specimen were similar to those for the SC and SF specimens, see Figures 29 and 30.

Corrosion Rates

Corrosion rates in the horizontal zone, Figures 31 and 32, were similar for both control specimens and were decreasing in time. In the vertical zone, Figures 33-36, corrosion rates measured on specimen BS-1 were lower than the ones measured on specimen BS-2. As shown in Figures 33 and 36 two bars had significantly higher corrosion rates than the other bars. Once the specimens were moved outdoors, corrosion rates decreased. Corrosion rates in the tidal zone also decreased once the specimens were moved outdoors. See Figures 37-40. Corrosion rates in the immersed zone for the two control specimens were similar to corrosion rates in the tidal zone and also decreased after moving the specimens outdoors, see Figures 41-42 and 43-44 for specimens BS-1 and BS-2, respectively.

The corrosion rate results indicate that the control specimens were in an active region of corrosion when they were kept indoors, since the corrosion rates were higher than $2 \mu\text{A}/\text{cm}^2$ and the corrosion rates measured outdoors were lower than indoors, see Figures 31-44. The data from the horizontal zone, Figures 31 and 32, agree with the potential data indicating lesser corrosion activity when the specimens were kept outdoors than indoors. Also, in the vertical zone the highest corrosion rates for the controls were observed in the right leg of BS-2 specimen, the same place where the most negative potentials were found, see Figures 33-36. Macrocell action is a probable explanation of differences in corrosion rates in the immersed and tidal zones between the BS-1 specimen, legs reinforcement not connected, and the BS-2 specimen, legs reinforcement connected, see Figures 37-44.

Corrosion rates in the horizontal zone, while the specimens were housed indoors, ranged from

1.46 to 2.86 $\mu\text{A}/\text{cm}^2$ for the FA specimen, from 3.01 to 6.32 $\mu\text{A}/\text{cm}^2$ for the SC specimen, from 2.32 $\mu\text{A}/\text{cm}^2$ to 3.32 $\mu\text{A}/\text{cm}^2$ for the SF specimen, and from 0.88 to 2.52 $\mu\text{A}/\text{cm}^2$ for the SFD specimen, see Figures 45-48. Some corrosion activity that was observed while the specimens were housed indoors, disappeared after the specimens were moved outdoors.

Corrosion rate readings in the vertical zone on left leg were similar to the readings on the right leg for the FA, SC, SF, and SFD specimens, see Figures 49-56. Rates were slightly lower than for the control concretes without mineral admixtures and slag. Corrosion rates in the tidal zone show similar trend as in the vertical zone, see Figures 57 and 64. Likewise, corrosion rates in the immersed zone show trends similar to that in the vertical and tidal zones, see Figures 68 and 72.

Chlorides

Chloride concentrations measured after 33 weeks of ponding are presented in Figure 73, for the tidal zone, and in Figure 74, for the immersed zone. Chloride concentrations measured after one year of ponding are presented in Figure 75 for the tidal zone, and in Figure 76 for the immersed zone. Chloride concentrations measured after 1.5 years of ponding are presented in Figures 77-80, for the horizontal, vertical, tidal, and immersed zones, respectively. Chloride concentration threshold of 0.71 kg/m^3 of concrete (8) was reached at the bar depth, 25 mm, between 33 weeks and 1 year of ponding for the control specimens in all exposure zones. However, none of the specimens with low permeable concrete has exceeded the chloride threshold in the first year of ponding. Between 1 and 1.5 years of ponding, the FA and SC specimens have exceeded the chloride threshold, but only in the horizontal zone. After 1.5 years of ponding, chloride concentrations in the remaining exposure zones, as well as for the SF and SFD specimens in all exposure zones, were below the chloride threshold.

Once, the chloride ion concentrations were measured, diffusion constants were calculated for all specimen types. The calculations were performed in accordance to Fick's Second Law of diffusion, see Equation 1 (11).

$$\frac{\partial C}{\partial t} = D_c \frac{\partial^2 C}{\partial x^2} \quad (1)$$

where: C = chloride ion concentration,
 D_c = diffusion coefficient,
 t = time, and
 x = depth.

The solution to the Equation 1 with a boundary condition of surface concentration, C_0 , being dependent on square root of time is given by Equation 2 (11).

$$C_{(x,t)} = k \sqrt{t} \left[e^{-x^2/4D_c t} - \frac{x\sqrt{\pi}}{2\sqrt{D_c t}} \left(1 - \operatorname{erf} \frac{x}{2\sqrt{D_c t}} \right) \right] \quad (2)$$

where $C_{(x,t)}$ = chloride ion concentration at depth x after time t [kg/m³ of concrete],
 erf = error function.
 k = materials characteristics coefficient dependent on surface concentration
($C_0 = k \sqrt{t}$)

Since the chloride concentrations were measured at three or four depths (only horizontal zone, 1.5 years of exposure) the “Least Squares Fit Concept”, as described by Weyers et al., was employed to obtain the best fit of the diffusion coefficient (13). Calculated diffusion coefficients corresponding to the minimum of the sum of squared errors, after 1.5 years of indoor exposure, are presented in Table 11.

Rapid Concrete Chloride Permeability

Rapid permeability of the A4 concrete after 28 days and 1 year of wet curing averaged 3135 and 1877 Coulombs, with standard deviations of 579 and 509 Coulombs, and coefficients of deviation of 0.185 and 0.271, respectively. Rapid permeability values for other specimens were significantly lower than for the controls, and are expressed as number of standard deviations below the average for the A4 concrete. After 28 days of wet curing, these numbers were 2.6, 2.5, 4.0, and 3.5 for the FA, SC, SF, and SFD specimens, respectively. After 1 year of wet curing they were 3.0, 2.3, 2.5, and 2.1 for the FA, SC, SF, and SFD specimens, respectively.

Visual Observations

Control Specimens

Figures 82-87 present visually observed cracks and rust stains in the BS-1, BS-2, FA, SC, SF, and SFD specimens, after approximately four months of outdoor exposure. As shown, most of cracking had occurred in the horizontal and vertical zones and over the bars that were not included in the corrosion condition assessment. For the BS-1 specimen one crack in the horizontal zone was found, see Figure 82. The crack with a rust spot was first observed after 54 weeks of exposure over the bar No. 4a, between points 4 and 8. Five smaller cracks were observed in the vertical zone, four of which were on the left leg and one on the right leg, see Figure 82. In the left leg, one crack was over the top mat reinforcing bar, two cracks over the bar No. 1a and one crack over the bar No. 1. In addition to the two cracks over the bar No. 1a, relatively large rust stains were also observed. The crack in the right leg was observed in the

upper right corner. It was the only crack progressing vertically and also the shortest crack of all cracks found in the BS-1 specimen. As shown in Figure 83, several cracks were found in the horizontal zone, as well as in the legs of the BS-2 specimen. The two cracks in the horizontal zone were found over the side bars, 1a and 4a. The bar No. 1a also caused cracking in the right leg, and the bar No. 4a in the left leg. These cracks appeared in the upper parts of the specimen's legs. Two rust spots were found in the lower part of the specimen: one over the bar No. 1 in the tidal zone, the other one was on the boundary between the tidal and immersed zones, see Figure 83. In addition, two structural cracks were formed while the specimen was being removed from the steel forms. These cracks progressed through the whole thickness of each leg. The structural crack in the left leg occurred in the vicinity of the bar No. 1a, while the crack in the right leg close to the bar from the bottom mat of the deck reinforcement.

Low Permeable Concretes

The FA specimen also had structural crack which occurred in the right leg close to the bar No. 1a in the vertical zone. In addition several cracks were found in the horizontal and vertical zones, see Figure 84. The cracks in the horizontal zone occurred over the bars No. 1, No. 3a, No. 4, and one crack, perpendicular to the main reinforcement, progressing from the bar No. 4. The crack over the bar No. 4, at the back side of the specimen, was first observed after 20 weeks of ponding. Also during the indoor exposure, after 30 weeks of ponding, cracks visible in the left and right legs were observed. The cracks in the left leg can be found in the vertical zone over the bars No. 1a and No. 1. The two cracks in the right leg are located above the structural crack over the bars from the top and bottom mats of deck reinforcement. Cracks in the SC specimen occurred only in the deck and left leg, see Figure 85. Cracking in the horizontal zone occurred over almost every bar, except the bar No. 1a, and they were found in a very early stage of indoor exposure. It is highly possible that all cracks found in the horizontal zone are the subsidence cracks. There was one crack in the left leg. It occurred over the bar from the top mat of deck reinforcement. In addition to cracking, a rust spot was found over the bar No. 3 in the vertical zone of the left leg, and it was first observed after 10 weeks of ponding. The SF specimen had one structural crack in the right leg, close to the bar from the deck bottom mat, one crack in the horizontal zone over the bar No. 1, and one rust spot over the bar No. 3a in the vertical zone of the left leg, see Figure 86. The SFD specimen had only two little cracks in the horizontal zone, see Figure 87. One crack occurred over the bar No. 1a and progressed diagonally towards the edge with the right leg. The other crack occurred between the bars No. 1 and No. 2 at the back of the specimen, and was perpendicular to these bars.

Discussion Summary

The structural cracks observed in some specimens appeared to have no influence on the corrosion development on the bars in the vicinity of the these cracks. Evidently the silicone rubber and duct tape protection provided an adequate repair.

Corrosion potentials observed in the horizontal zone of BS-1 and BS-2 specimens suggest the possibility of an active corrosion process development during indoor exposure. This was confirmed by the corrosion rate results which indicate that the control specimens were in an active region of corrosion when they were kept indoors. Macrocell action is a probable explanation of differences in corrosion rates in the immersed and tidal zones between the BS-1 specimen, legs reinforcement not connected, and the BS-2 specimen, legs reinforcement connected. Potential and corrosion rate data for the LP concretes were inconclusive.

The results of chloride testing indicate that the amount of chlorides present at the bar level is more than sufficient for corrosion to occur for the control specimens, however, it still is very low for the specimens with low permeable concretes. Based on chloride data it appears that the specimens with silica fume are the least prone to chloride ingress. Specimens with fly ash and slag cement will allow for greater intrusion of chlorides, but still much less than the controls. This is confirmed by comparing diffusion coefficients: they are more than 3 times lower for the specimens made with concrete with mineral admixtures, as compared to the controls. Chloride concentration data agree with the rapid permeability test results which also show a positive influence of mineral admixtures on concrete chloride ion blocking abilities.

The cracking, other than structural, appeared to be related to the reinforcing steel corrosion. The bars No. 1a and No. 4a in the horizontal zone were expected to corrode first since they were exposed to more severe condition than any other bar. The chlorides diffused from the top, 25 mm of the cover depth in the horizontal zone, and from the side, 25 mm cover depth in the leg. This behavior was especially observed in the control, BS-1 and BS-2, specimens. The largest number of cracks and the highest severity was observed in the control specimens and the FA specimen. It is believed that crack over the bar No. 4, at the back side of the FA specimen, was caused by the corrosion of the hook used for lifting the specimen. Nevertheless, the cracks in the vertical zone are clearly related to the corrosion of the underlaying bars. The cracks in the horizontal zone of the SC specimen were probably caused by the subsidence cracking, since no corrosion products were visible, typical for cracks caused by corrosion. Obviously the crack in the upper part of the left leg is corrosion related. The least affected specimens by corrosion were the SF and SFD specimens with one and two cracks, respectively.

Low permeable concretes provide a much better level of protection against chloride intrusion than the A4 concrete alone. Concretes with fly ash or slag cement may provide the same protection as concrete with silica fume, as long as the concretes are allowed to cure for a longer period of time without salt application. Application of a corrosion inhibitor causes the beneficial elevation of the chloride threshold and in result an increase in time to EFSL.

SERVICE LIFE ESTIMATES

Service lives of A4 and LP concretes were determined from the results of the laboratory and field

investigations. The laboratory study was described in previous chapters. The field investigation consisted of sampling bridge decks for chloride concentration profiles and measuring cover depths. Three 17-years-old structures in the state of Virginia, SN 1026, SN 1029, and SN 8003, were selected for the purpose of the study. Additional 18 bridge decks throughout Virginia were selected for cover depth measurements only.

Cover depths were measured on 21 bridge decks with an average close to 120 readings per deck. A total of 2498 measurements were recorded. Concrete powder samples were collected from twelve locations from each out of three bridge decks. At each location, a sample set consisting of chloride samples from the following depths: 13 mm (6 to 19 mm), 25 mm (19 to 32 mm), 38 mm (32 to 44 mm), and 51 mm (44 to 57 mm), was collected. Sample sets collected at six locations on the SN 8003 bridge deck included two additional samples from depths of 64 mm (57 to 70 mm) and 76 mm (70 to 83 mm). The total number of concrete powder samples collected from the three bridge decks was 156 (48, 48, and 60).

As with the laboratory specimens, powdered concrete samples from the top 6 mm were discarded due to high variability of chloride content close to the surface. Also, chloride concentration measured at the 13 mm depth are referred to as surface concentration.

Field concrete powder samples were analyzed for chloride concentrations in accordance with ASTM C-114 (8). The average surface chloride concentrations was 4.46 kg/m^3 with the standard deviation of 2.36 kg/m^3 . The results indicate that surface concentration was distributed according to gamma function with parameters $\alpha = 3.56$ and $\beta = 1.25$. Cumulative distribution function (CDF) of the surface concentration is presented in Figure 88. The procedure used to calculate field diffusion coefficients was similar to the one used for the laboratory data. The difference was in the solution of the diffusion equation. It has been shown that the for the field data, surface concentration is relatively constant at a depth of 13 mm (13). Thus, a boundary condition with a surface concentration being constant applies, and Equation 3 was used for D_c determinations.

$$C_{(x,t)} = C_0 \left(1 - \text{erf} \frac{x}{2\sqrt{D_c t}} \right) \quad (3)$$

where: $C_0 =$ surface concentration

Diffusion coefficients were calculated for each location. For the three bridges and 12 locations from each bridge, 35 values (one outlier was excluded) averaged for $D_c = 38.4 \text{ mm}^2/\text{year}$. It has been observed that the diffusion coefficients were also distributed according to the gamma function. The parameters α and β were 1.42 and 27.05, respectively. The CDF of the diffusion coefficients is presented in Figure 89.

The presented methodology is based on data from the horizontal exposure zone, but the

procedure is applicable to other exposure zones as well. Laboratory and field data were used to determine time to corrosion initiation for all concrete types. Calculations were performed by an interactive solution of Equation 3 and solving it for time, t . The following four parameters were used to solve Equation 3: chloride concentration threshold, $C_{(x, t)}$, surface concentration, C_0 , reinforcing steel cover depth, x , and diffusion coefficient, D_c .

A value of 0.89 kg/m^3 of concrete was taken for all concrete types, except the SFD concrete, as a chloride concentration threshold. Since the corrosion inhibitor elevates the threshold, a double value of chloride concentration threshold, 1.78 kg/m^3 of concrete, was used for the SFD concrete for illustration purposes only. The manufacturer stated the threshold level for the DCI-S dosage of 20 l/m^3 of concrete used in the laboratory specimen is $5.9 \text{ kg chloride/m}^3$ of concrete.

Surface concentration of 4.05 , and 7.63 kg/m^3 of concrete were used in the analysis. These values were taken from the field surface concentration distribution, see Figure 88, and correspond to 50 and 90% of the CDF, respectively.

It has been shown that about 12% of the reinforcement is capable of causing corrosion damage requiring immediate repair or rehabilitation (11). Therefore, all calculations use 12% cover depth, a cover depth for 12% of the reinforcing steel, rather than the mean value. Based on 2498 readings from 21 bridge decks in Virginia, cover depths were found to be normally distributed with the mean of 65 mm and standard deviation of 9.1 mm. The average 12% cover depth was equal to 54 mm.

Diffusion coefficients of laboratory specimens could not be used directly in the analysis because laboratory exposure conditions were different from the field conditions. Since no field data is available on LP concretes, a relationship between laboratory and field diffusion coefficients had to be established. To properly simulate field conditions a modified diffusion coefficient, see Equation 4, was used.

$$D_{c(\text{modified})} = D_{c(\text{field})} \cdot D_{c(\text{lab specimen})} / D_{c(\text{control})} \quad (4)$$

where: $D_{c(\text{lab specimen})}$ = diffusion coefficient of a considered concrete type (laboratory specimen),
 $D_{c(\text{control})}$ = diffusion coefficient of a control specimen (D_c of the CTL 1 specimen was used for calculations), and
 $D_{c(\text{field})}$ = diffusion coefficient of a field structure.

Equation 4 shows that for the control specimen, $D_{c(\text{modified})}$ will always be equal to $D_{c(\text{field})}$ simply because $D_{c(\text{lab specimen})}$ is the same as, or equal to, $D_{c(\text{control})}$. Exact modeling of the field conditions by the control specimen was intentional, especially that concrete bridge decks and laboratory control specimens were made with the same specification concrete, A4 concrete. Note that diffusion coefficients of laboratory specimens are fixed values, while $D_{c(\text{field})}$ has a distribution, see Figure 89. Values of 29.9 and $81.1 \text{ mm}^2/\text{year}$ corresponding to 50% (mean) and 90% of the

field D_c population, respectively, were used in the analysis. For the A4 concrete, $D_{c(\text{modified})}$ was equal to the field value, $29.9 \text{ mm}^2/\text{year}$. For the FA, SC, SF, and SFD concretes, $D_{c(\text{modified})}$ was 6.1, 7.7, 3.9, and $11.3 \text{ mm}^2/\text{year}$, respectively.

Figure 90 presents the corrosion initiation times, as a function of cover depth, for the A4 concrete. The interpretation is that the time to corrosion initiation for 12 % reinforcement and the mean values of D_c and C_0 , at 54 mm depth, is 33 years. In other words, 50% of VA bridge decks will reach chloride threshold in less than 33 years. One can also see that for a small percentage of bridge decks, 10% [$\text{CDF}(C_0) > 90\%$ and $\text{CDF}(D_c) > 90\%$,] corrosion initiation will occur in less than 7.5 years. Corrosion initiation times, as a function of cover depth, for the FA, SC, SF, and SFD concretes are presented in Figures 91, 92, 93, and 94, respectively. It is apparent that these concretes would provide much better corrosion protection. Even for both $\text{CDF}(D_c)$ and $\text{CDF}(C_0)$ of 90%, less than 10% of the bridge decks, at 54 mm depth, initiation times increase from 7.5 years for the A4 concrete to 36, 29, 56, and 93 years for the FA, SC, SF, and SFD concretes, respectively.

The end of functional service life (EFSL) is defined as the condition of a bridge element requiring immediate repair or rehabilitation. In the presented analysis, time till EFSL was taken as the corrosion initiation time plus seven years, which is a reasonable estimate for corrosion development and resultant deterioration. All calculations were performed for the average 12% cover depth of 54 mm. Since the surface concentration and the diffusion coefficient variables have own distributions, probability considerations could be introduced into the analysis. For example, a time equivalent to 10% probability of EFSL for A4 concrete would be calculated with values of D_c and C_0 corresponding to 90% ($100\% - 90\% = 10\%$) of the respective CDFs. A relationship between the time till EFSL and its probability for A4 concrete is presented in Figure 95. Another curve, designated as SHRP, also presented in Figure 95 is the curve from the SHRP study on field performance of 120 Virginia bridge decks (13). The conclusion of the SHRP study was that the time till EFSL for an average bridge deck in Virginia would be 36 years with a standard deviation of 13 years. The modeled time to EFSL for the mean, 50% probability, bridge deck with A4 concrete is 40 years, see Figure 95. The four years difference, $40 - 36$, is very little, especially that the SHRP study was done on bridges that were built when specifications required $w/c = 0.46$ and 51 mm cover depth. Current Virginia specifications for the A4 concrete require $w/c = 0.45$ and 64 mm cover. Thus, the model proves to be valid. Similar analysis was performed on all other concretes and the prediction results are presented in Figure 96. The beneficial use of mineral admixtures and SF with DCI-S corrosion inhibitor is evident even at low probabilities of EFSL.

The assumption that the distributions of C_0 and D_c are fairly representative of the whole population of Virginia bridges is reasonable because the average service life for Virginia bridge decks with bare steel is 36 years using a specification concrete with w/c of 0.46 and 51 mm cover depth. Using the mean C_0 and D_c values and seven years from the corrosion initiation to spalling, the average service life is about 40 years for a specification concrete with w/c of 0.45 and 64 mm cover. Thus, the presented model is appropriate for service life determinations.

The benefit of having D_c and C_0 distributions is that predictions can be made not only for the average, but for any percentile of bridge decks.

As seen in Figure 95, low permeable concretes require much more time to EFSL than the A4 concrete. This behavior is attributed to pozzolanic reaction of mineral admixtures. Even though the FA and SC concretes yield lower times to EFSL than the concrete with silica fume, one should not overlook their excellent properties. The particles of fly ash and slag cement are about 100 times larger than the silica fume particles, thus the pozzolanic reaction of these materials is much slower. This can be seen by comparing rapid permeability results at 28 days and 1 year, see Figure 81. Laboratory study, as all laboratory studies, required accelerated tests and chloride ingress was very fast. At early ages the FA and SC concretes were more vulnerable to chloride attack than the SF concrete simply because the concrete matrix was not developed to the same extent. It is believed that their performance would be better if chlorides were introduced at a later time.

CONCLUSIONS

The addition of mineral admixtures and slag to A4 concrete can reduce the infiltration of chloride ion and provide for structures with a much longer service life.

RECOMMENDATIONS

It is recommended that annual monitoring of the specimens be continued until more cracking has occurred to better estimate the service life extension provided by mineral admixtures and mineral admixture with corrosion inhibitor used in the construction of concrete bridge components in Virginia. The specimens with low permeable concretes and one control specimen, BS-2, should be taken to the Hampton Road north tunnel island and placed in the brackish water to a depth of the immersed zone at low tide for further exposure to chloride ions. The BS-1 specimen should remain in an outdoor exposure in Southwest Virginia like the Civil Engineering Materials Research Laboratory in Blacksburg, Virginia.

Even though the presented D_c and C_0 distributions provide good basis for service life analysis, more field studies are needed to have a better representation of bridge conditions in Virginia. Also, calculated times to EFSL for concretes with mineral admixtures need to be verified.

REFERENCES

1. Weyers, R.E. et. al. (November 1995). *Protocol for In-Service Evaluation of Bridges with Epoxy-Coated Reinforcing Steel*, NCHRP 10-37B, Final Report, p.110.
2. Clear, K.C. (December 1992). *Effectiveness of Epoxy-Coated Reinforcing Steel - Final Report*, Canadian Strategic Highway Research Program, Ottawa, Ontario, p.128.
3. Sagues, A.A., et. al. (May 1994). *Corrosion of Epoxy-Coated Rebar in Florida Bridges*, College of Engineering, University of South Florida, p.70.
4. Weyers, R.E., et. al. (October 1997). *Field Investigation of the Corrosion Protection Performance of Bridge Decks and Piles Constructed with Epoxy-Coated Reinforcing Steel in Virginia*, VTRC 98-R4, Virginia Transportation Research Council, Charlottesville, Virginia, p. 34.
5. Krauss, P.D., D.B. McDonald and M.R. Sherman (June 1996). *Corrosion Investigation of Four Bridges Built Between 1973 and 1978 Containing Epoxy-Coated Reinforcing Steel*, Minnesota Department of Transportation, MN/RC - 96/25, St. Paul Minnesota, p. 163.
6. Newhouse, Charles D., *Corrosion Rates and the Time to Cracking of Chloride Contaminated Reinforced Concrete Bridge Components*, Master's Thesis, Blacksburg, VA, December, 1993.
7. SHRP-S / FR-92-110, *Condition Evaluation of Concrete Bridges Relative to Reinforcement Corrosion*, Volume 8: Procedure Manual, 1992.
8. ASTM C-114 *Standard Test Methods for Chemical Analysis of Hydraulic Cement, Section 19: Chloride (Reference Test Method)*.
9. ASTM C 876 *Standard Test Method for Half Cell Potentials of Reinforcing Steel in Concrete*.
10. ASTM C 1202, *Standard Test Method for Electrical Indication of Concrete's Ability to resist Chloride Ion Penetration*.
11. Crank, J., *Mathematics of Diffusion*, The University Press, Oxford, UK, 1970.
12. Whiting, D., "Rapid Determination of the Chloride Permeability of Concrete," Final Report No. FHWA/RD-81/119, Federal Highway Administration, August 1981, NTIS No. PB 82140724.
13. SHRP-S-668, *Concrete Bridge Protection and Rehabilitation: Chemical and Physical Techniques*, Service Life Estimates, 1994.

Table 1. Specimen Configuration.

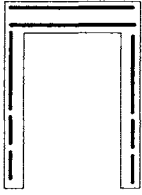
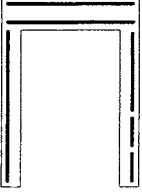
Specimen Legs' Reinforcement	A4 Concrete	A4 Concrete with Admixtures (cement replacement)			
	No Admixtures	Fly Ash	Slag Cement	Silica Fume	Silica Fume & DCI-S Corr. Inhibitor
	Bare Steel	Bare Steel	Bare Steel	Bare Steel	Bare Steel
 Type I	BS-1 (Control 1)				
 Type II	BS-2 (Control 2)				
 Type III		FA	SC	SF	SFD

TABLE 2. Recommended Action for Chloride Content Measurements.

Chloride Concentration	Recommendation
< 0.59 kg/m ³	leave intact
0.59 - 1.19 kg/m ³	questionable area
> 1.19 kg/m ³	remove concrete below bar level or replace entire section

TABLE 3. Interpretation of Potential Readings.

Voltmeter Reading	Interpretation
greater than -200 mV	90% probability of no corrosion
from -200 mV to -350 mV	uncertain
less than -350 mV	90% probability of active corrosion

TABLE 4. Data interpretation for the 3LP Device.

i_{corr}	Interpretation
$< 0.21 \mu\text{A}/\text{cm}^2$	no damage expected
$0.21 - 1.07 \mu\text{A}/\text{cm}^2$	damage possible in 10-15 years
$1.07 - 10.7 \mu\text{A}/\text{cm}^2$	damage possible in 2-10 years
$> 10.7 \mu\text{A}/\text{cm}^2$	damage possible in less than 2 years

TABLE 5. Physical and Chemical Properties of Bare Steel.

Physical Properties:

Yield Point [MPa]	425 - 473
Tensile Strength [MPa]	645 - 703
% Elongation [200 mm]	10

Chemical Properties:

C [%]	0.38 - 0.43
Mn [%]	0.83 - 1.00
P [%]	0.01
S [%]	0.03 - 0.05

TABLE 6. Concrete Mixture Proportions.

Specimen	BS-1, BS-2	FA	SC	SF	SFD
Ingredients [kg/m ³ of concrete]					
Cement	377	320	226	351	351
Fly Ash	-	75	-	-	-
Slag Cement	-	-	151	-	-
Silica Fume	-	-	-	26	26
#78 Coarse Aggregate	867	867	867	867	867
Fine Aggregate	864	825	854	856	848
Water	170	170	170	170	153
Corrosion Inhibitor [l/m ³ of concrete]:					
DCI-S	-	-	-	-	20
Admixtures [ml/100 kg of cement]:					
HRWR: WRDA-19	1215, 914	847	682	1063	1605
AEA: Daravair-M	72, 69	78	70	69	87

TABLE 7. Cement Properties (as Provided by the Manufacturer).

Chemical Test Data		Physical Test Data	
SiO ₂	22.1	Fineness - Blaine	3760
Al ₂ O ₃	4.29	Fineness - Wagner	2212
Fe ₂ O ₃	2.83	Autoclave Expansion	0.05
CaO	63.4	Initial Set (H:min.)	2:25
MgO	2.86	Final Set (H:min.)	3:35
SO ₃	2.23	Vicat (min.)	95
Total Alkalies	0.62	Air Content (Mortar)	6.6
Insoluble Residue	---	Compressive Strength [MPa]	
Ignition Loss	1.1	1 day	15.0
C ₃ S	51.3	3 day	27.4
C ₃ A	6.58	7 day	35.5

TABLE 8. Fresh Concrete Properties.

Specimen	Water/Cement Ratio	Slump [mm]	Air [%]	Temperature [C]	Density [g/cm ³]
BS-1	0.46	191	6.2	25	2.34
BS-2	0.44	203	5.5	26	2.34
FA	0.44	203	3.1	27	2.41
SC	0.44	165	8.5	24	2.24
SF	0.44	178	5.7	23	2.32
SFD	0.45	64	4.5	29	2.36

TABLE 9. Compressive Strengths.

Specimen	Average Compressive Strength (MPa)				
	3 days	7 days	28 days	56 days	1 year
BS-1	39	48	58	62	72
BS-2	35	40	48	54	63
FA	28	36	48	58	68
SC	18	29	42	44	52
SF	31	39	54	53	63
SFD	28	42	62	61	73

TABLE 10. Rapid Concrete Chloride Permeability.

Specimen	Water/Cement	Permeability [Coulomb]	
	Ratio	28 days	1 year
BS-1	0.46	3049	1816
BS-2	0.44	3120	2048
FA	0.44	1653	332
SC	0.44	1700	708
SF	0.44	815	584
SFD	0.46	1130	814

TABLE 11. Diffusion Coefficients.

Specimen	Diffusion Coefficient [mm ² /year]			
	Horizontal Zone	Vertical Zone	Tidal Zone	Immersed Zone
BS-1	138	135	85	112
BS-2	135	109	113	113
FA	28	10	16	16
SC	35	20	17	21
SF	18	24	21	18
SFD	19	25	17	18

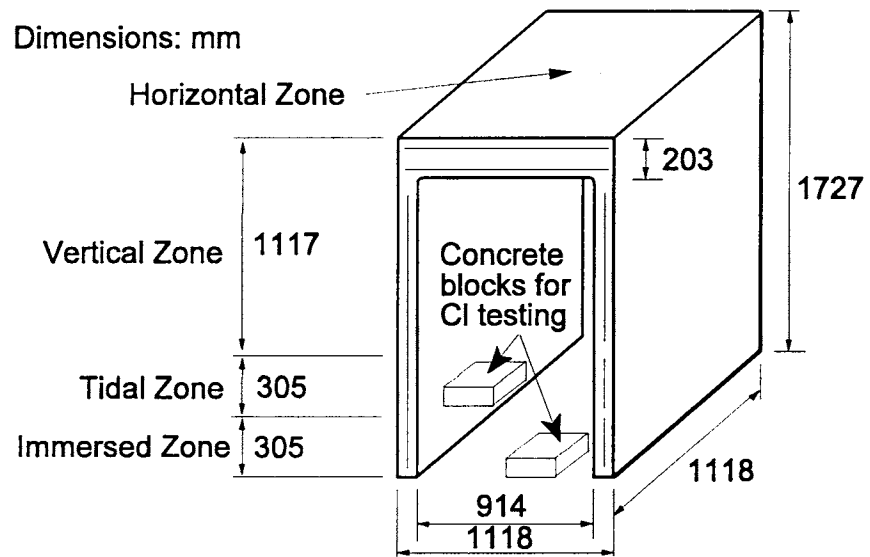


FIGURE 1. Specimen Configuration.

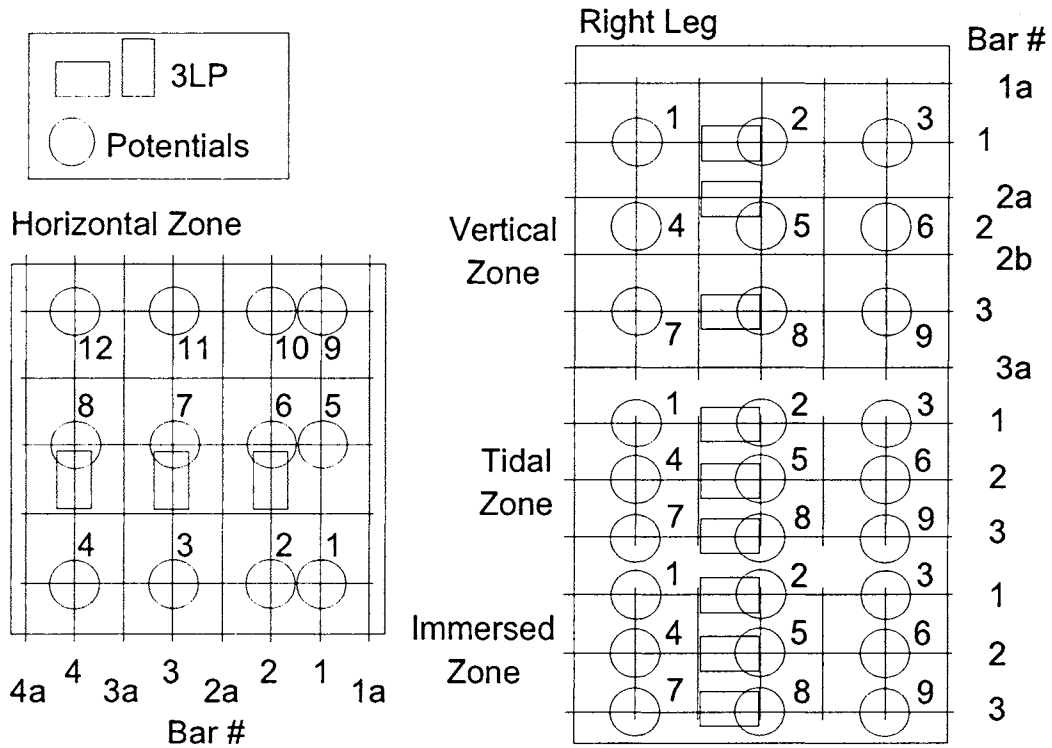


FIGURE 2. Measurement Plan.

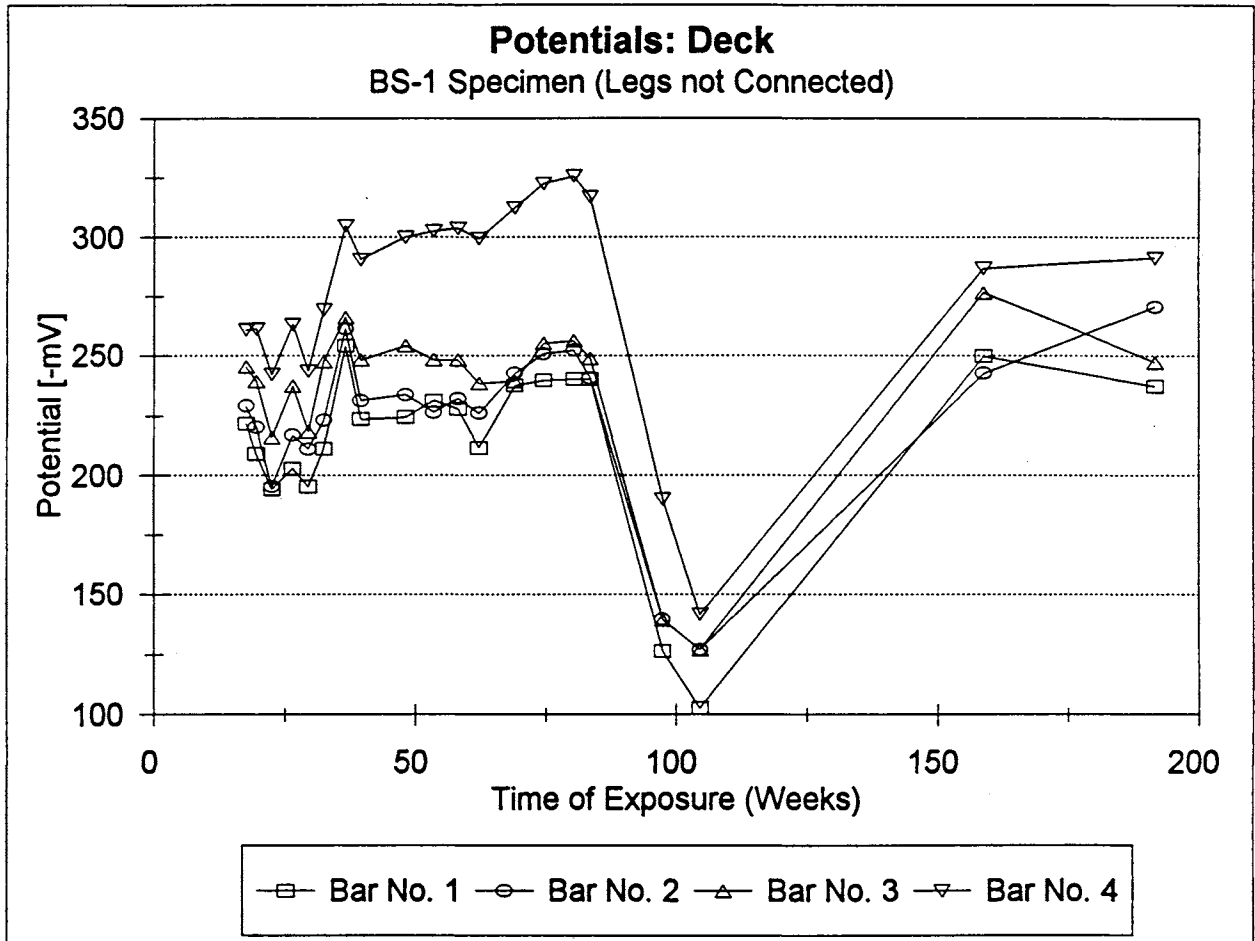


FIGURE 3. Corrosion Potentials in the Horizontal Zone, BS-1 Specimen (Control 1).

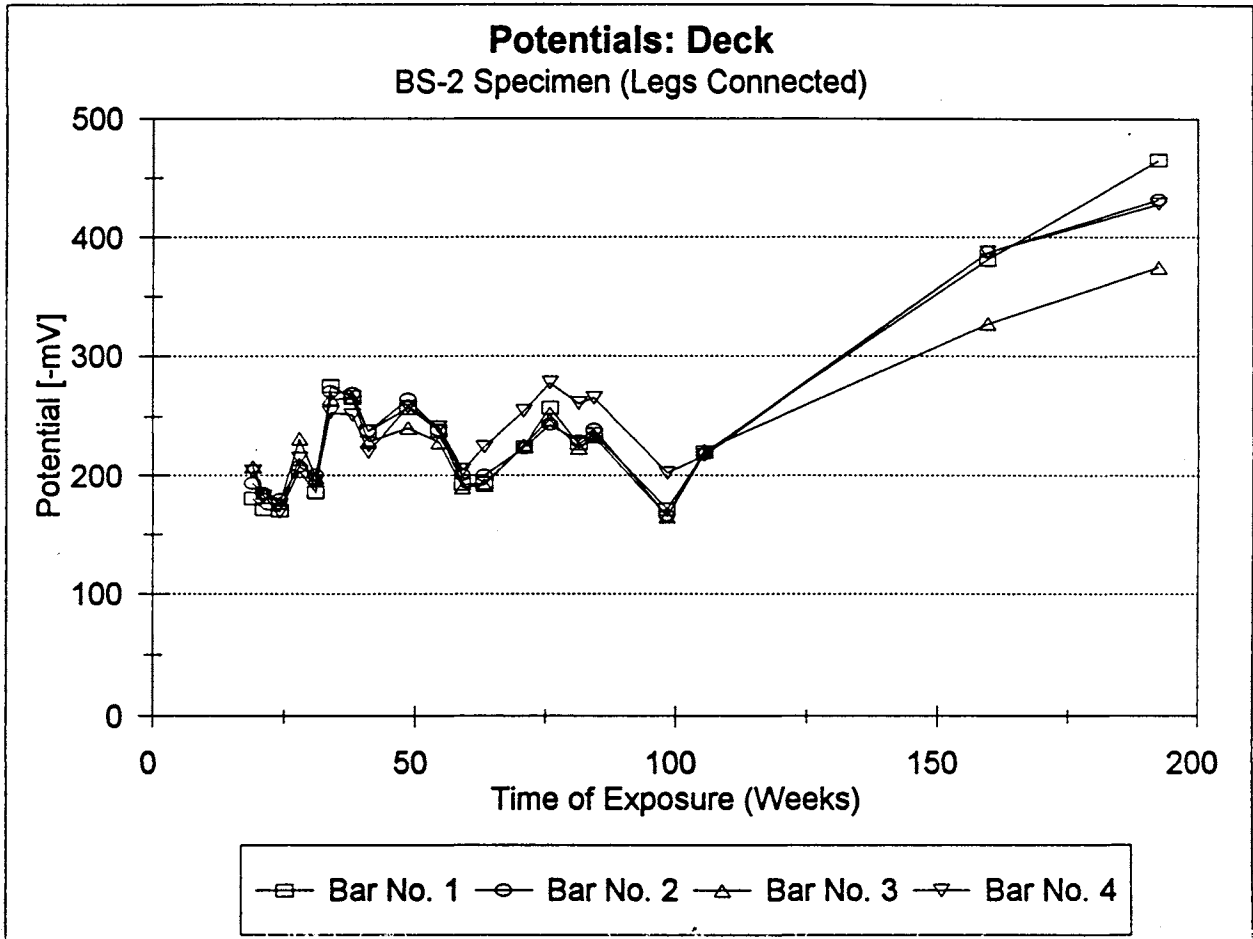


FIGURE 4. Corrosion Potentials in the Horizontal Zone, BS-2 Specimen (Control 2).

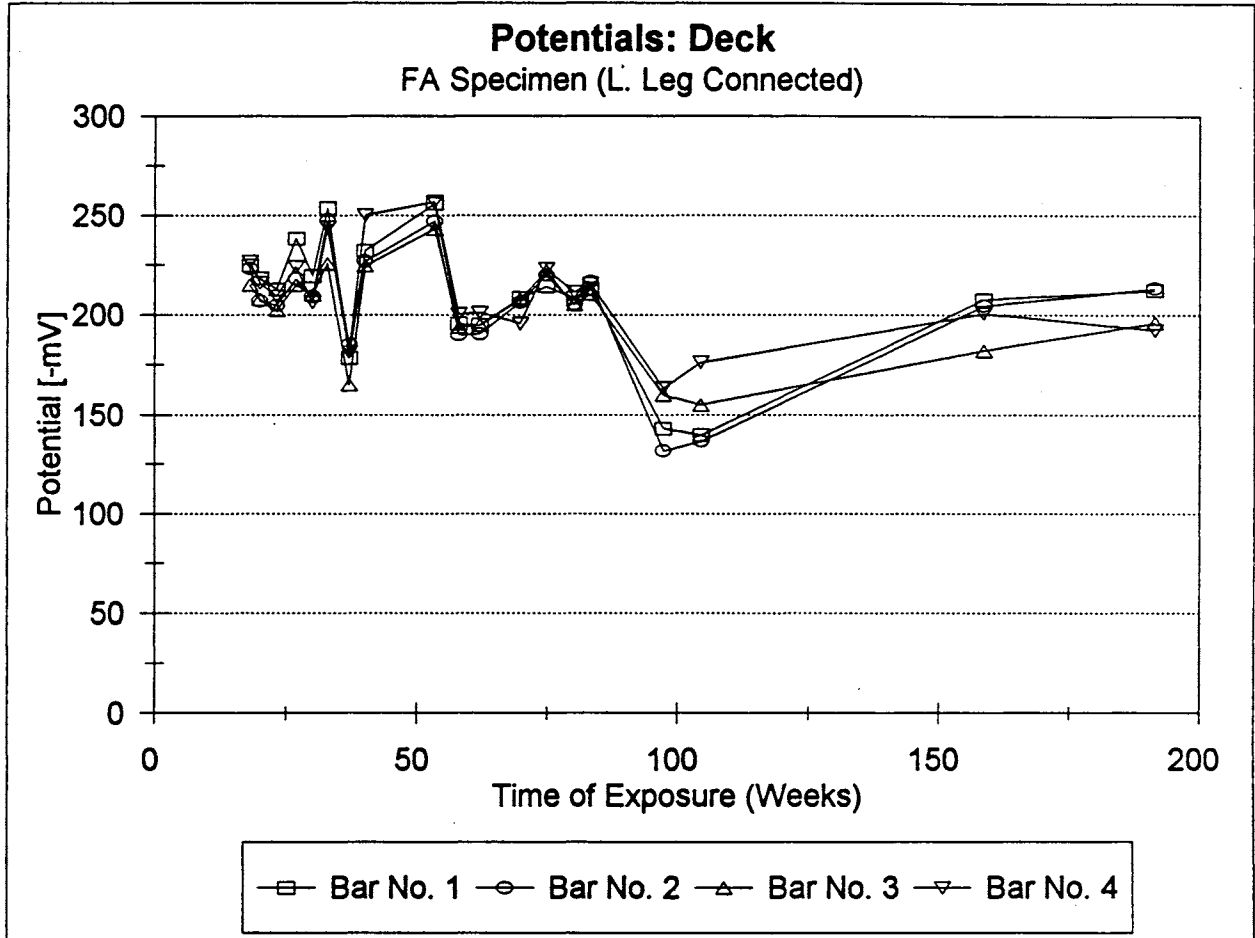


FIGURE 5. Corrosion Potentials in the Horizontal Zone, FA Specimen.

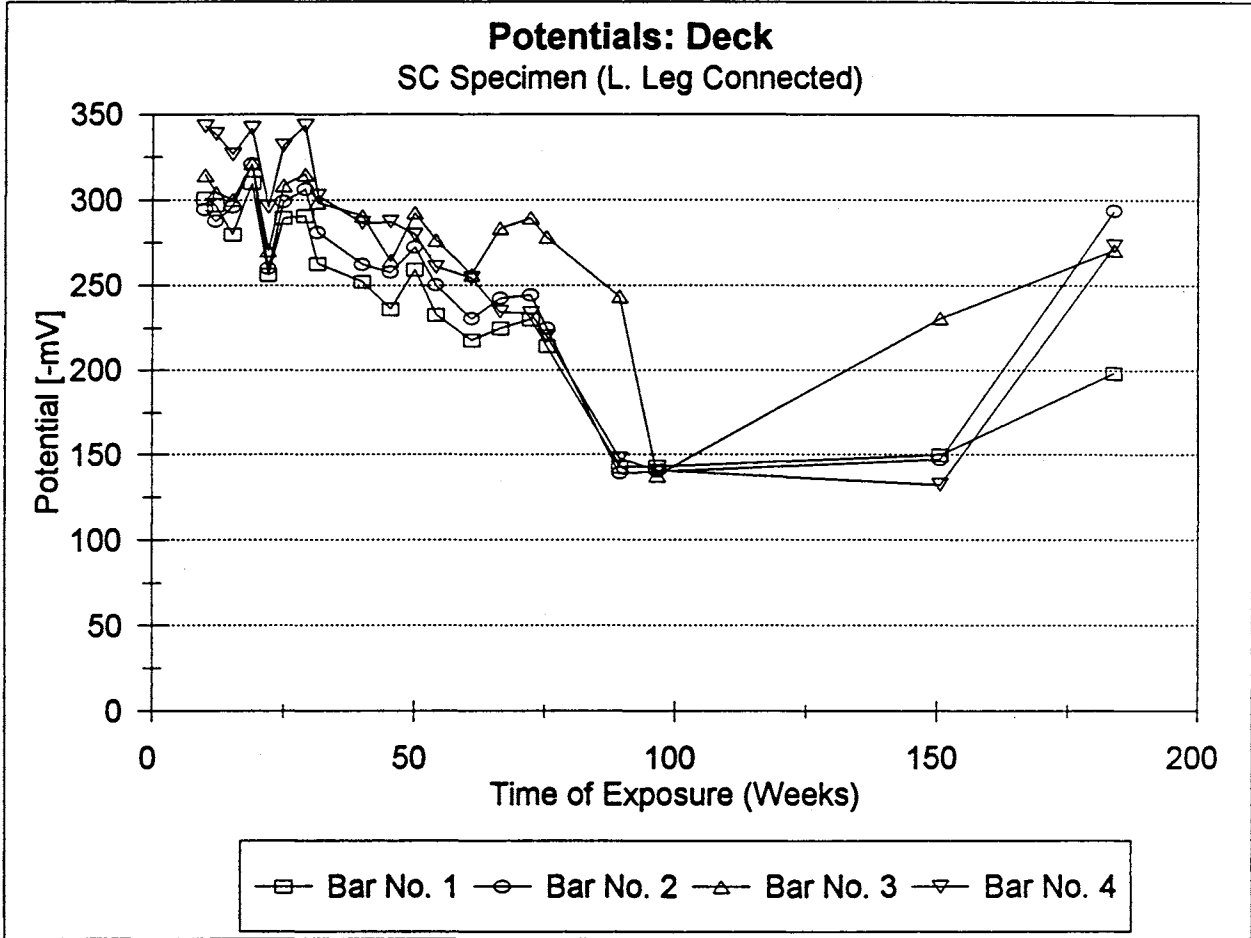


FIGURE 6. Corrosion Potentials in the Horizontal Zone, SC Specimen.

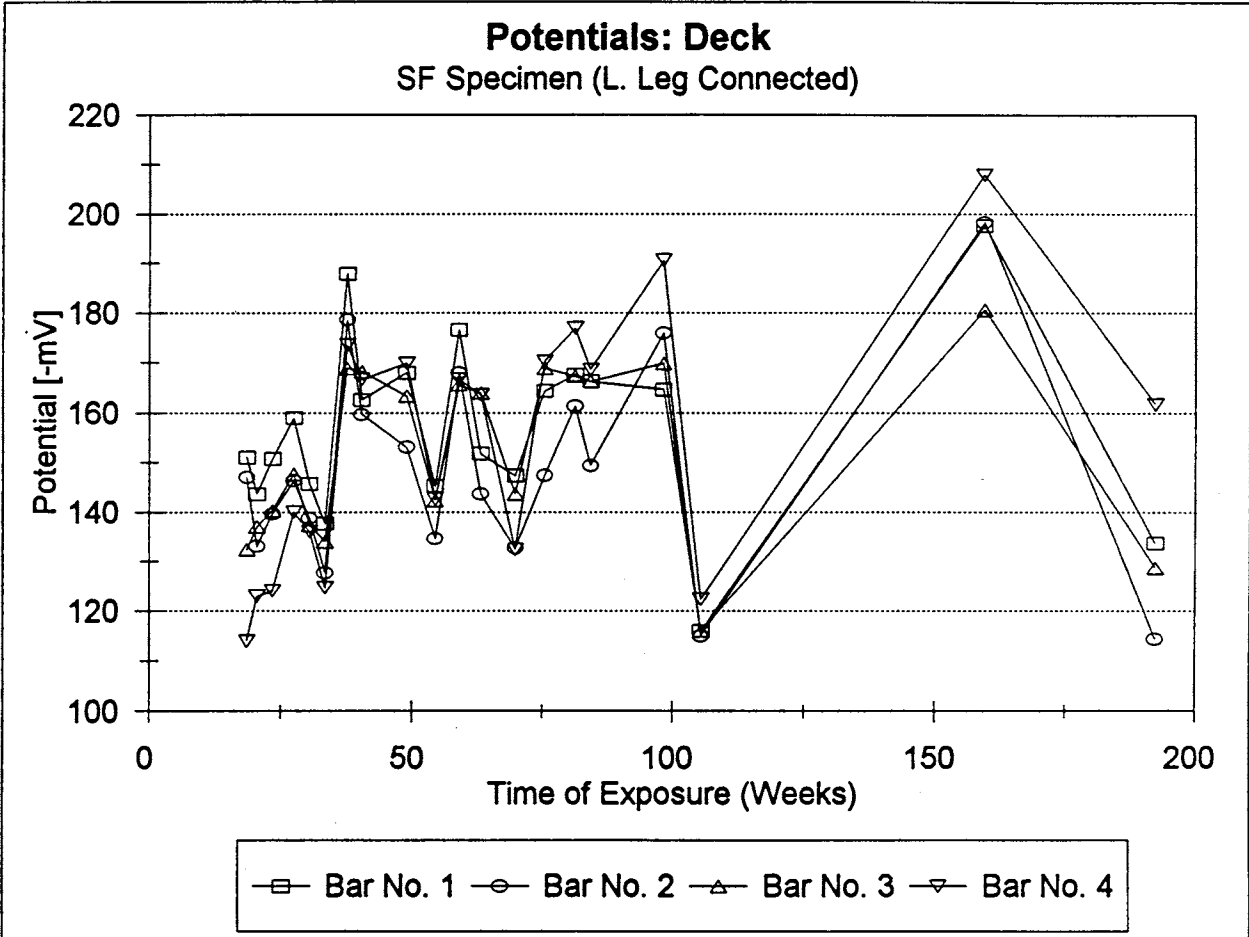


FIGURE 7. Corrosion Potentials in the Horizontal Zone, SF Specimen.

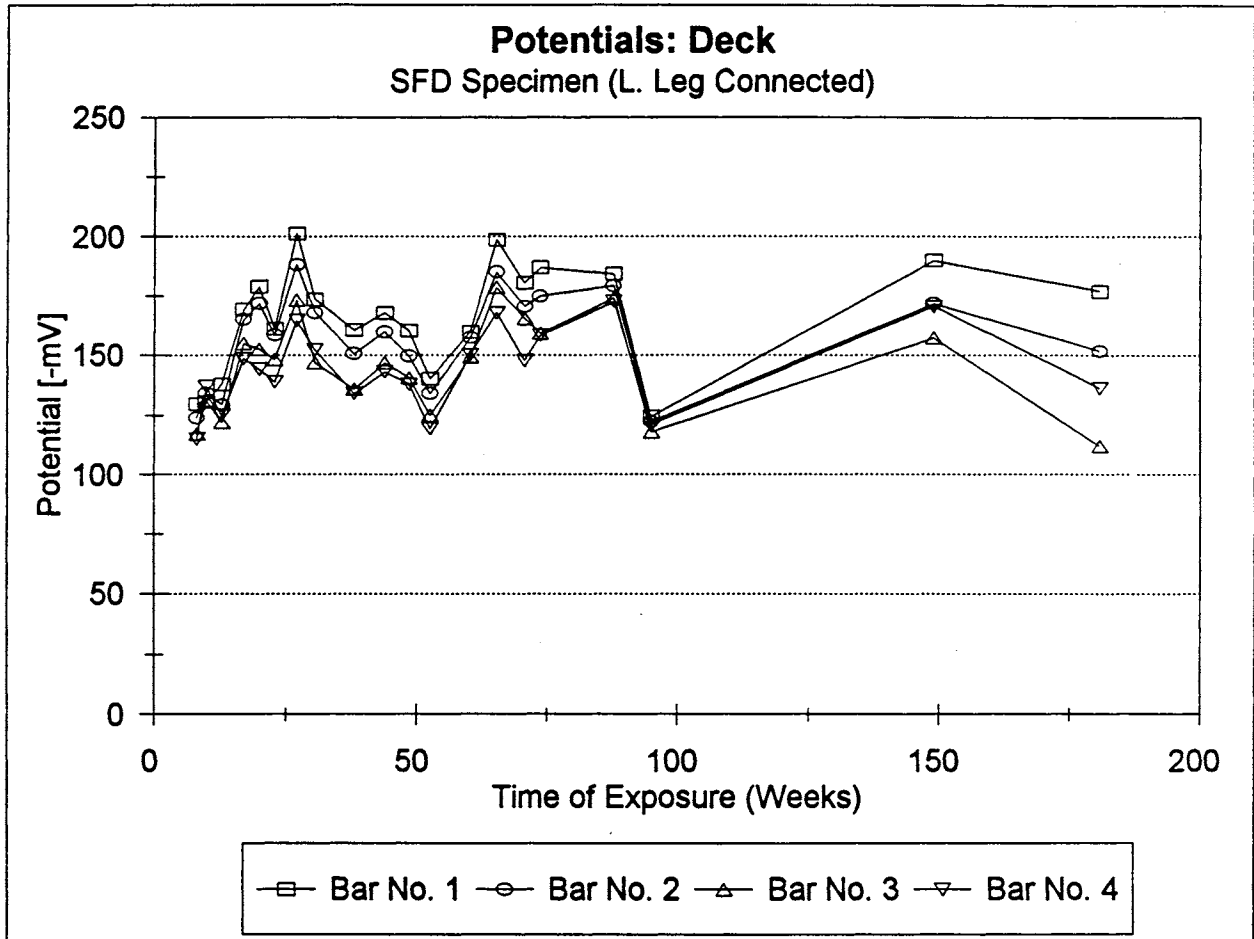


FIGURE 8. Corrosion Potentials in the Horizontal Zone, SFD Specimen.

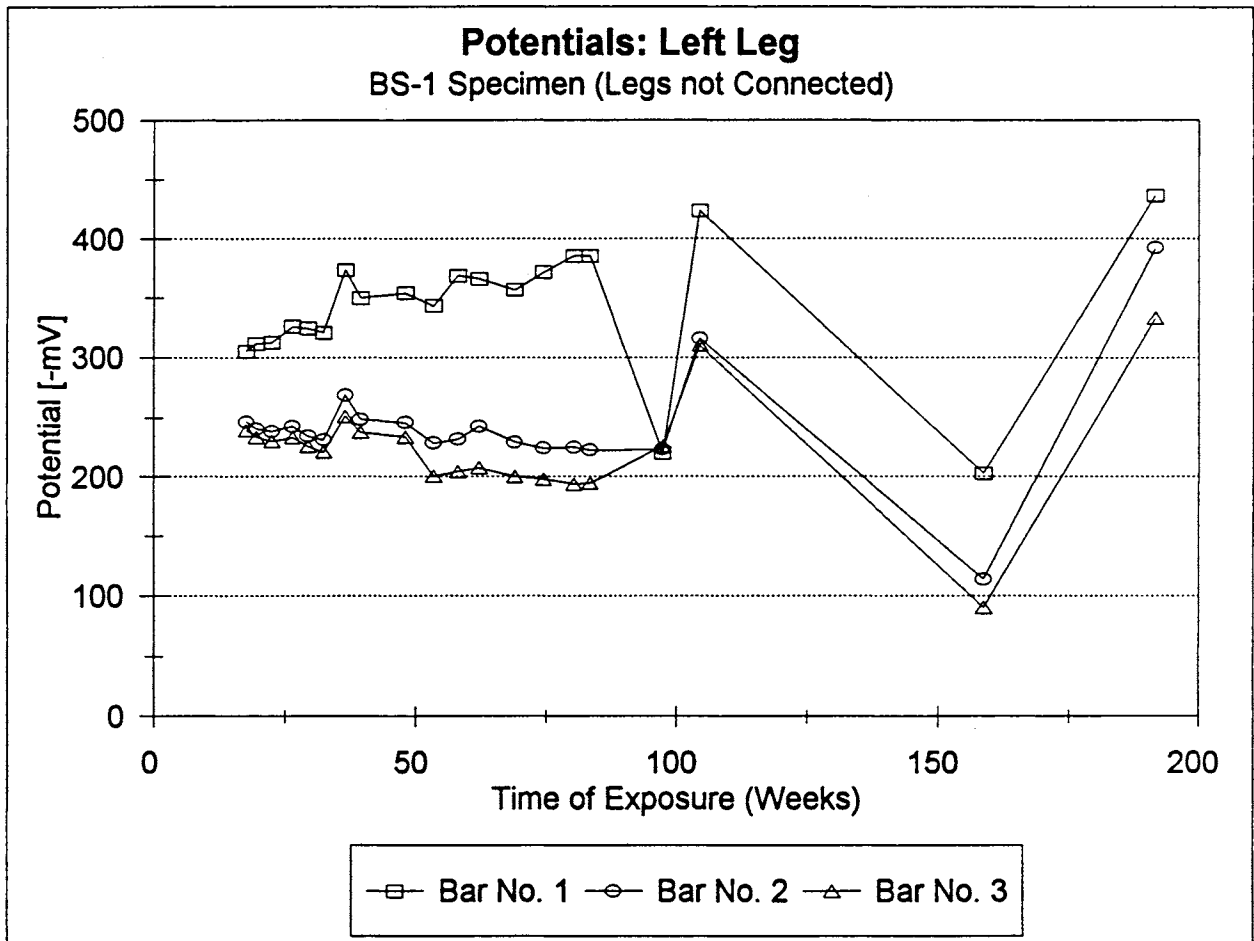


FIGURE 9. Corrosion Potentials in the Vertical Zone, Left Leg, BS-1 Specimen (Control 1).

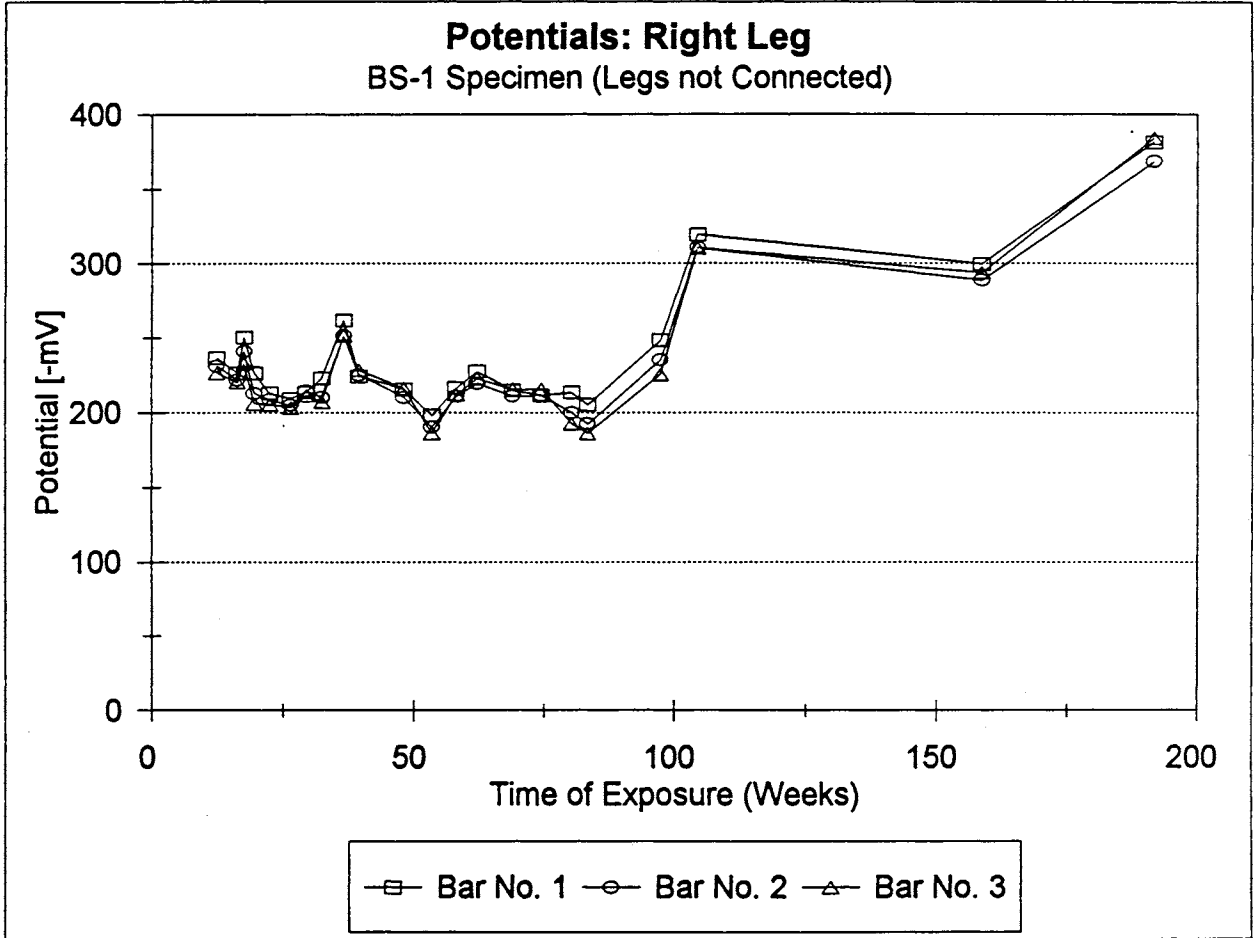


FIGURE 10. Corrosion Potentials in the Vertical Zone, Right Leg, BS-1 Specimen (Control 1).

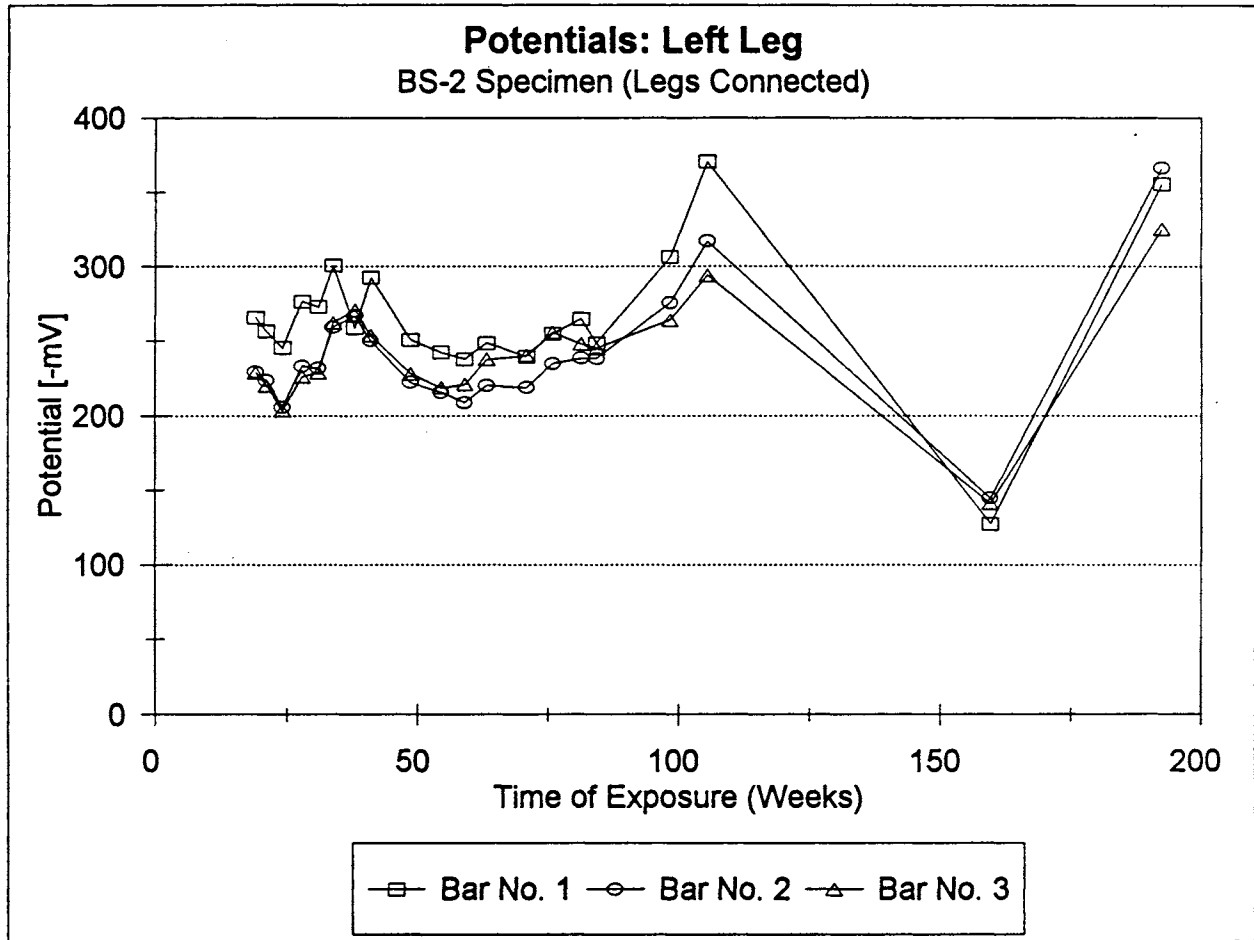


FIGURE 11. Corrosion Potentials in the Vertical Zone, Left Leg, BS-2 Specimen (Control 2).

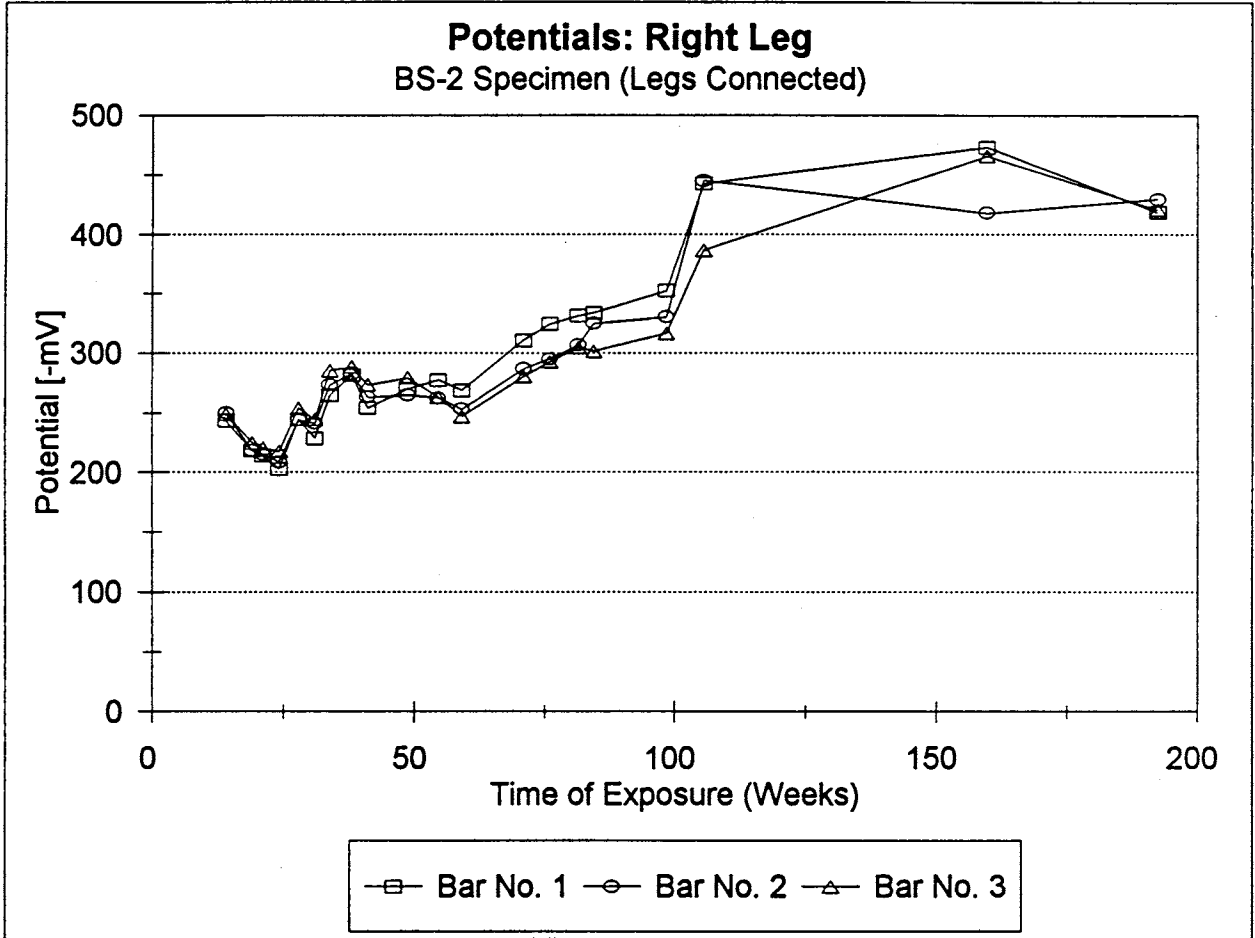


FIGURE 12. Corrosion Potentials in the Vertical Zone, Right Leg, BS-2 Specimen (Control 2).

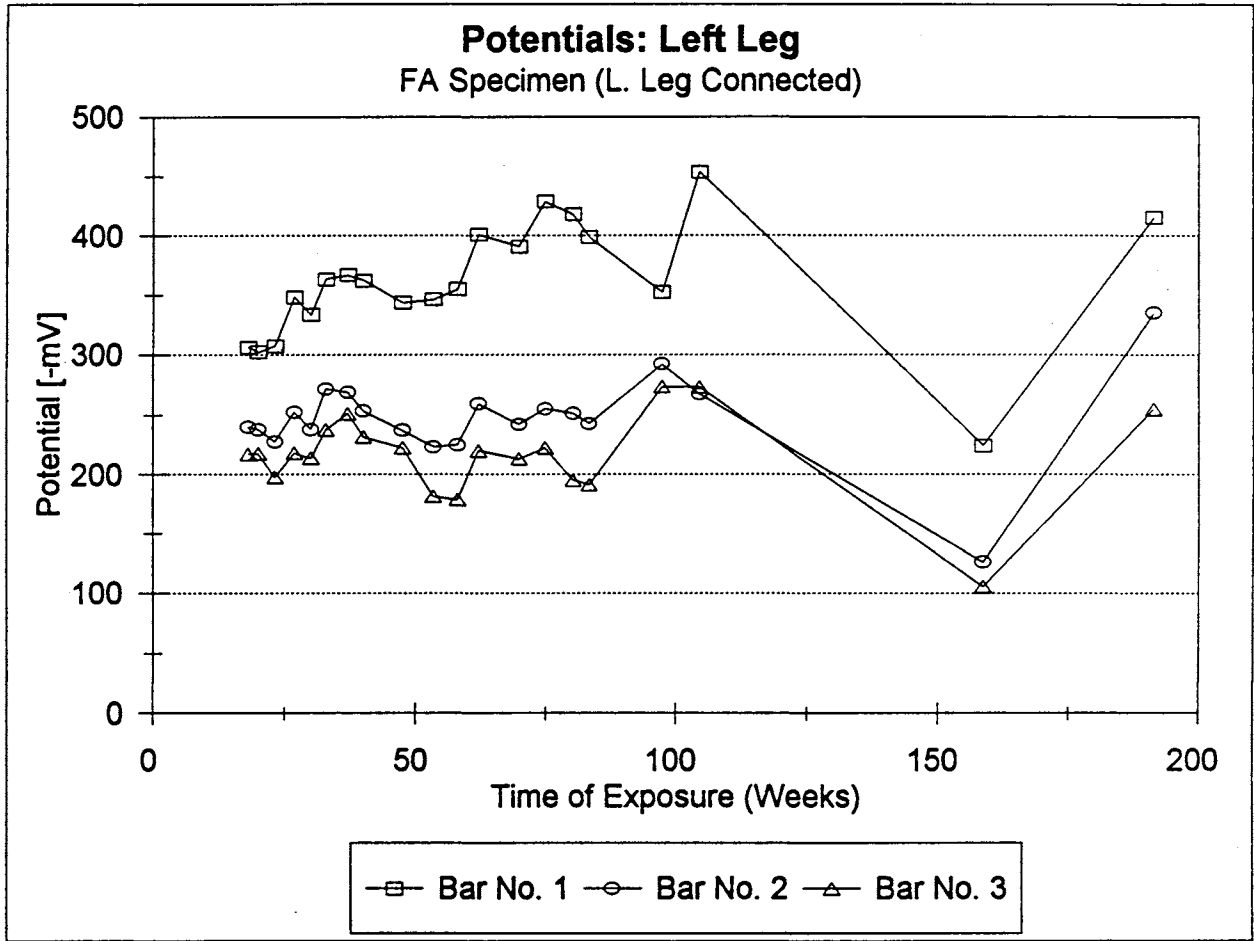


FIGURE 13. Corrosion Potentials in the Vertical Zone, Left Leg, FA Specimen.

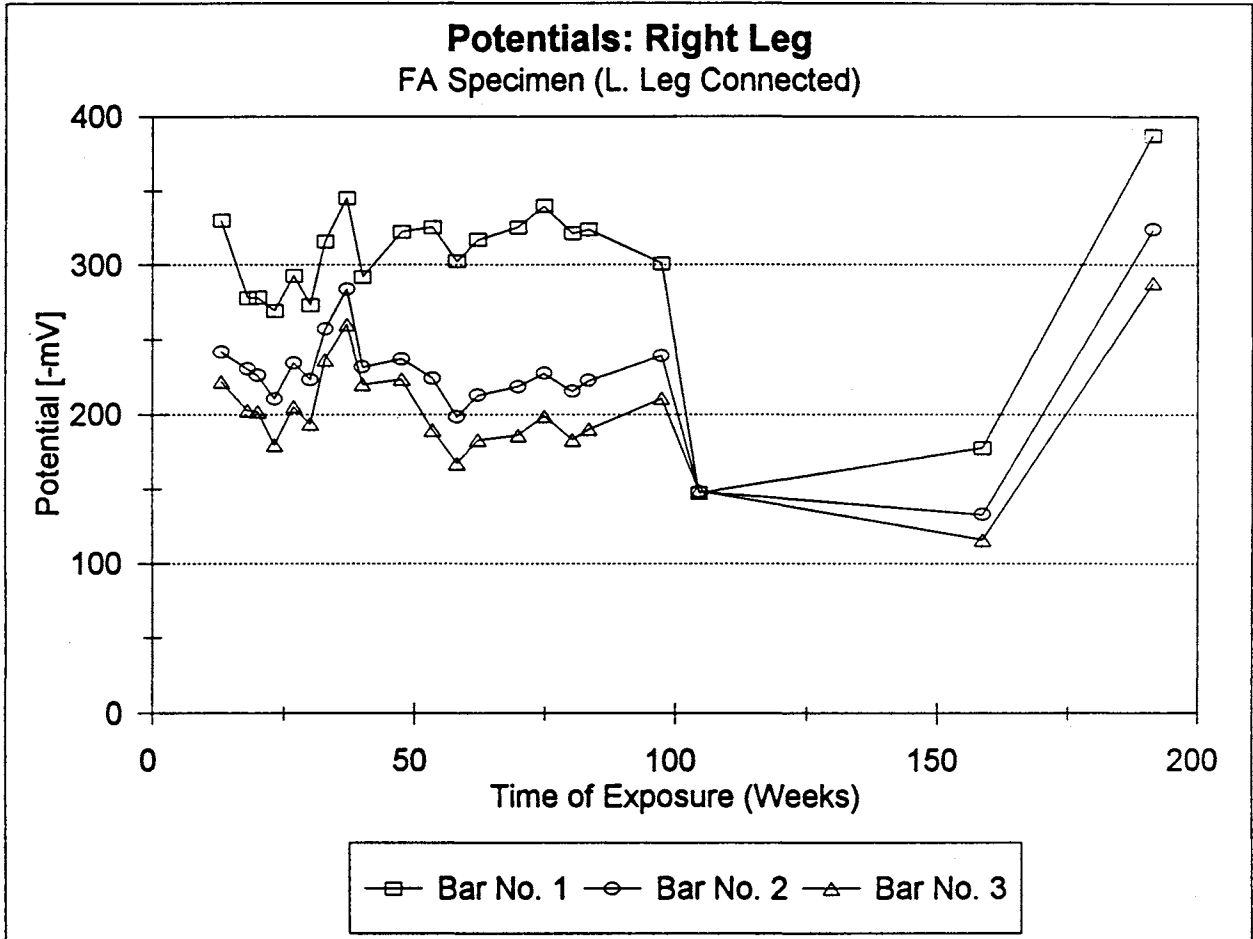


FIGURE 14. Corrosion Potentials in the Vertical Zone, Right Leg, FA Specimen.

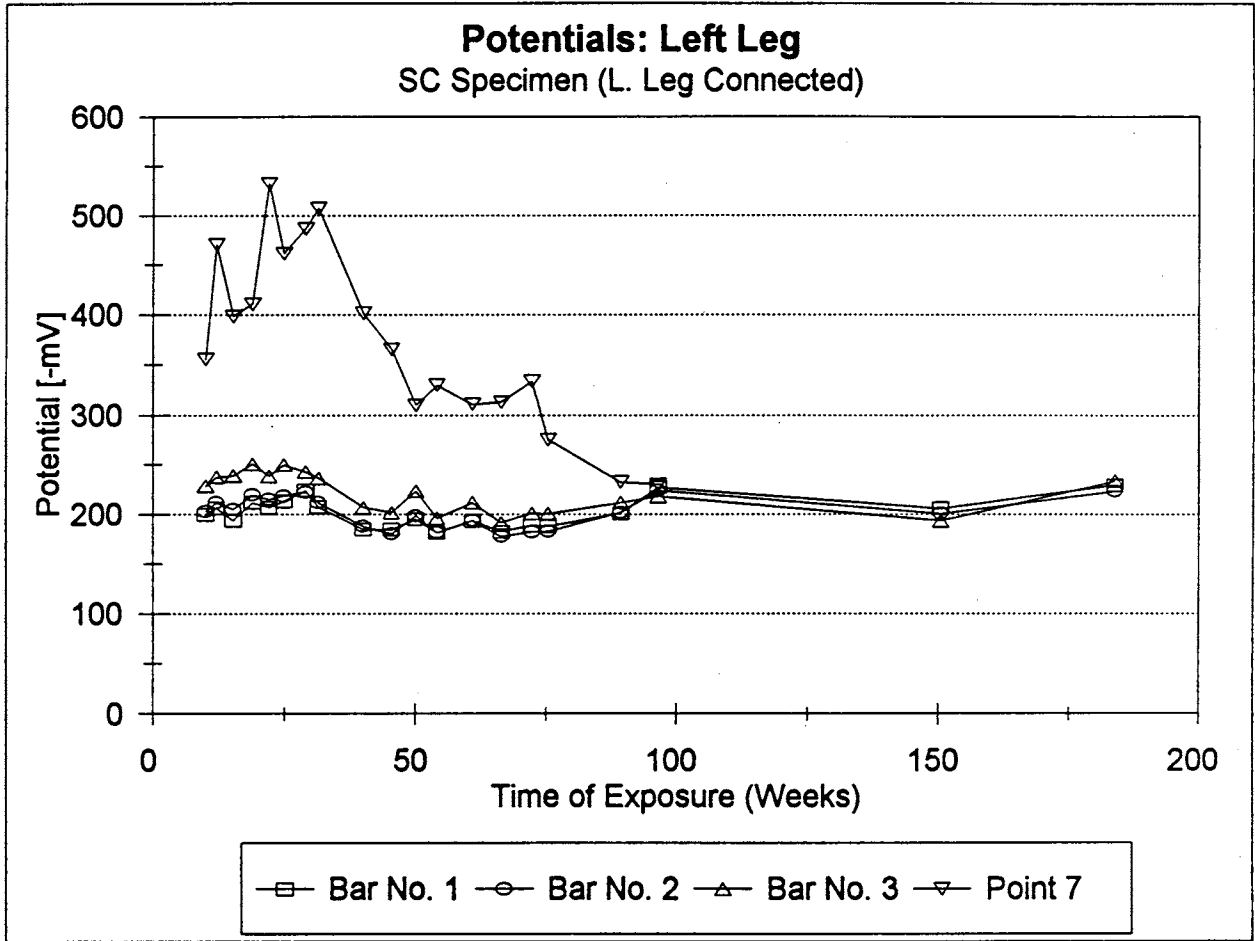


FIGURE 15. Corrosion Potentials in the Vertical Zone, Left Leg, SC Specimen.

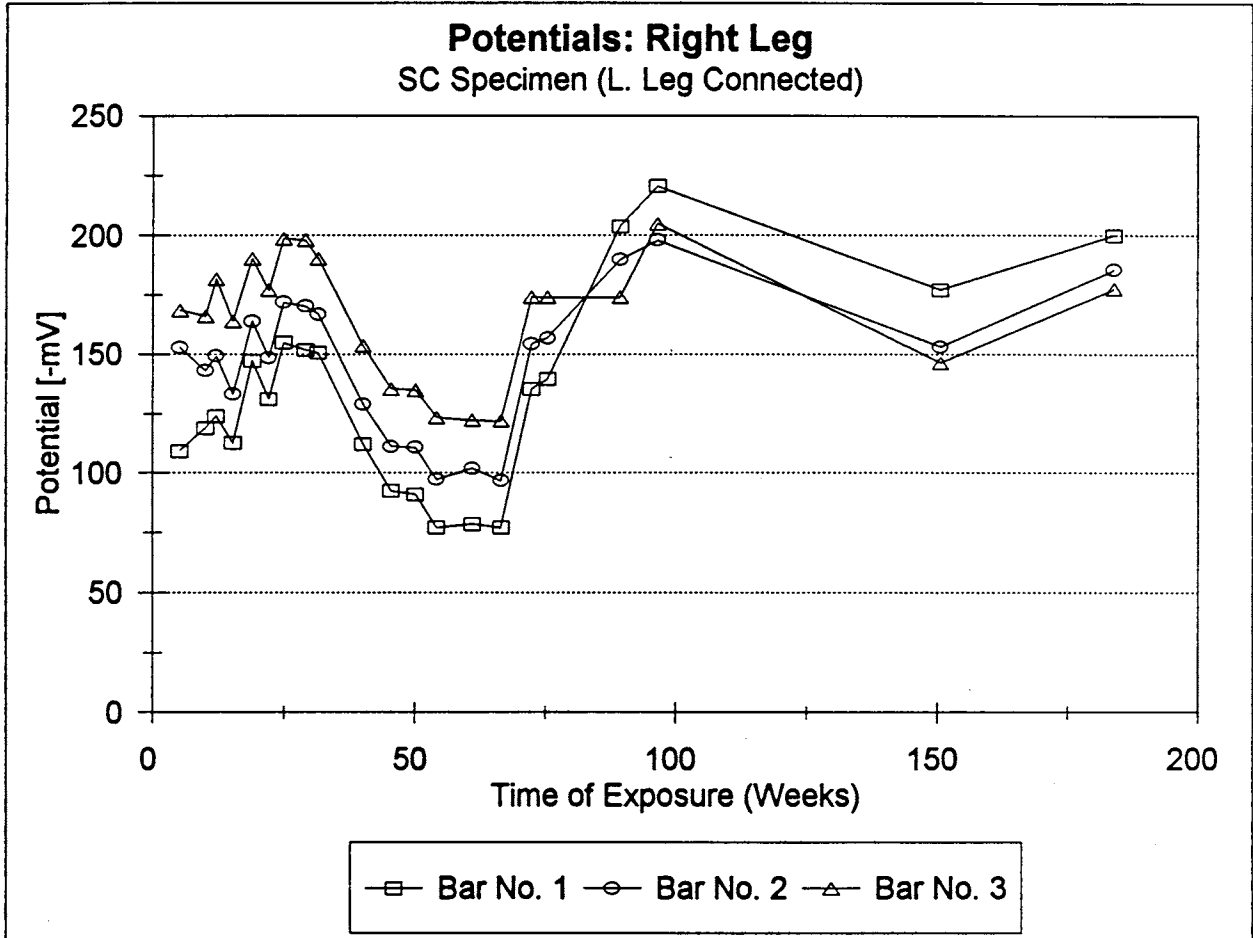


FIGURE 16. Corrosion Potentials in the Vertical Zone, Right Leg, SC Specimen.

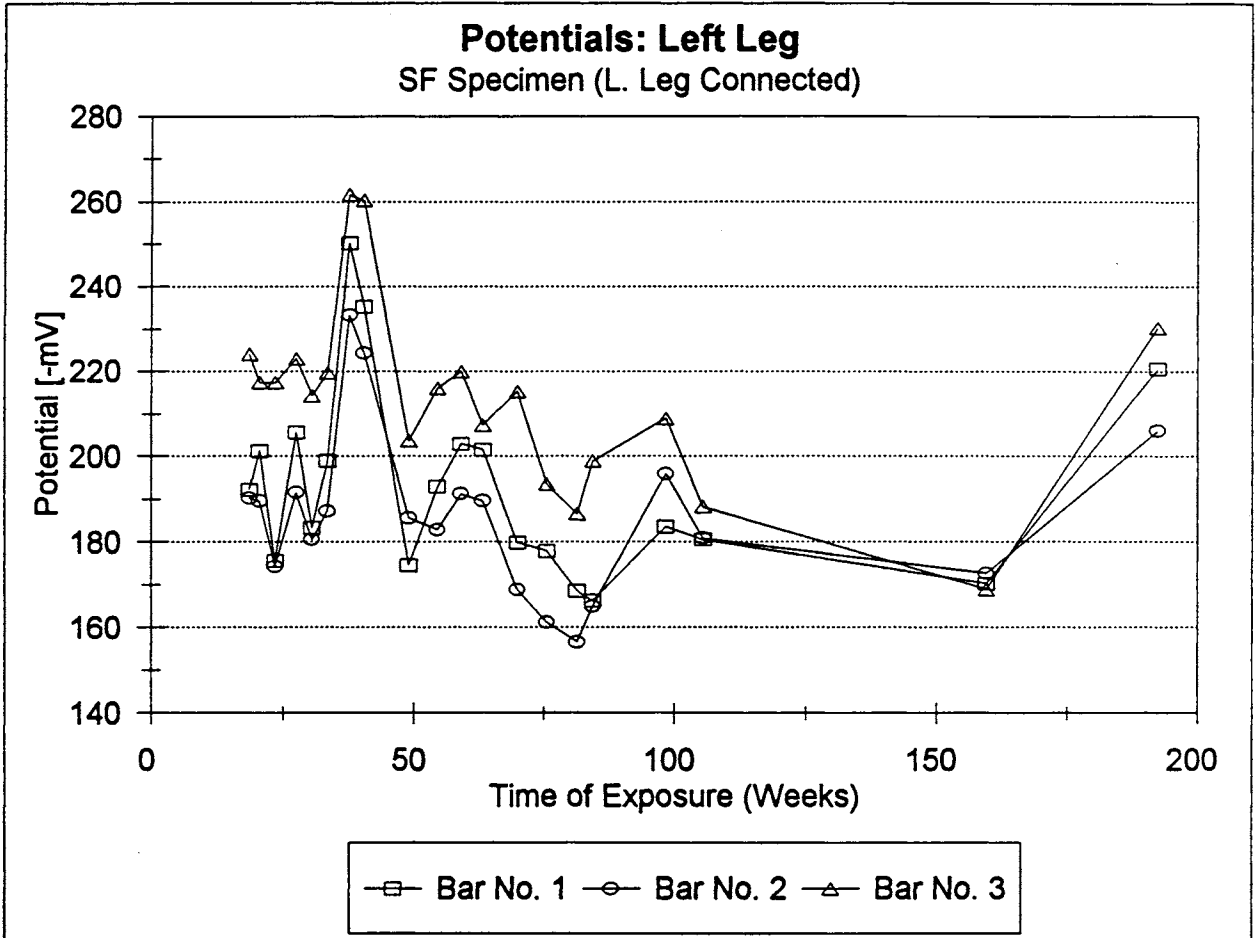


FIGURE 17. Corrosion Potentials in the Vertical Zone, Left Leg, SF Specimen.

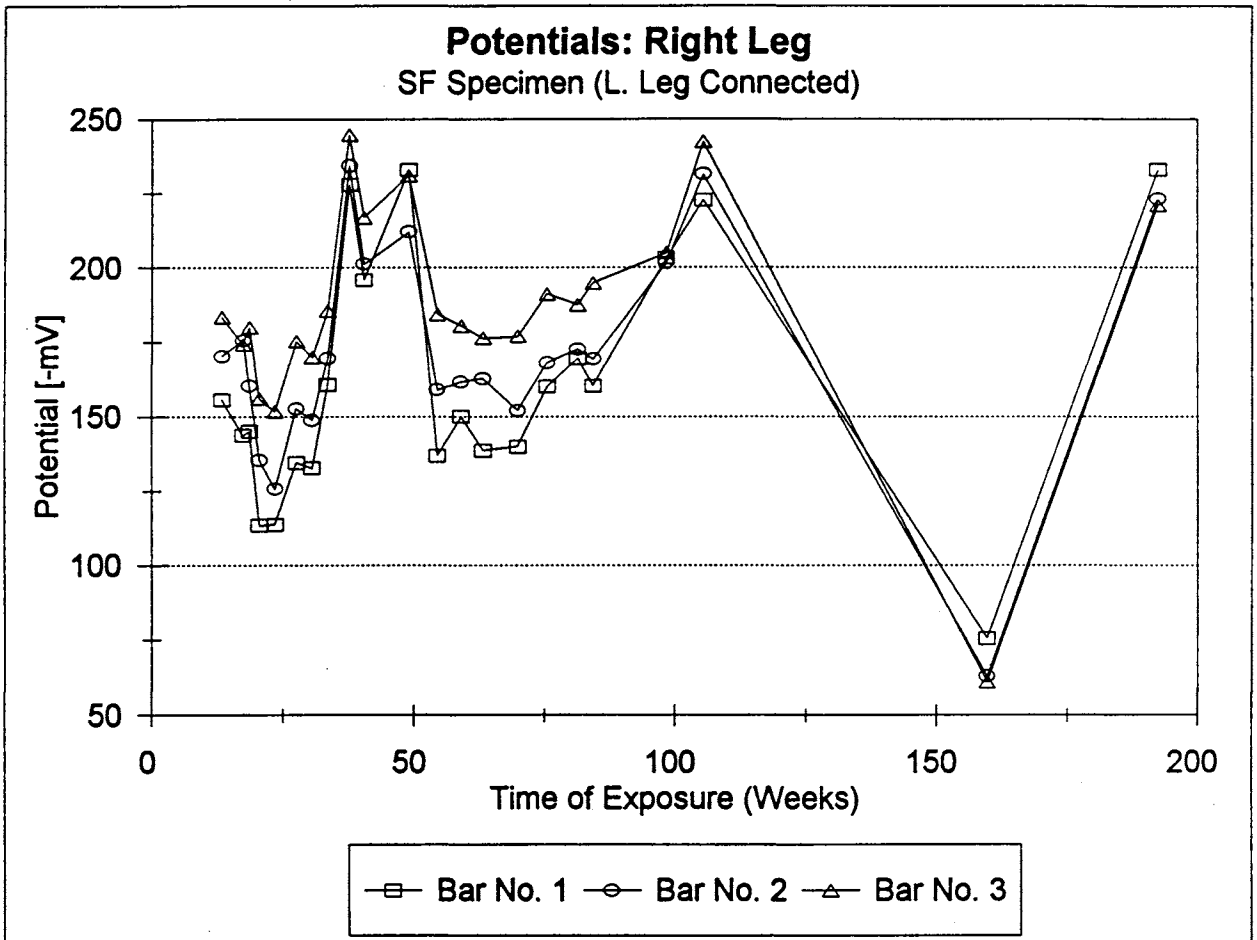


FIGURE 18. Corrosion Potentials in the Vertical Zone, Right Leg, SF Specimen.

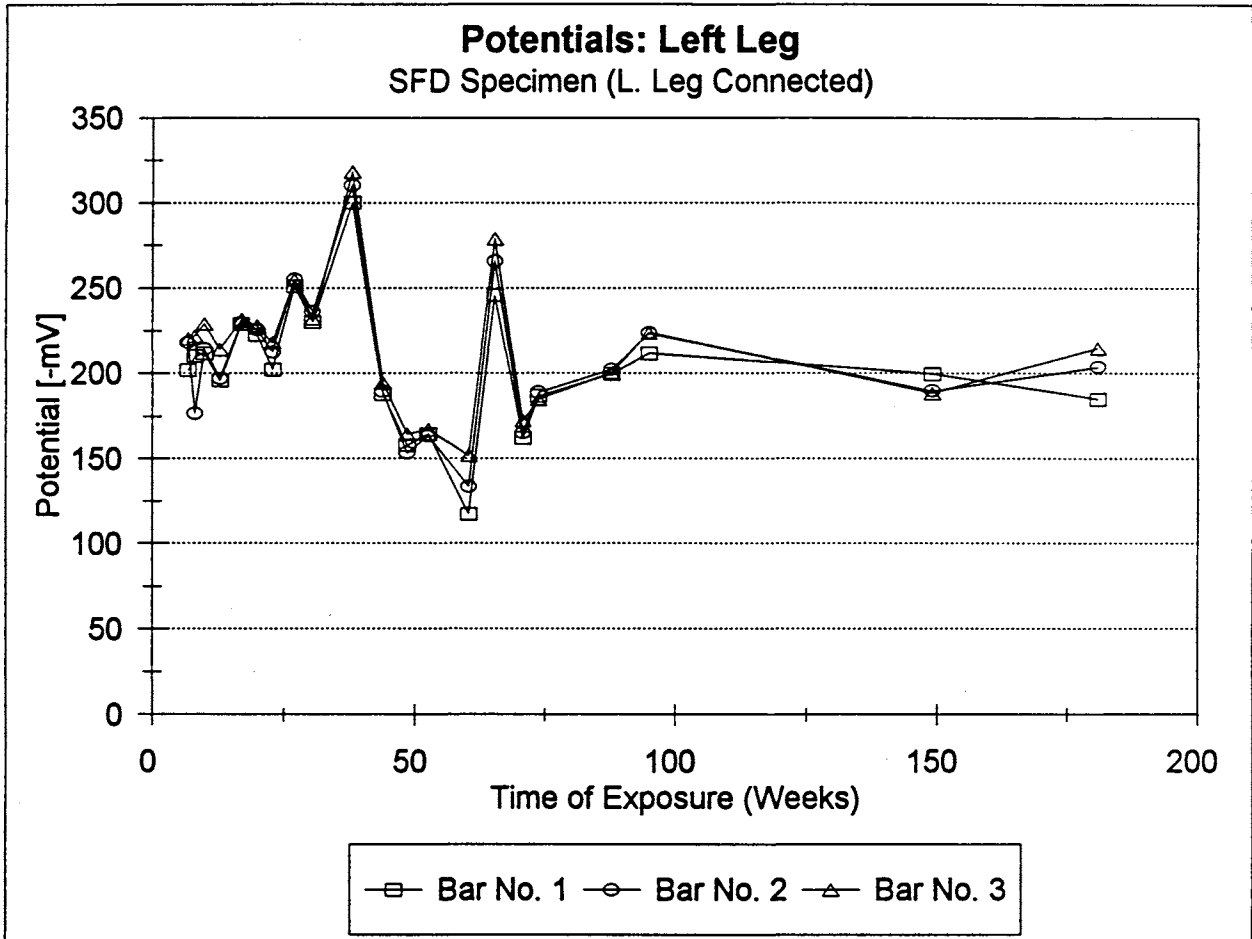


FIGURE 19. Corrosion Potentials in the Vertical Zone, Left Leg, SFD Specimen.

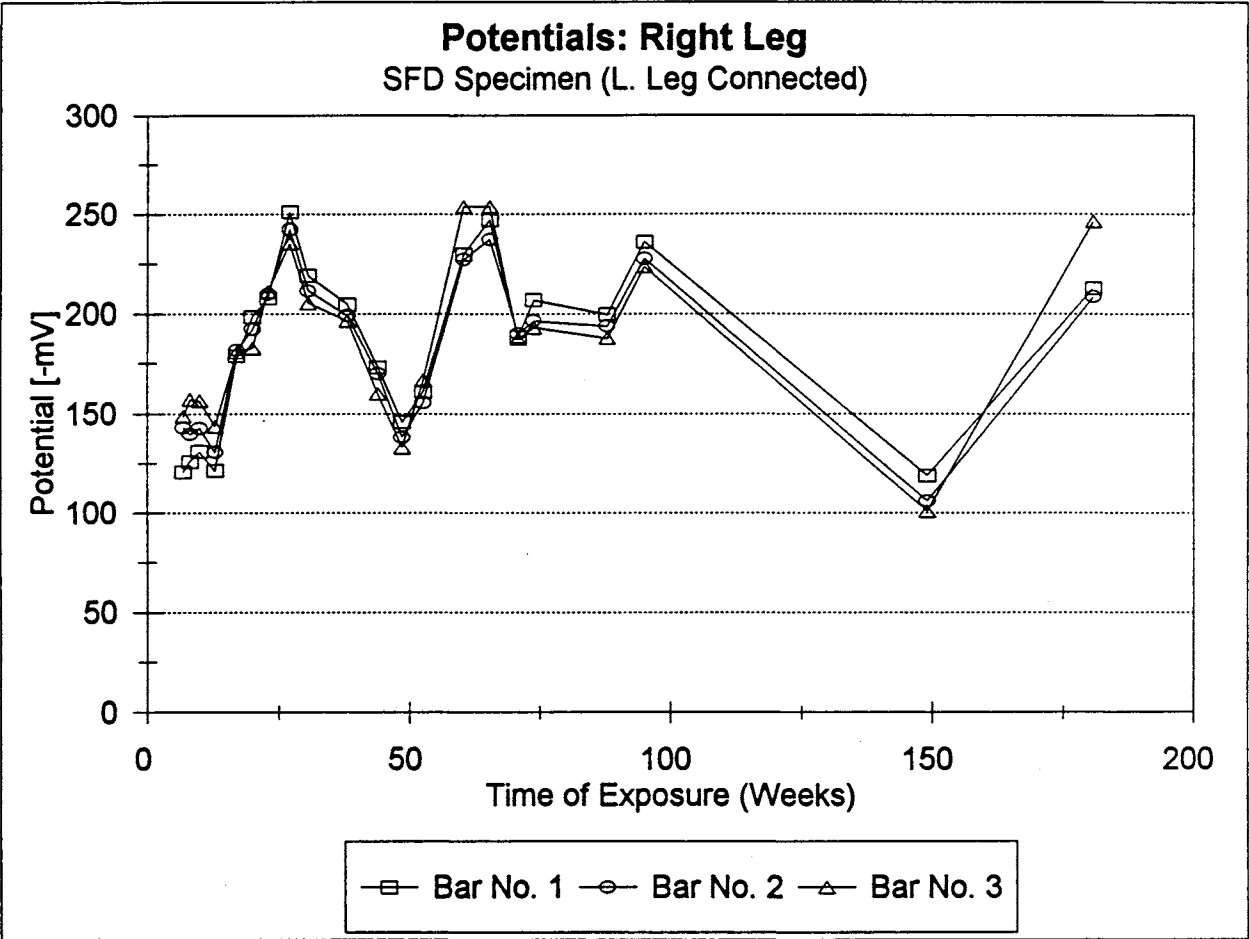


FIGURE 20. Corrosion Potentials in the Vertical Zone, Right Leg, SFD Specimen.

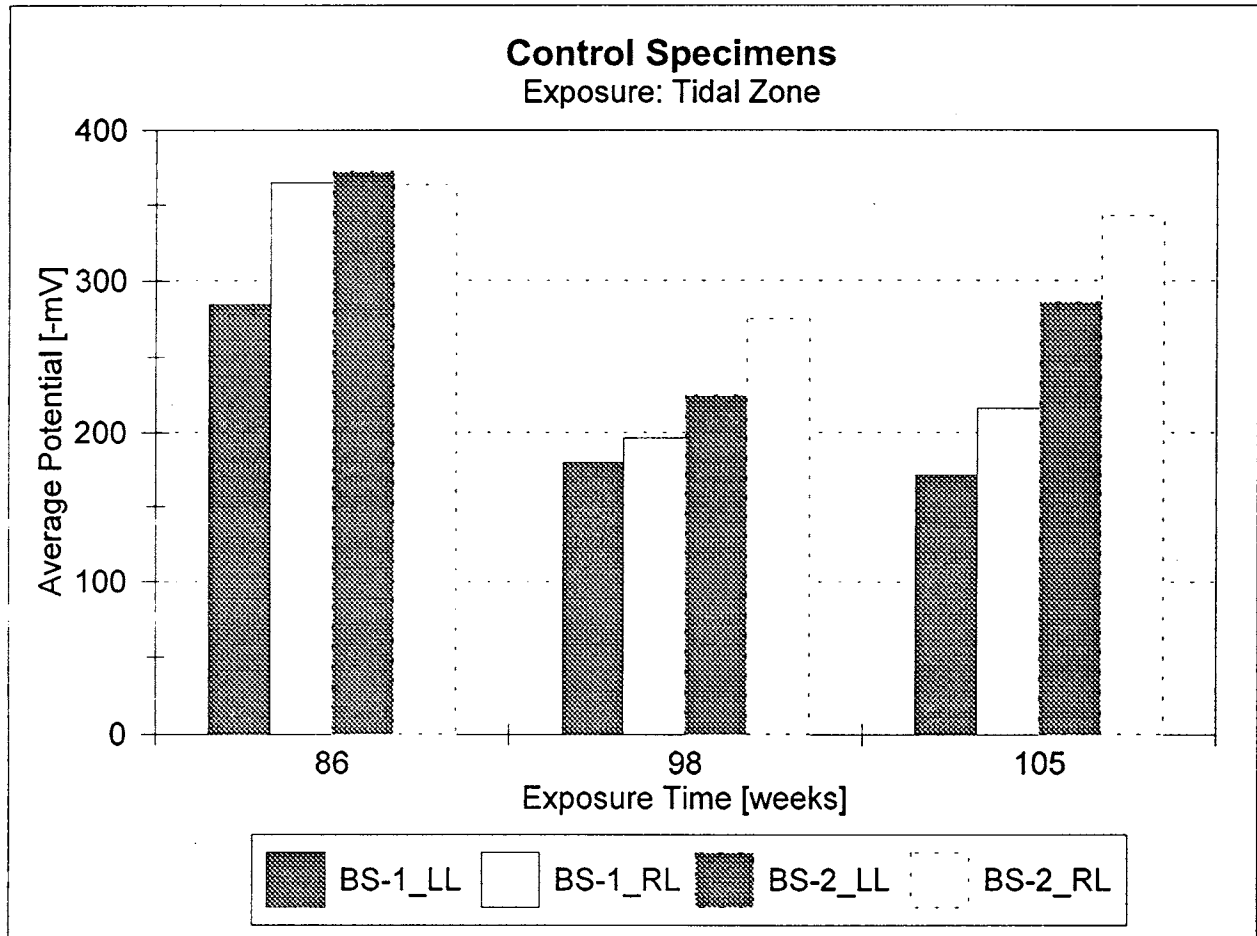


FIGURE 21. Corrosion Potentials in the Tidal Zone, Left and Right Legs, BS-1 and BS-2 Specimens.

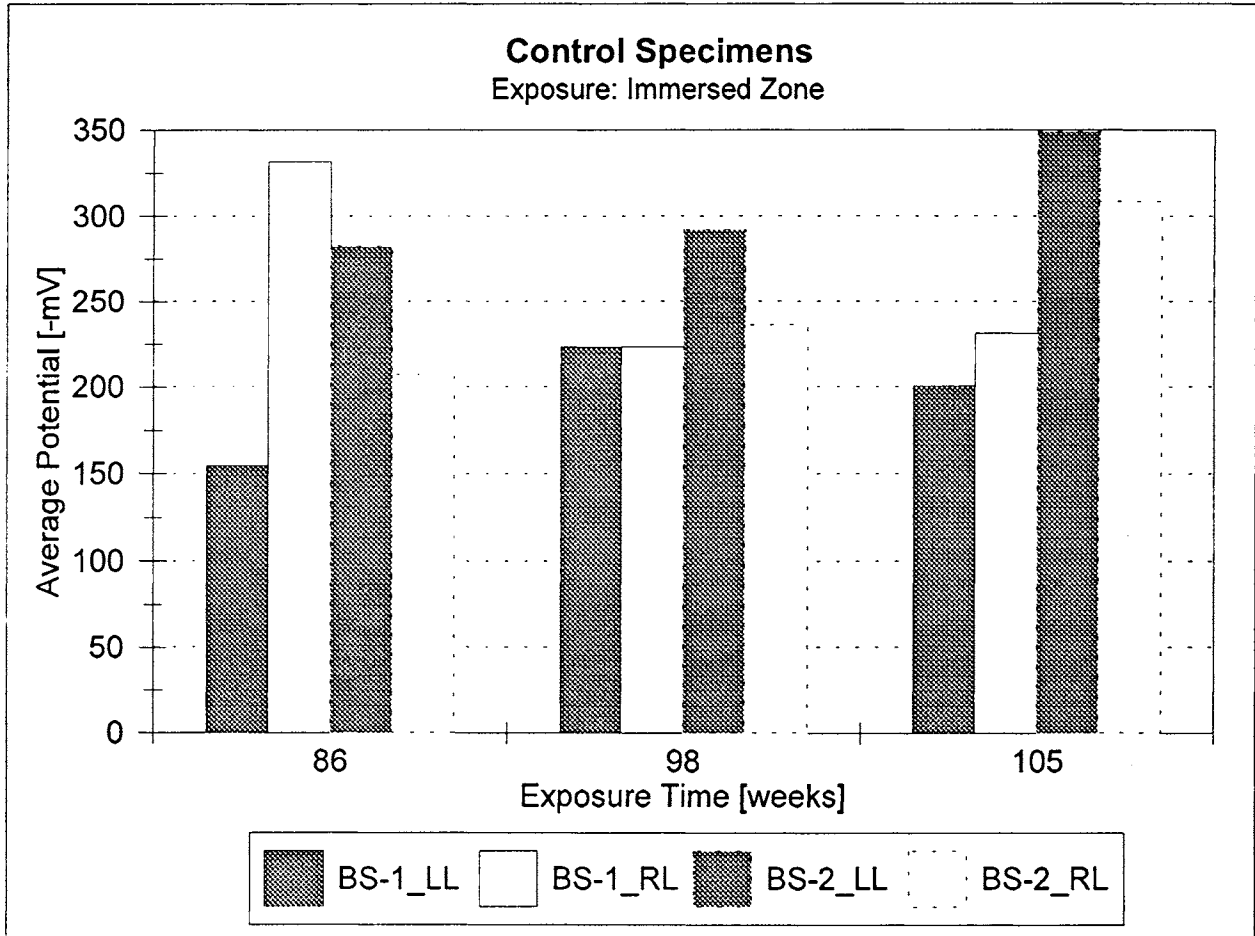


FIGURE 22. Corrosion Potentials in the Immersed Zone, Left and Right Legs, BS-1 and BS-2 Specimens.

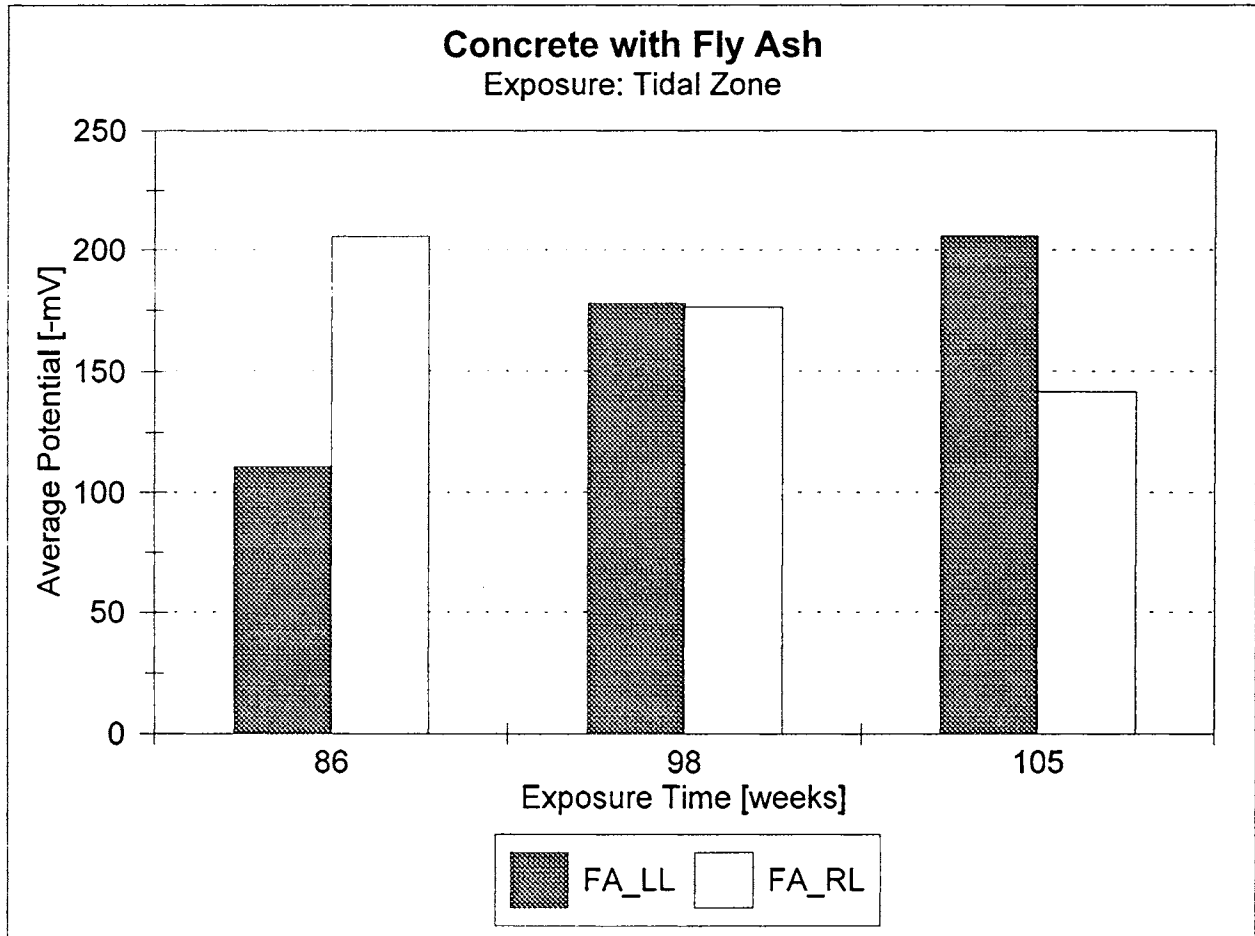


FIGURE 23. Corrosion Potentials in the Tidal Zone, Left and Right Legs, FA Specimen.

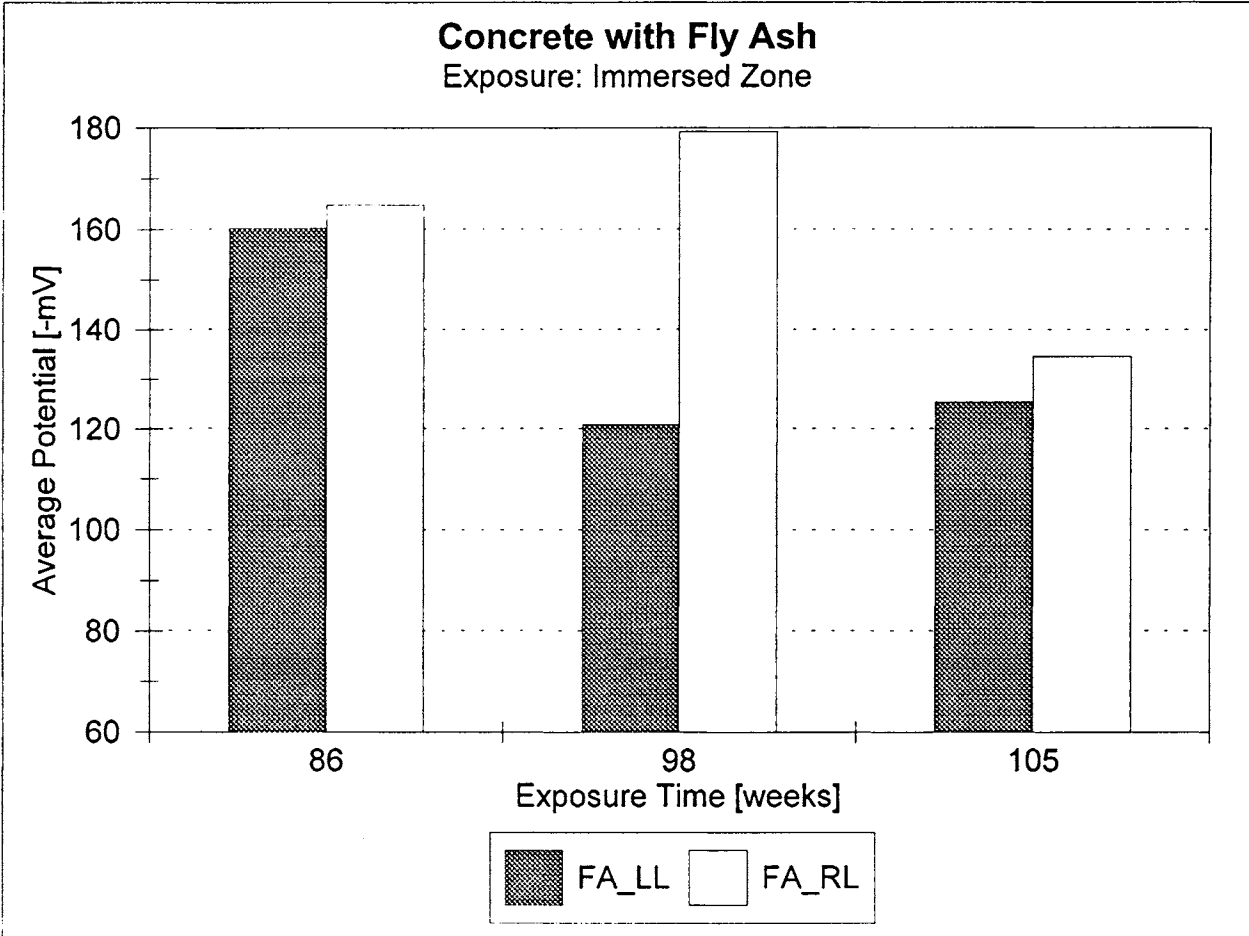


FIGURE 24. Corrosion Potentials in the Immersed Zone, Left and Right Legs, FA Specimen.

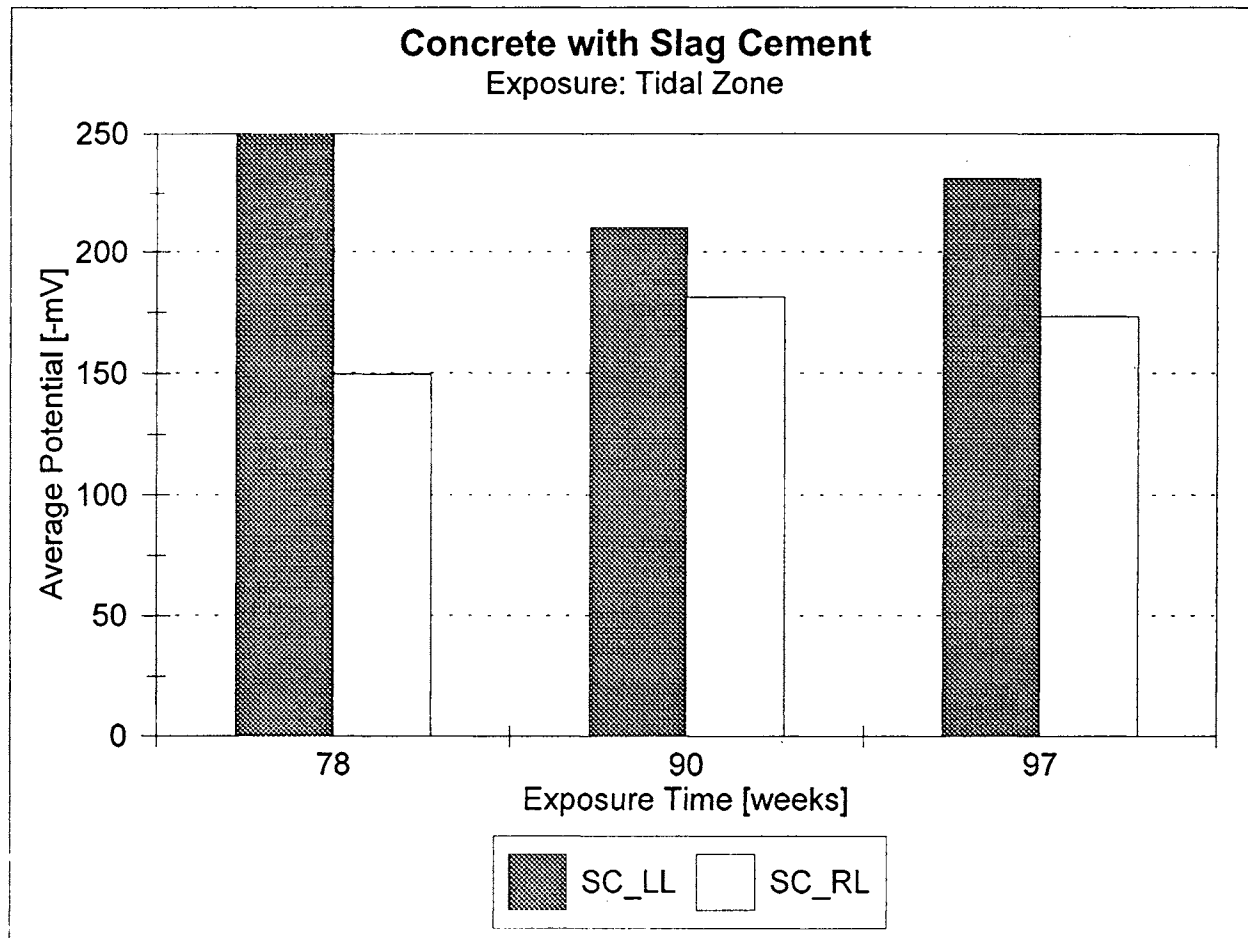


FIGURE 25. Corrosion Potentials in the Tidal Zone, Left and Right Legs, SC Specimen.

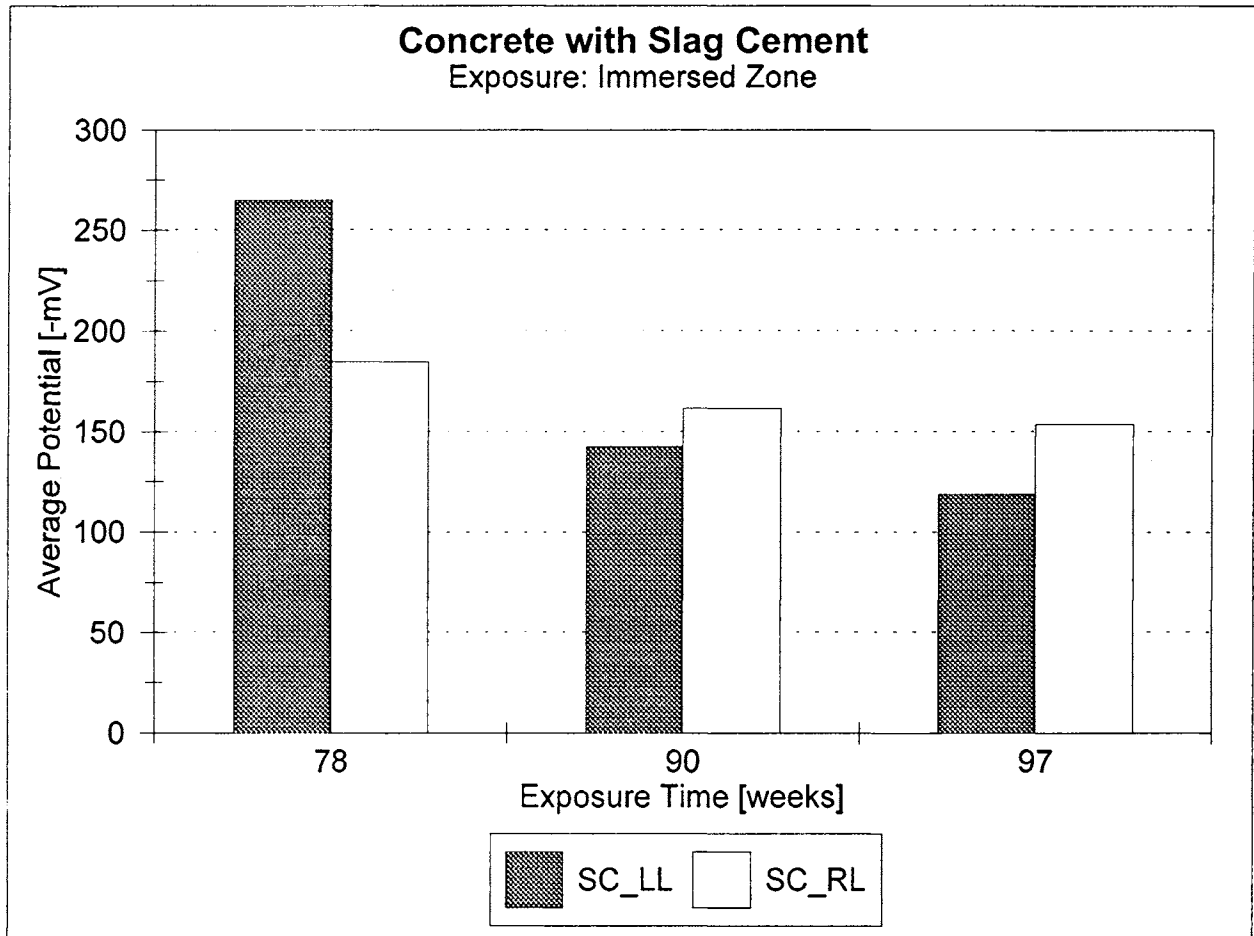


FIGURE 26. Corrosion Potentials in the Immersed Zone, Left and Right Legs, SC Specimen.

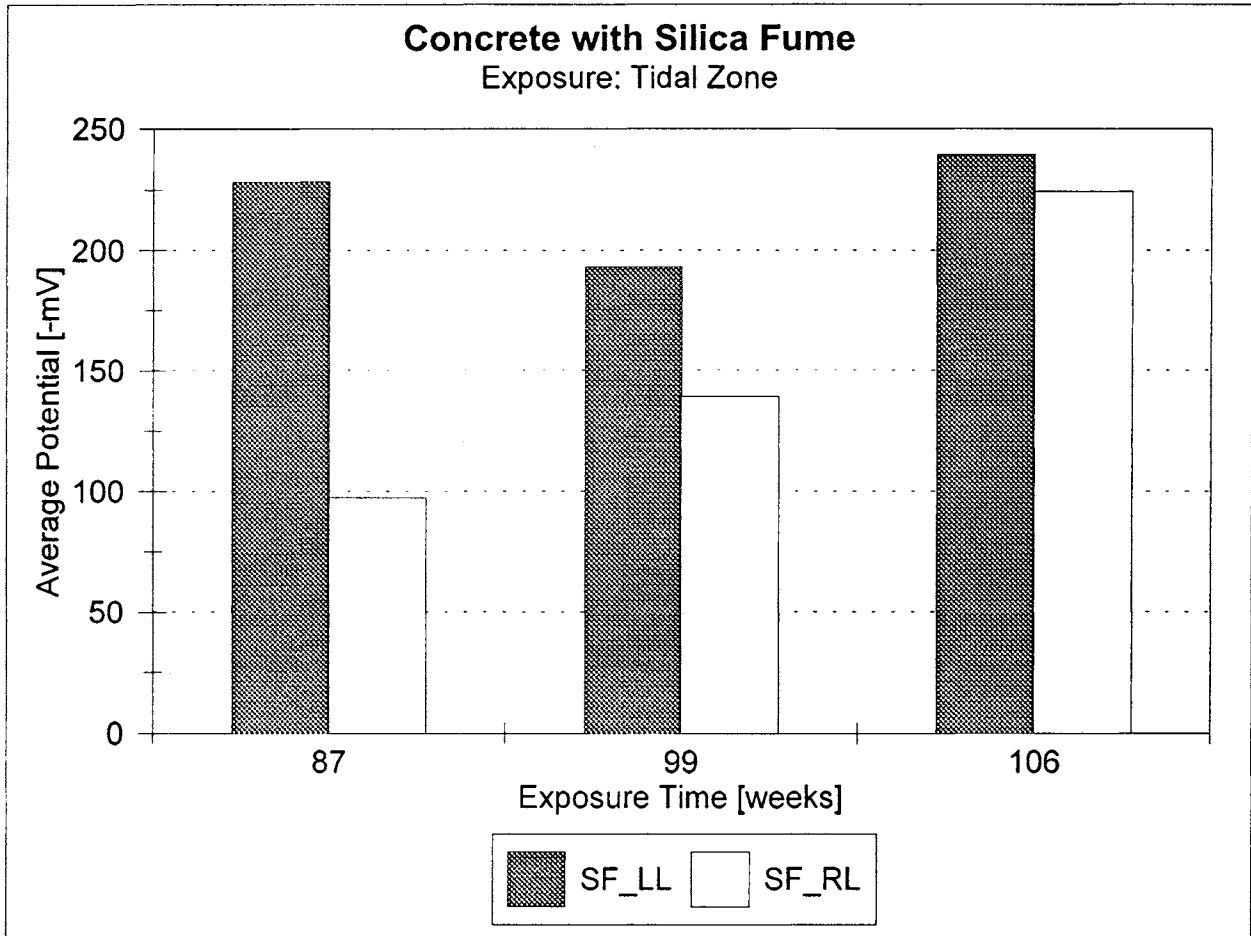


FIGURE 27. Corrosion Potentials in the Tidal Zone, Left and Right Legs, SF Specimen.

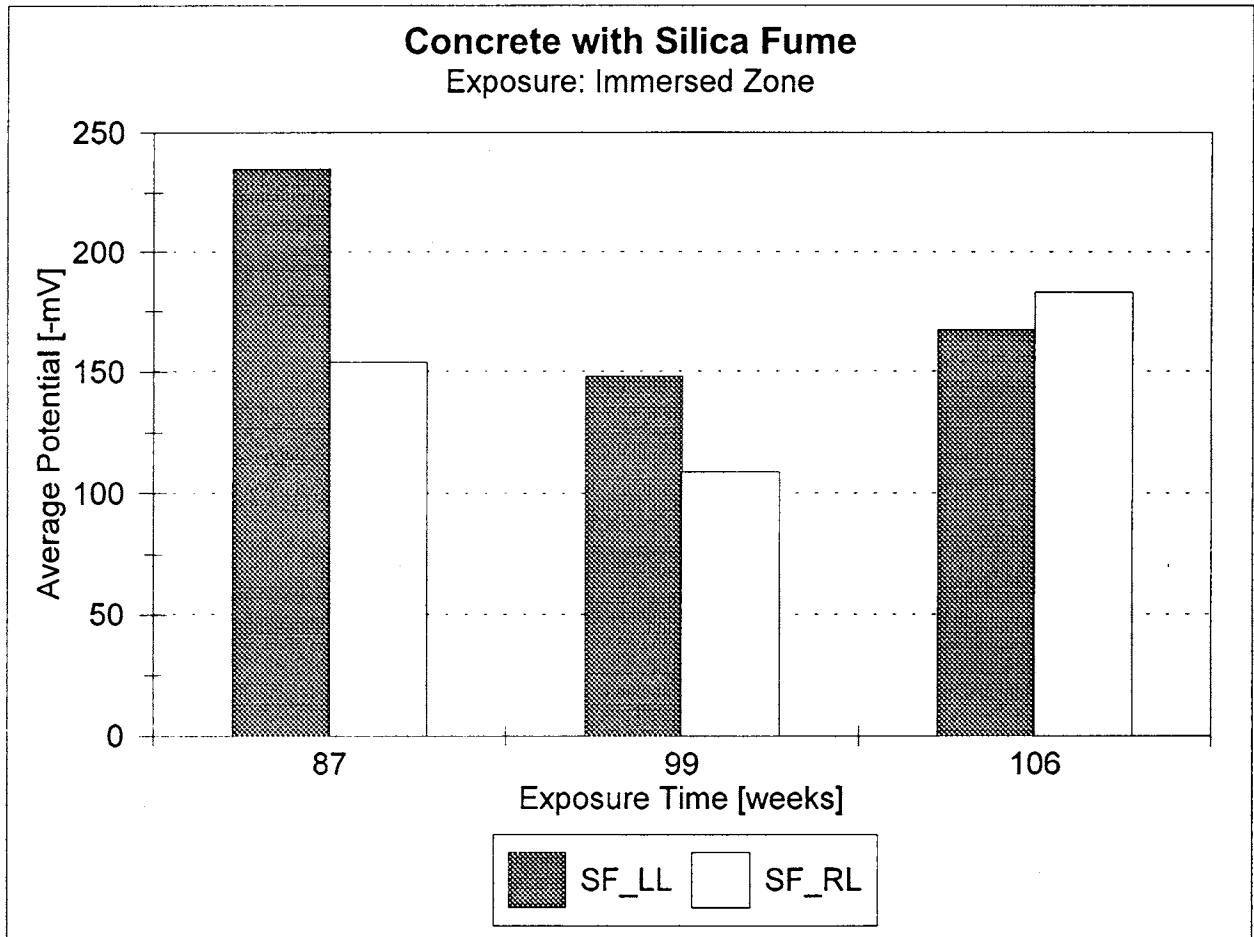


FIGURE 28. Corrosion Potentials in the Immersed Zone, Left and Right Legs, SF Specimen.

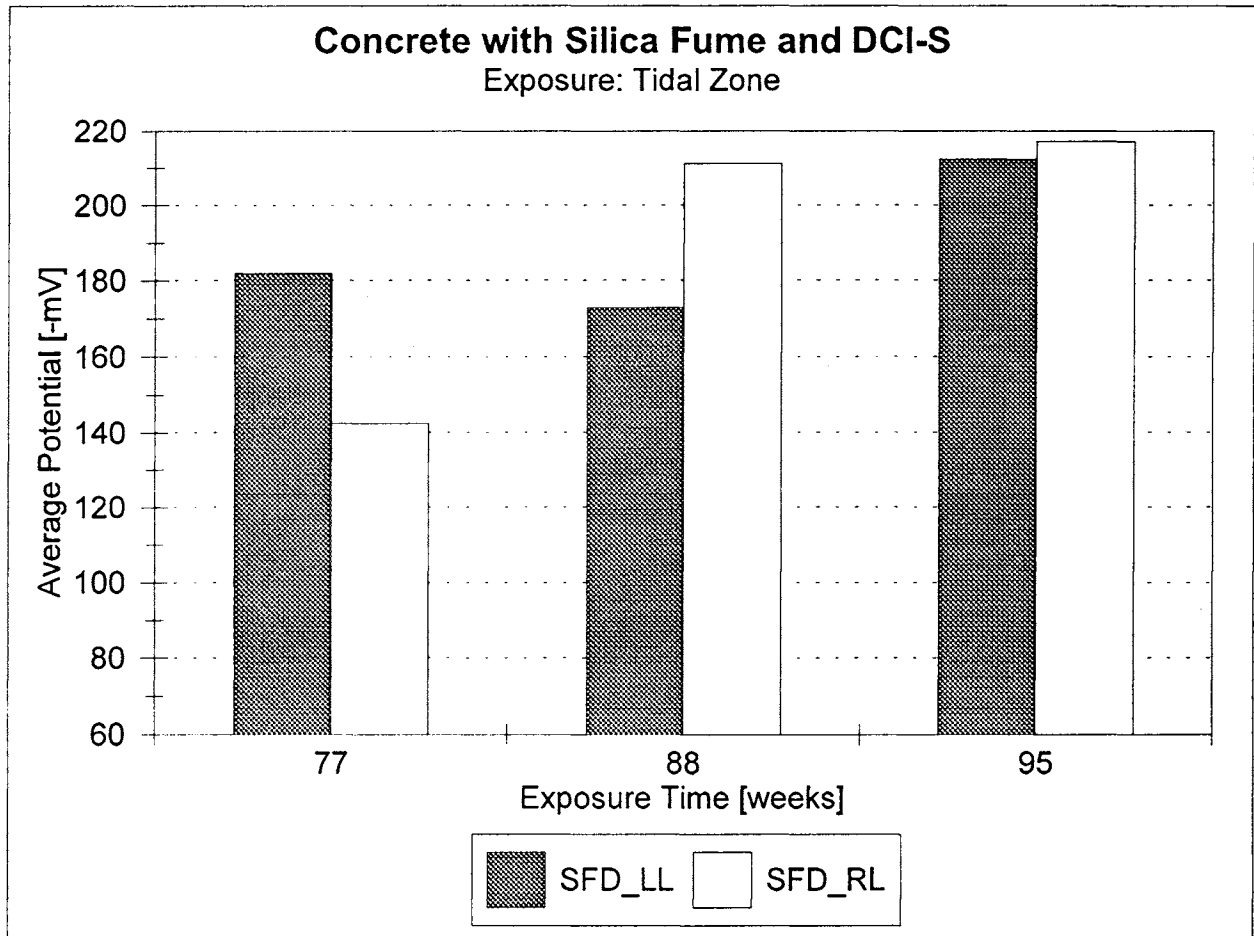


FIGURE 29. Corrosion Potentials in the Tidal Zone, Left and Right Legs, SFD Specimens.

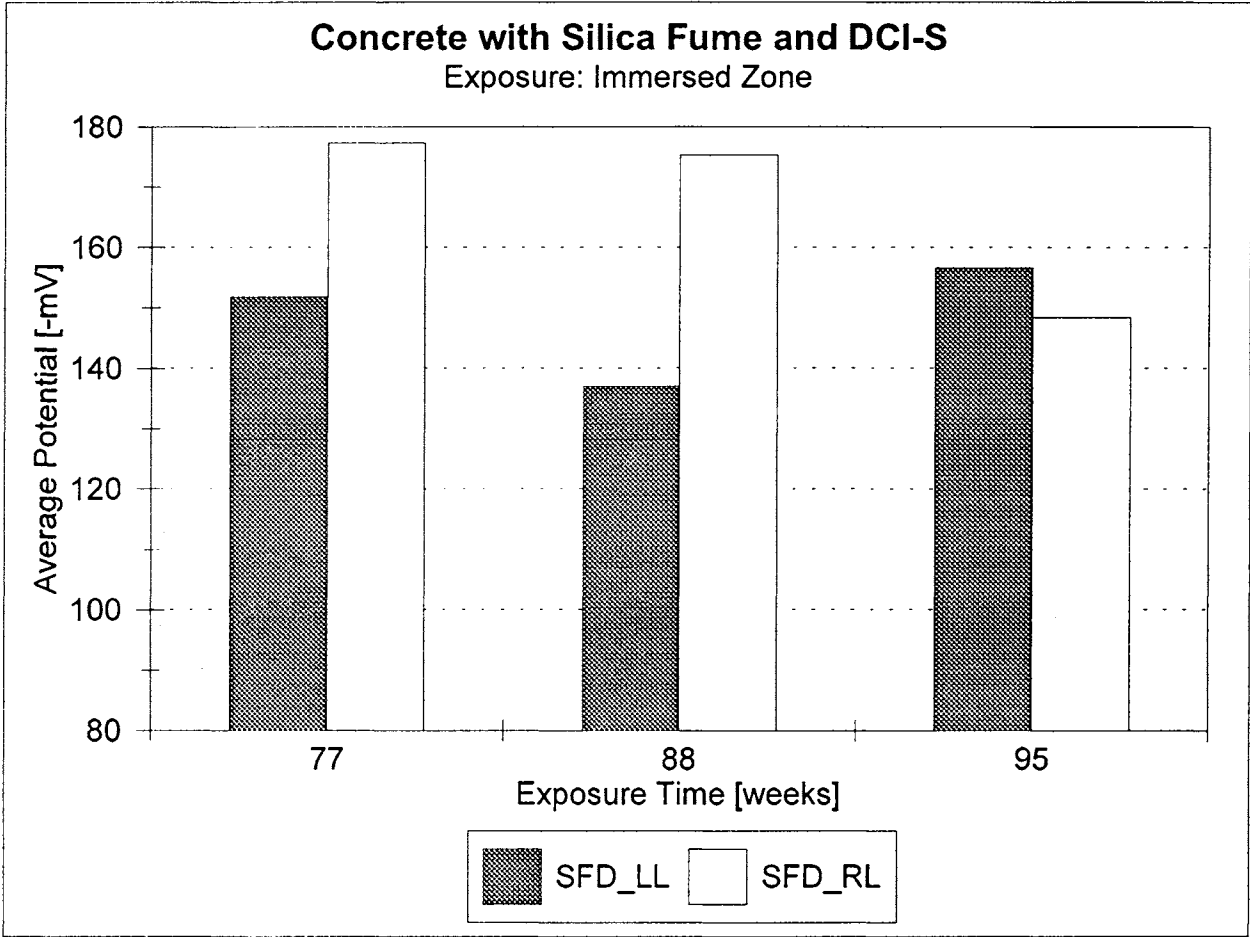


FIGURE 30. Corrosion Potentials in the Immersed Zone, Left and Right Legs, SFD Specimens.

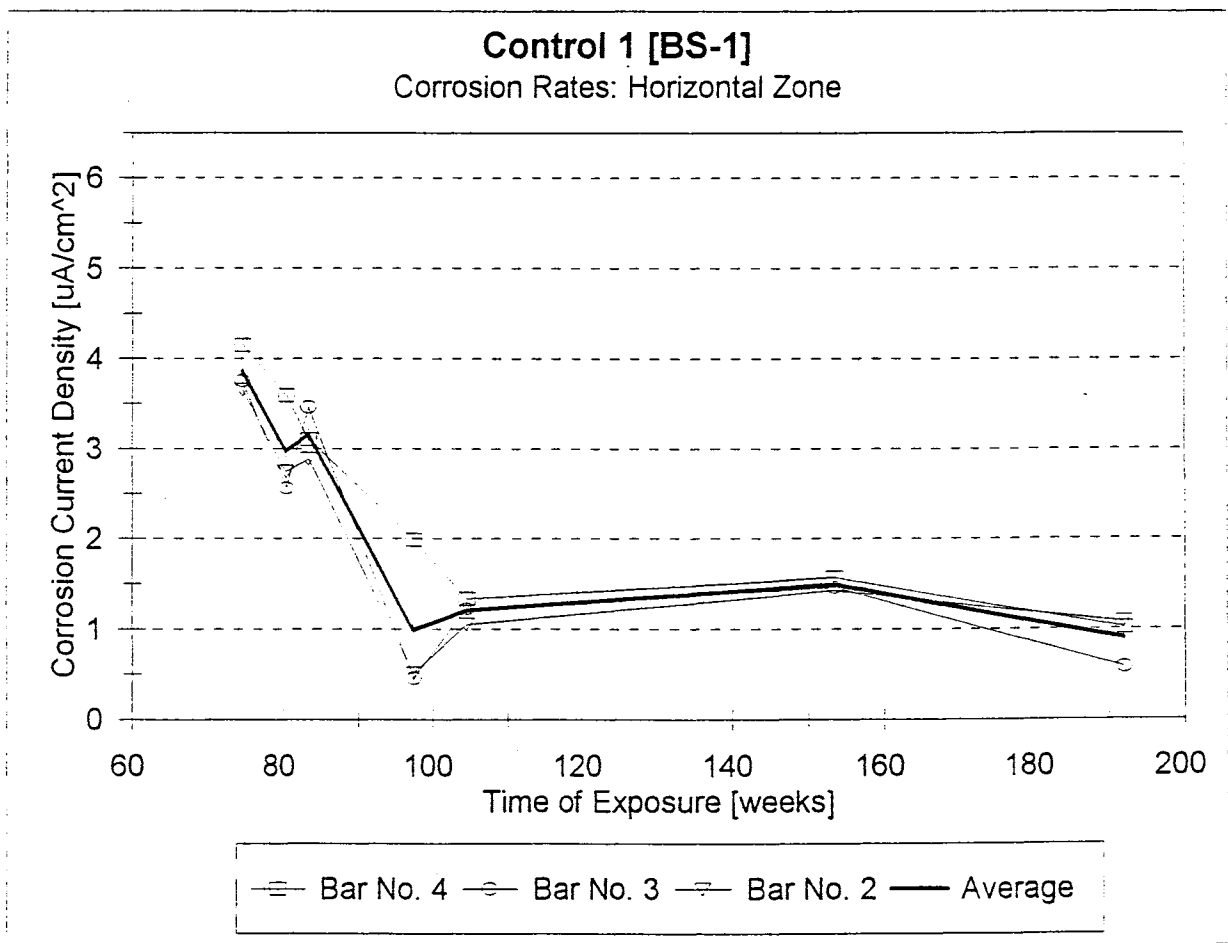


FIGURE 31. Corrosion Rates in the Horizontal Zone, BS-1 Specimen.

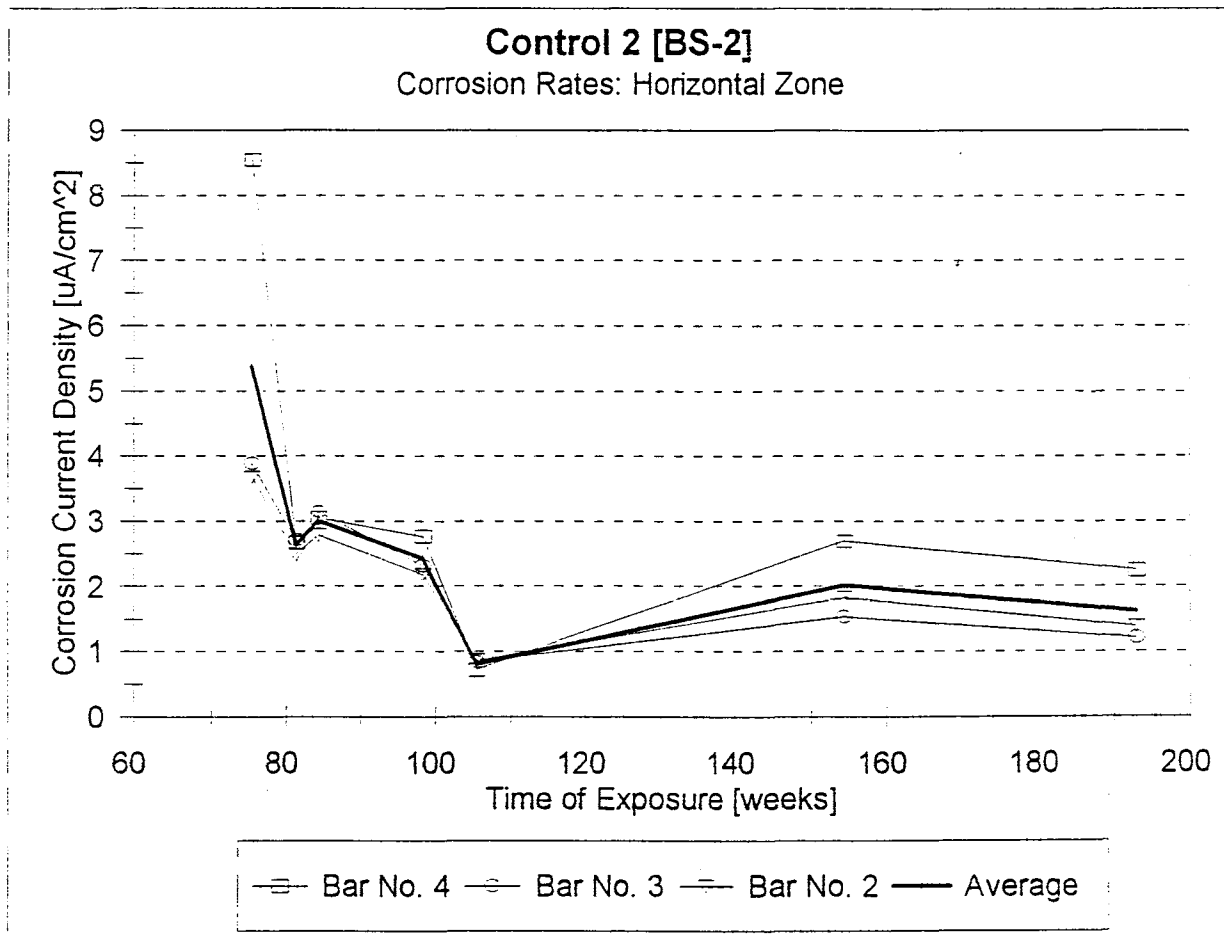


FIGURE 32. Corrosion Rates in the Horizontal Zone, BS-2 Specimen.

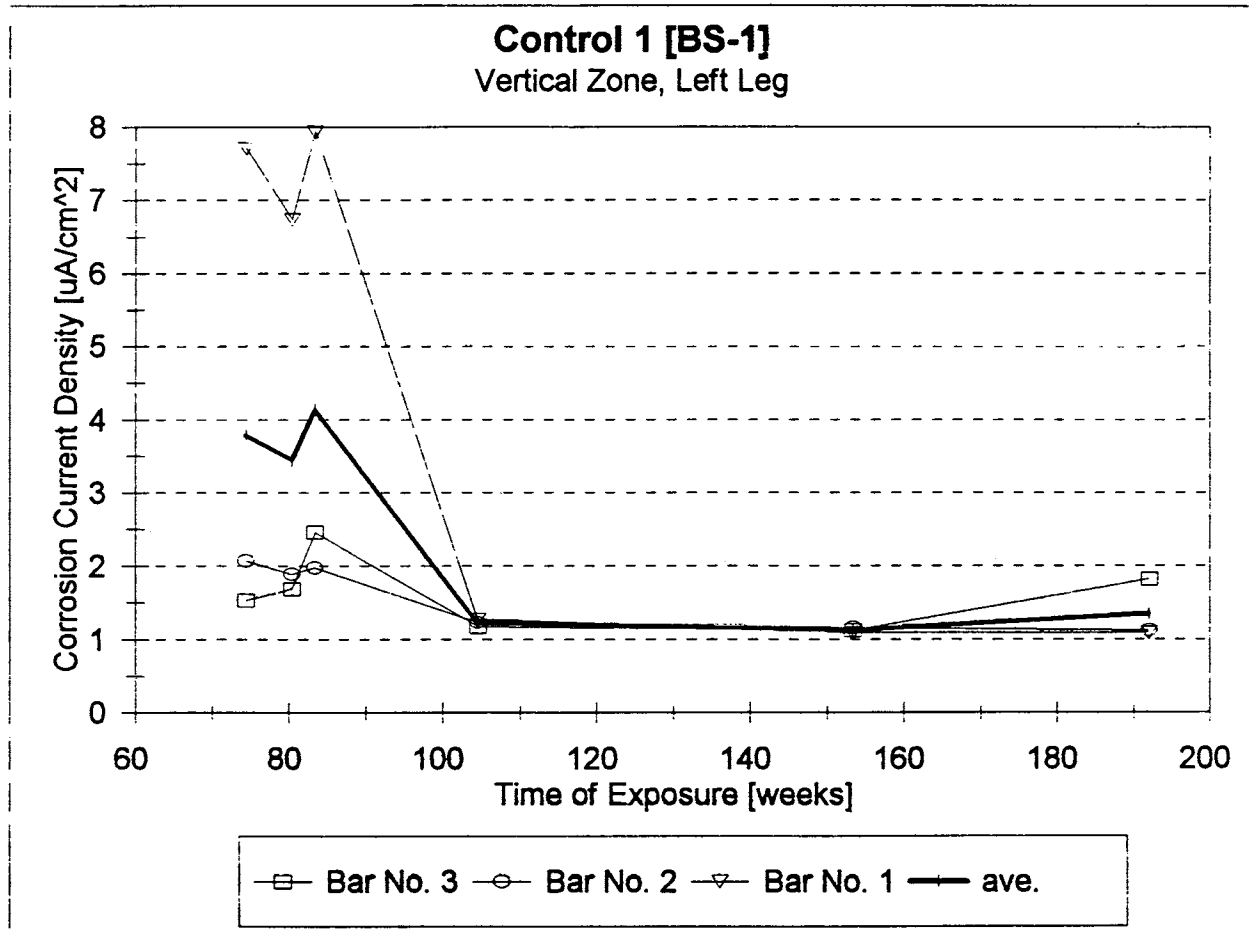


FIGURE 33. Corrosion Rates in the Vertical Zone, Left Leg, BS-1 Specimen.

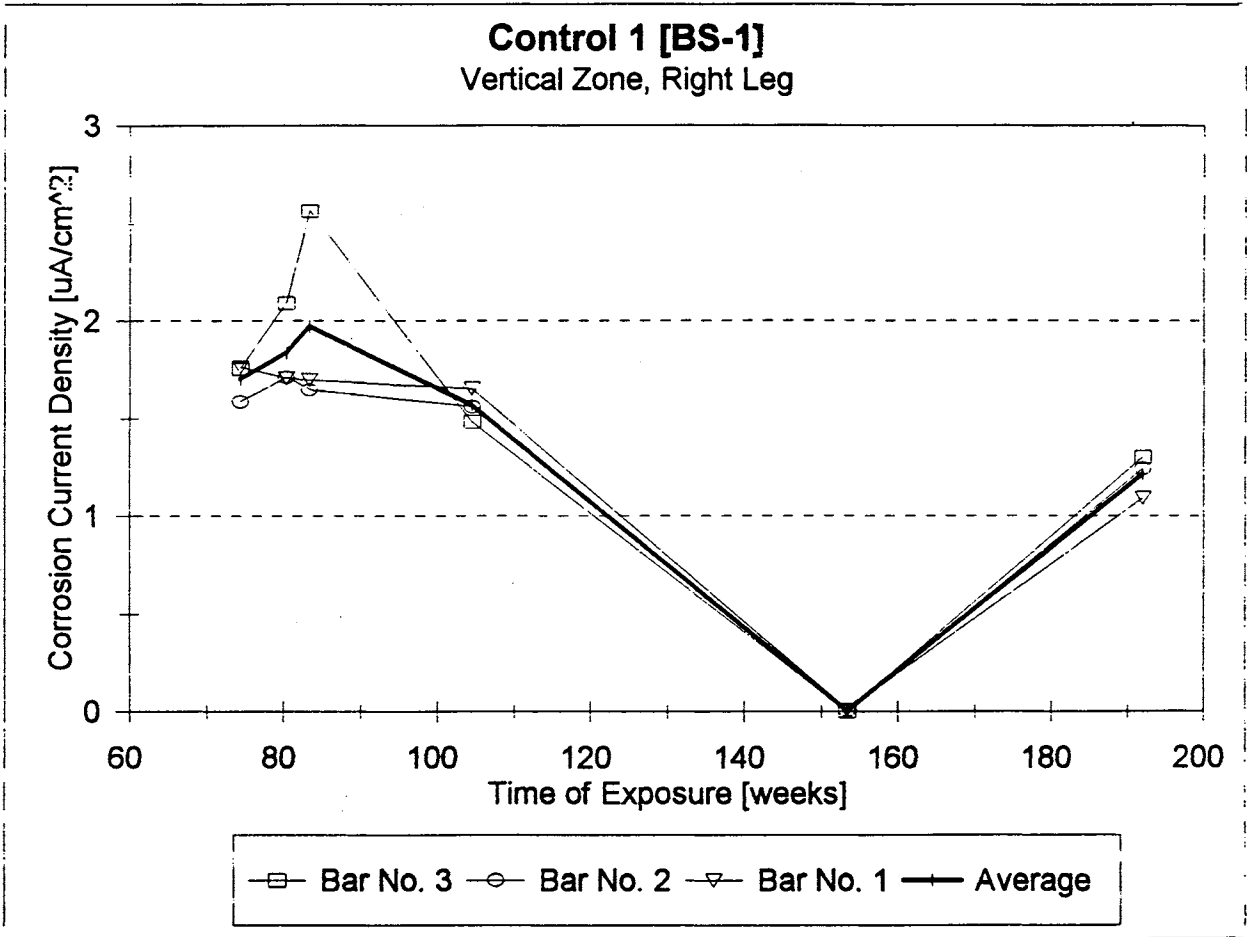


FIGURE 34. Corrosion Rates in the Vertical Zone, Right Leg, BS-1 Specimen.

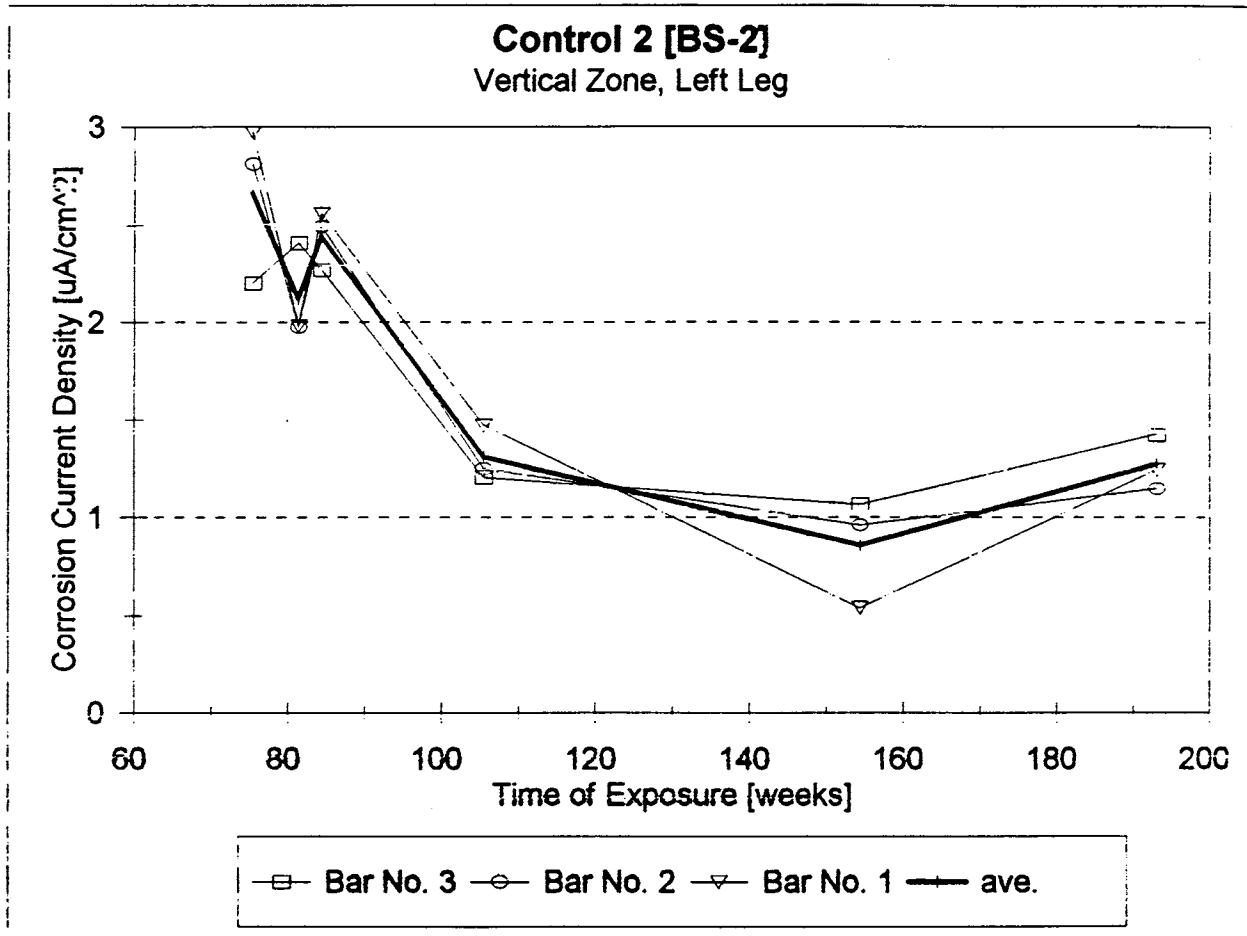


FIGURE 35. Corrosion Rates in the Vertical Zone, Left Leg, BS-2 Specimen.

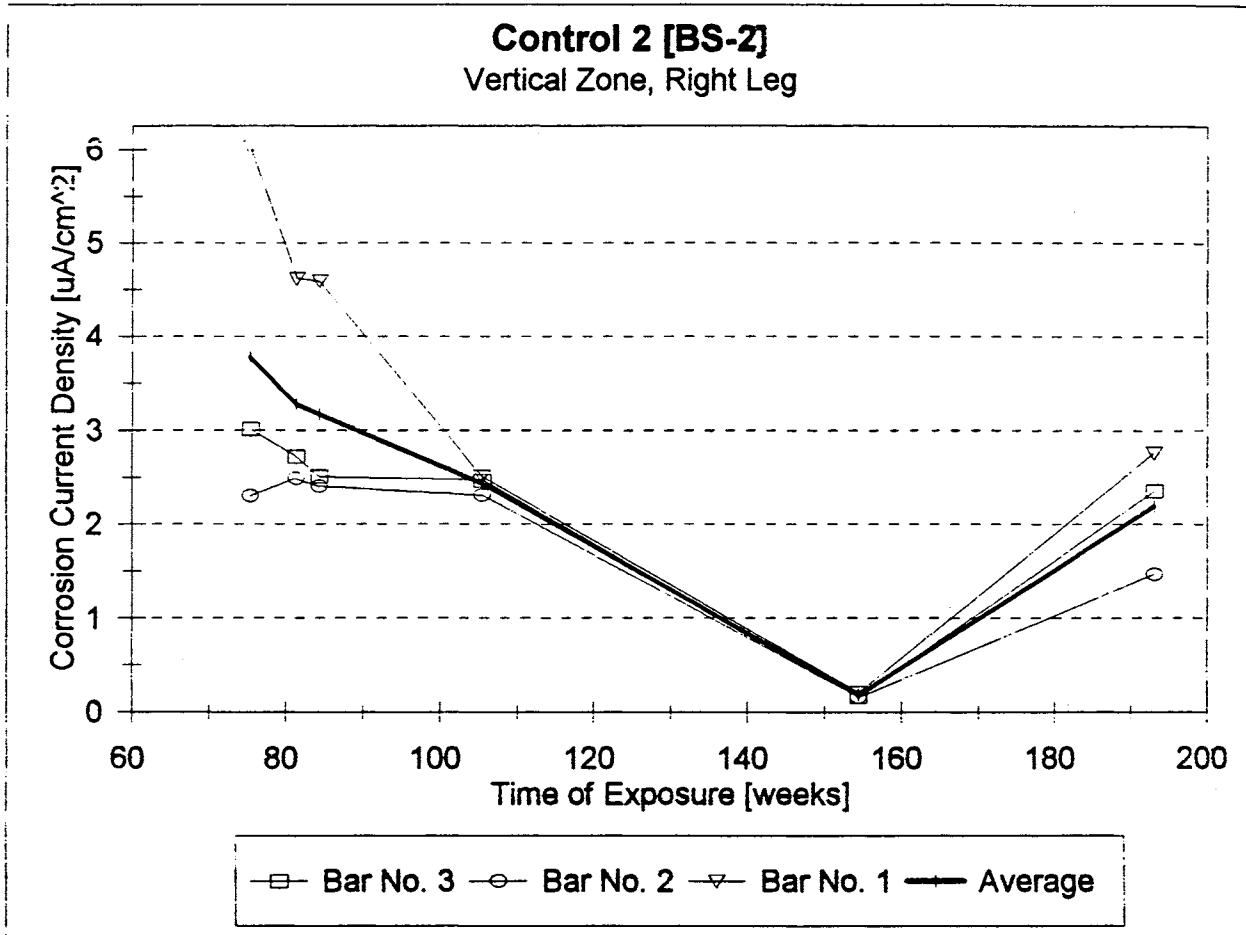


FIGURE 36. Corrosion Rates in the Vertical Zone, Right Leg, BS-2 Specimen.

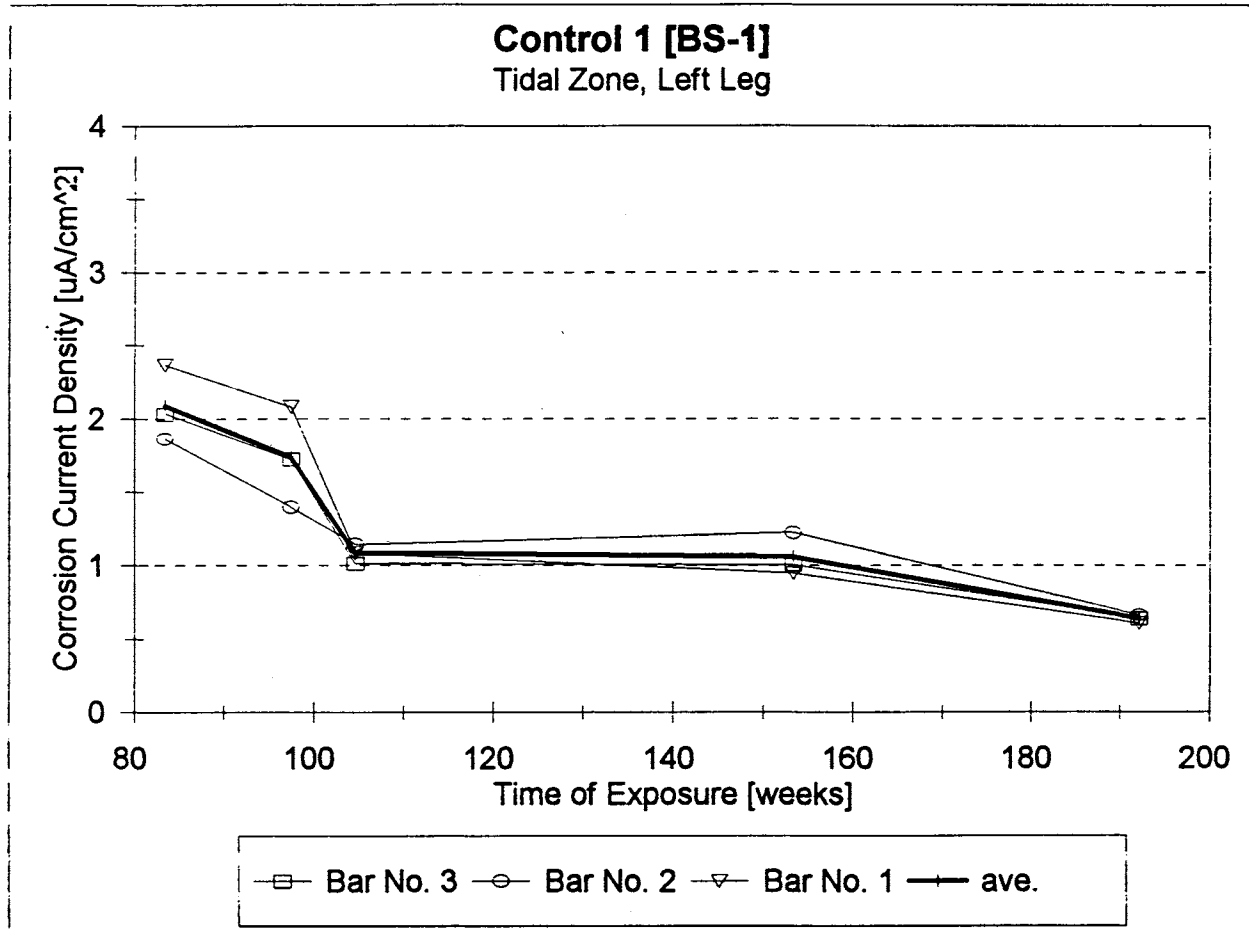


FIGURE 37. Corrosion Rates in the Tidal Zone, Left Leg, BS-1 Specimen.

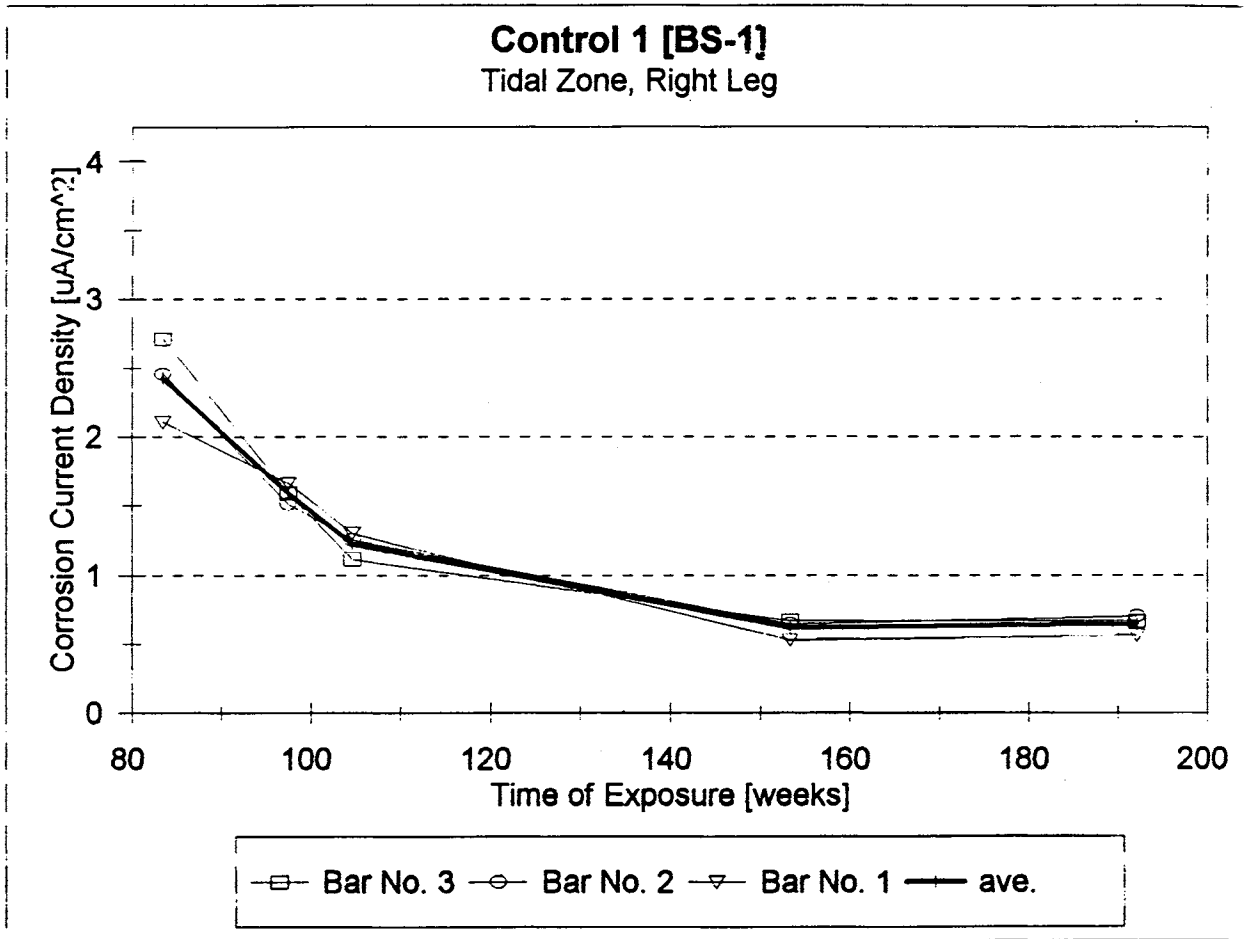


FIGURE 38. Corrosion Rates in the Tidal Zone, Right Leg, BS-1 Specimen.

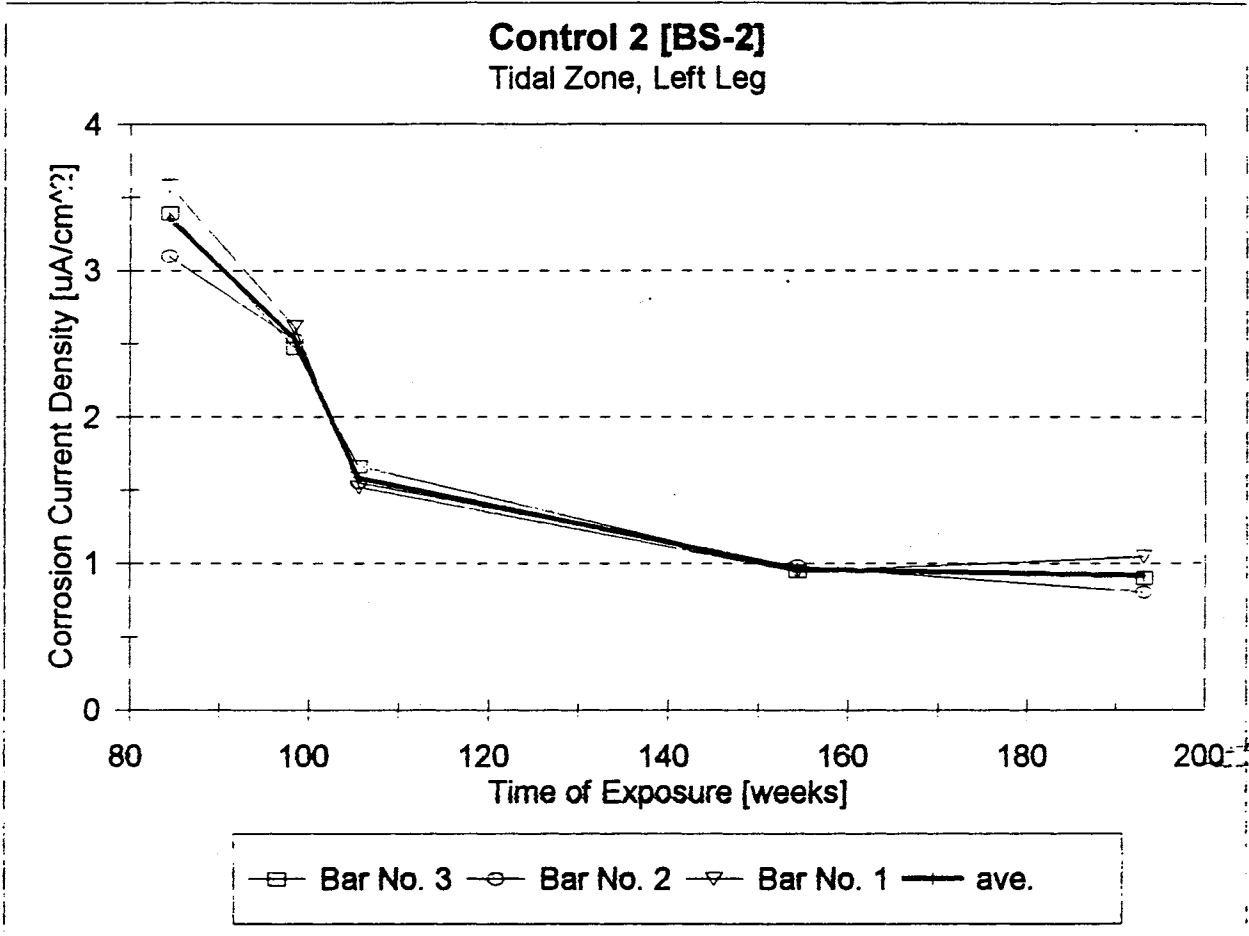


FIGURE 39. Corrosion Rates in the Tidal Zone, Left Leg, BS-2 Specimen.

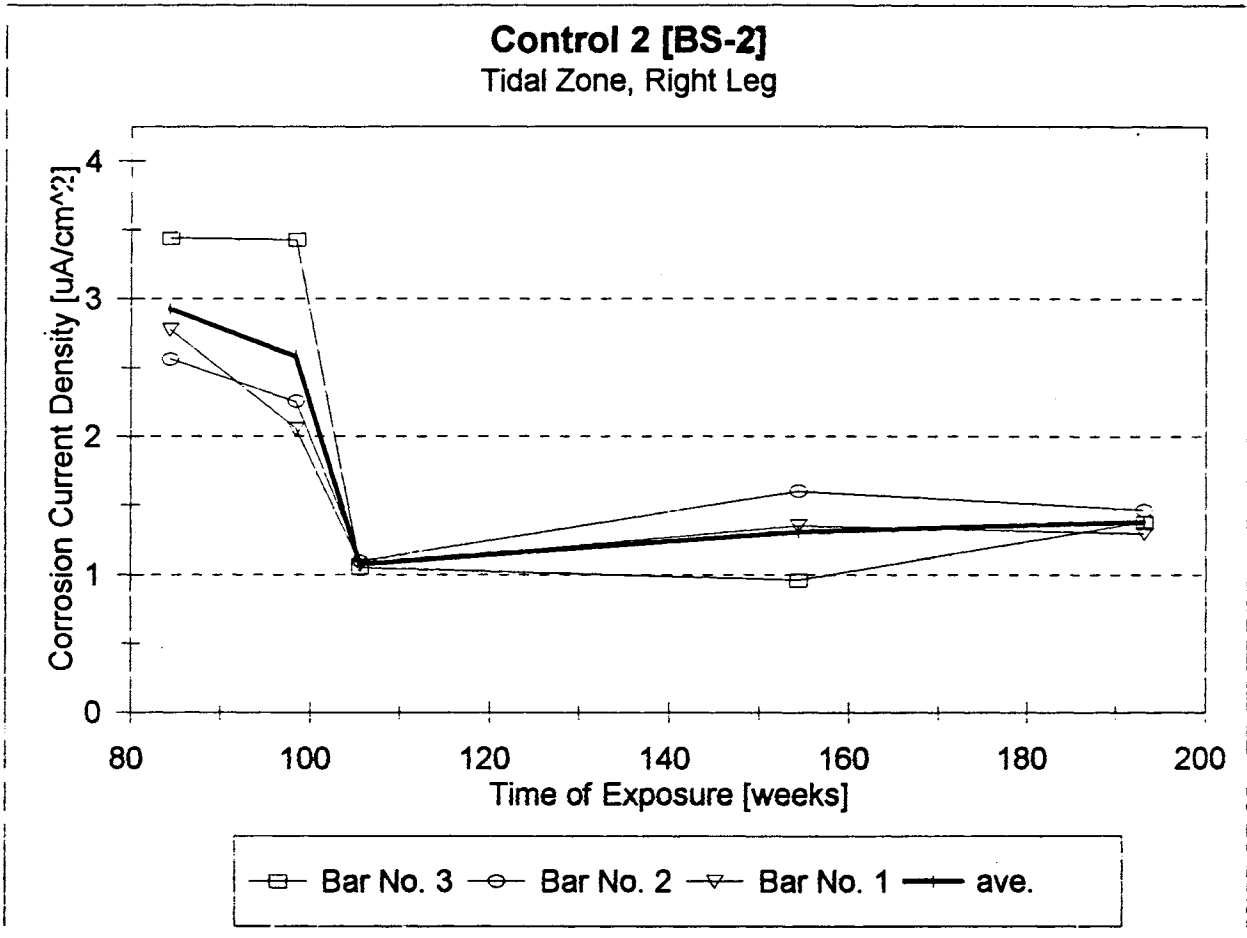


FIGURE 40. Corrosion Rates in the Tidal Zone, Right Leg, BS-2 Specimen.

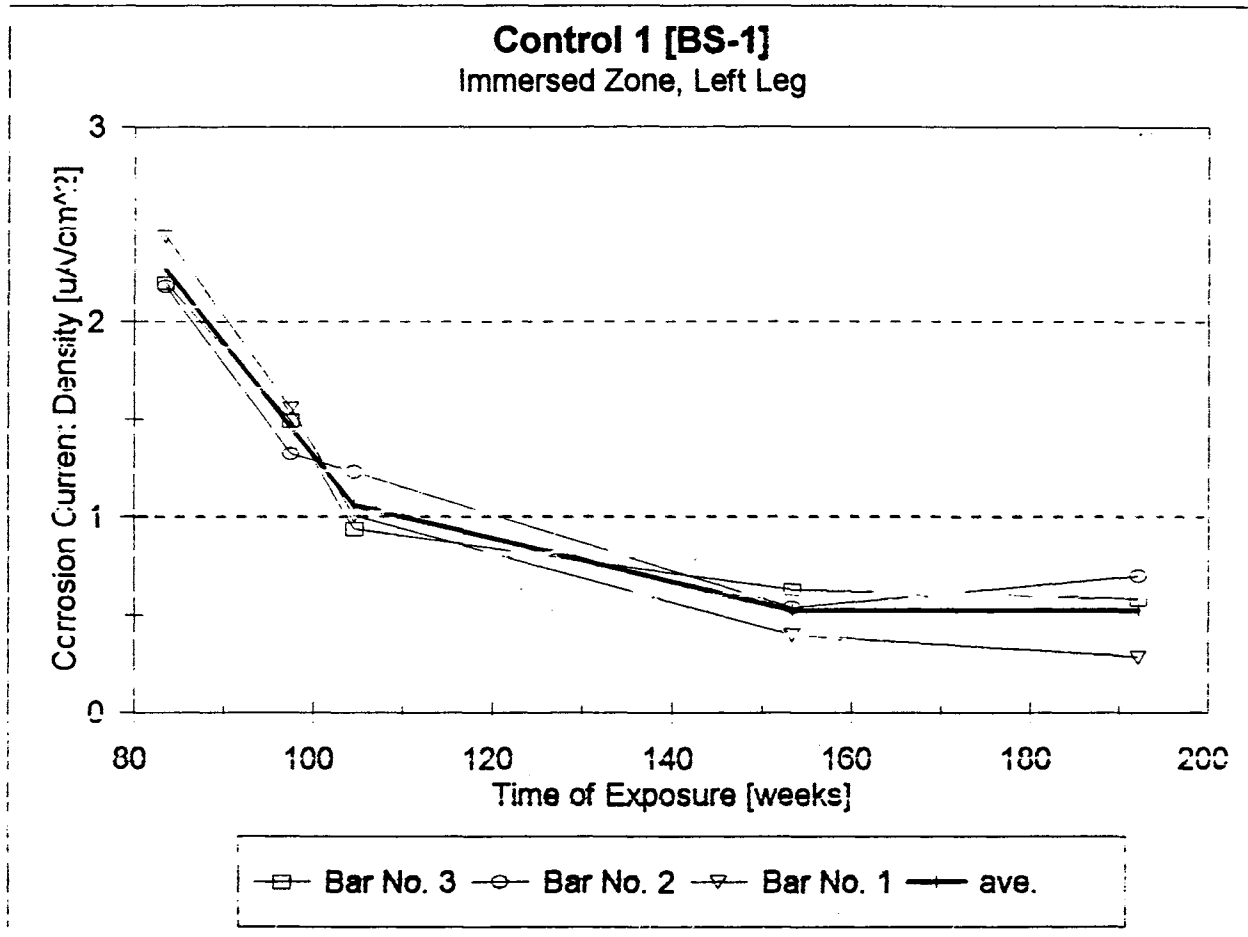


FIGURE 41. Corrosion Rates in the Immersed Zone, Left Leg, BS-1 Specimen.

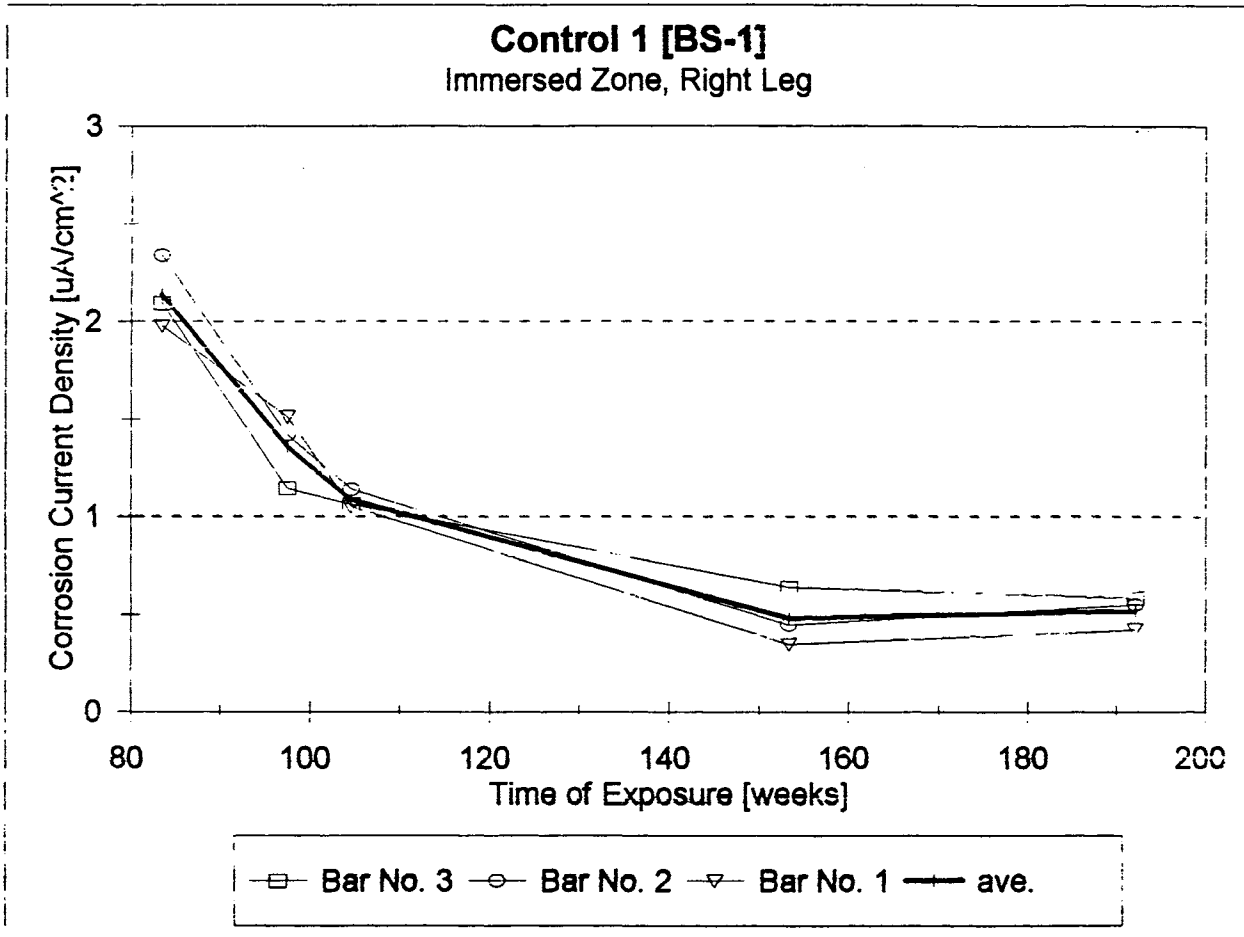


FIGURE 42. Corrosion Rates in the Immersed Zone, Right Leg, BS-1 Specimen.

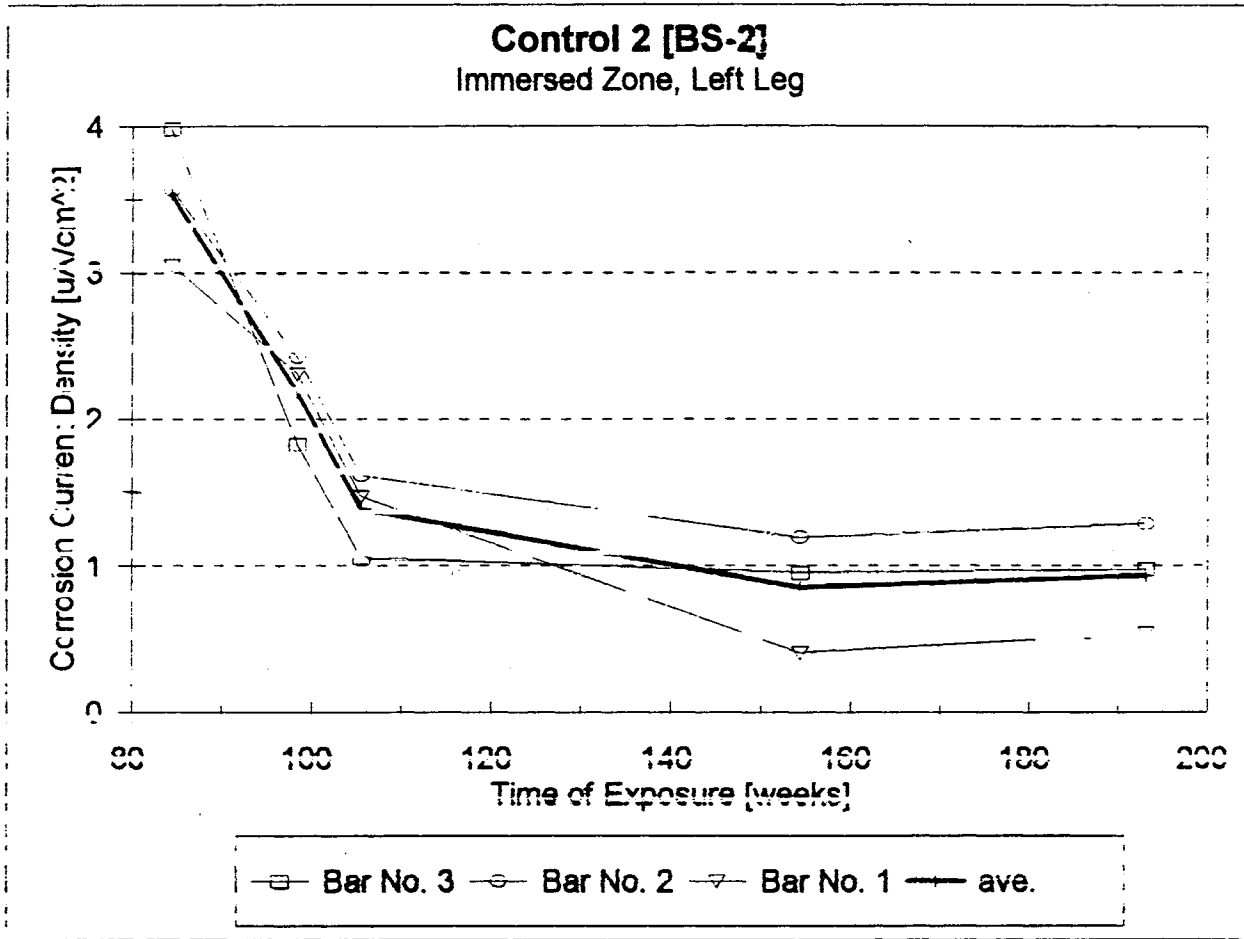


FIGURE 43. Corrosion Rates in the Immersed Zone, Left Leg, BS-2 Specimen.

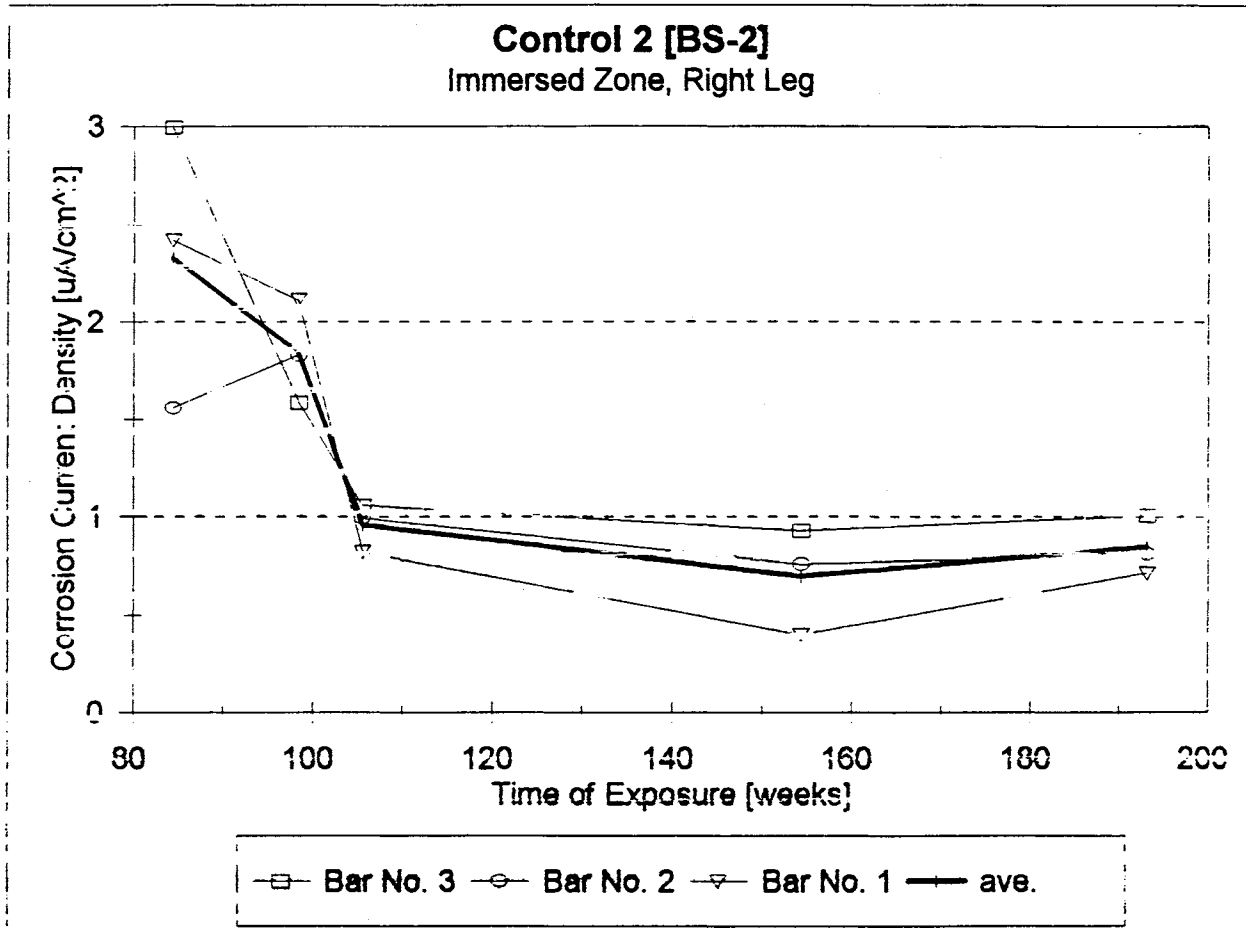


FIGURE 44. Corrosion Rates in the Immersed Zone, Right Leg, BS-2 Specimen.

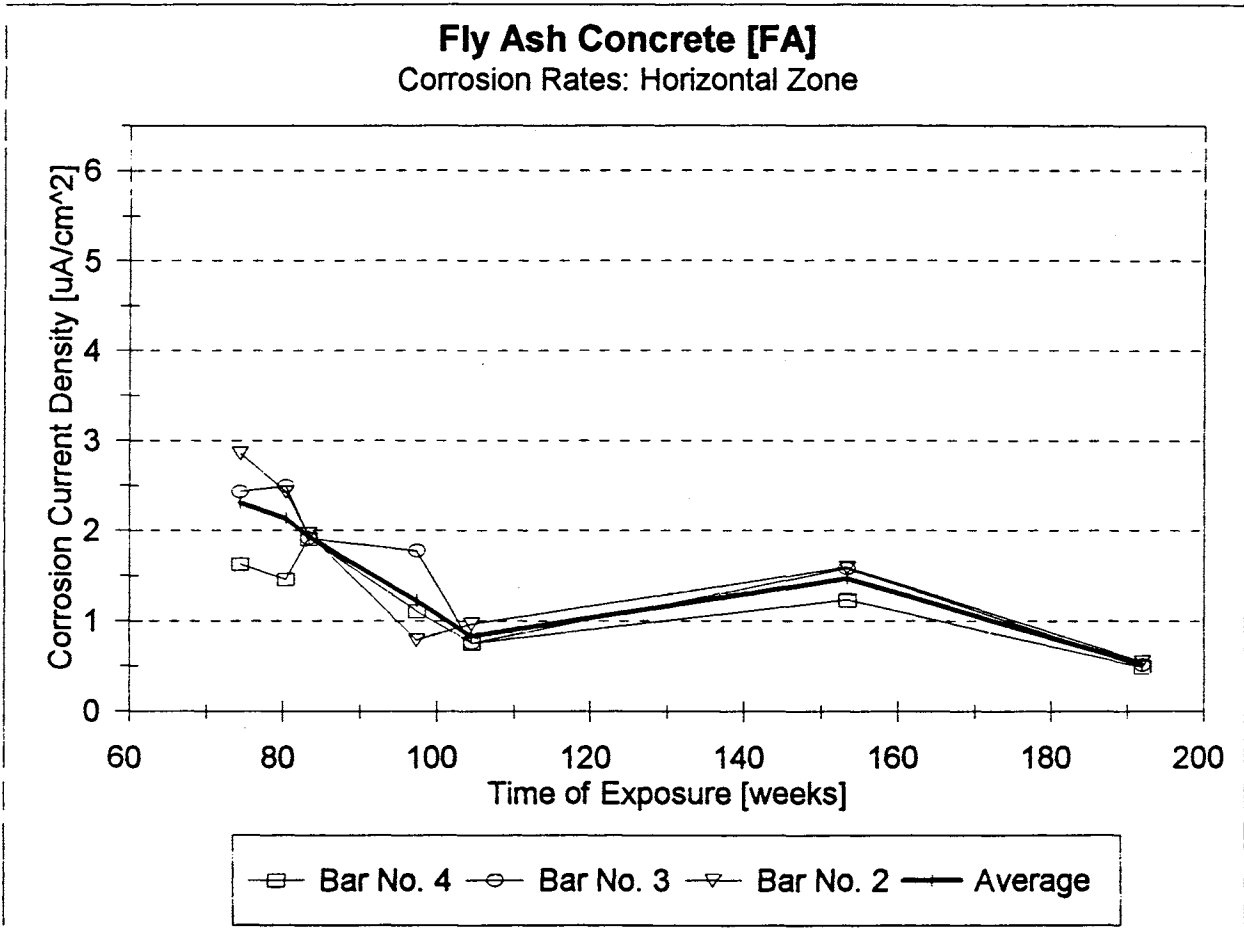


FIGURE 45. Corrosion Rates in the Horizontal Zone, FA Specimen.

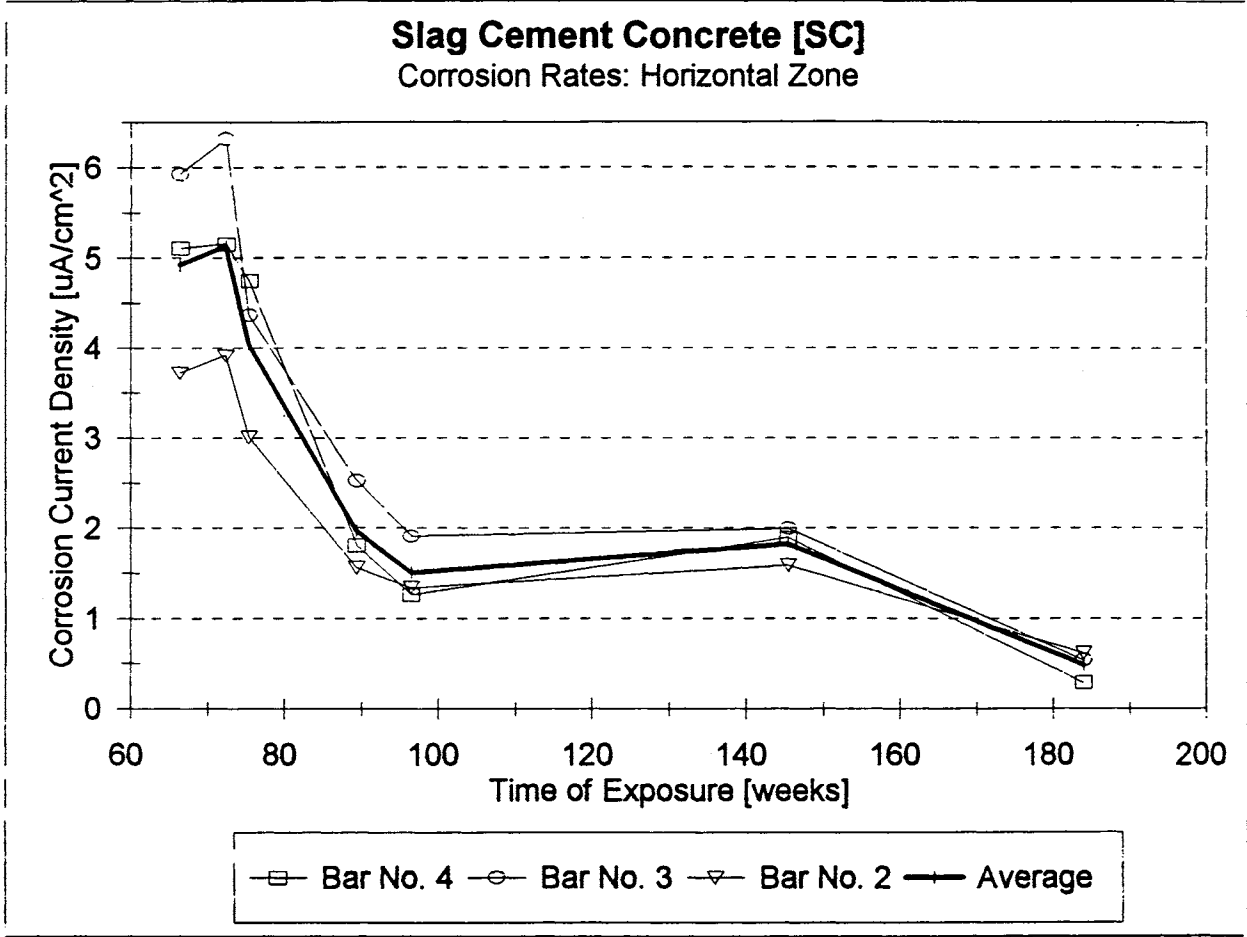


FIGURE 46. Corrosion Rates in the Horizontal Zone, SC Specimen.

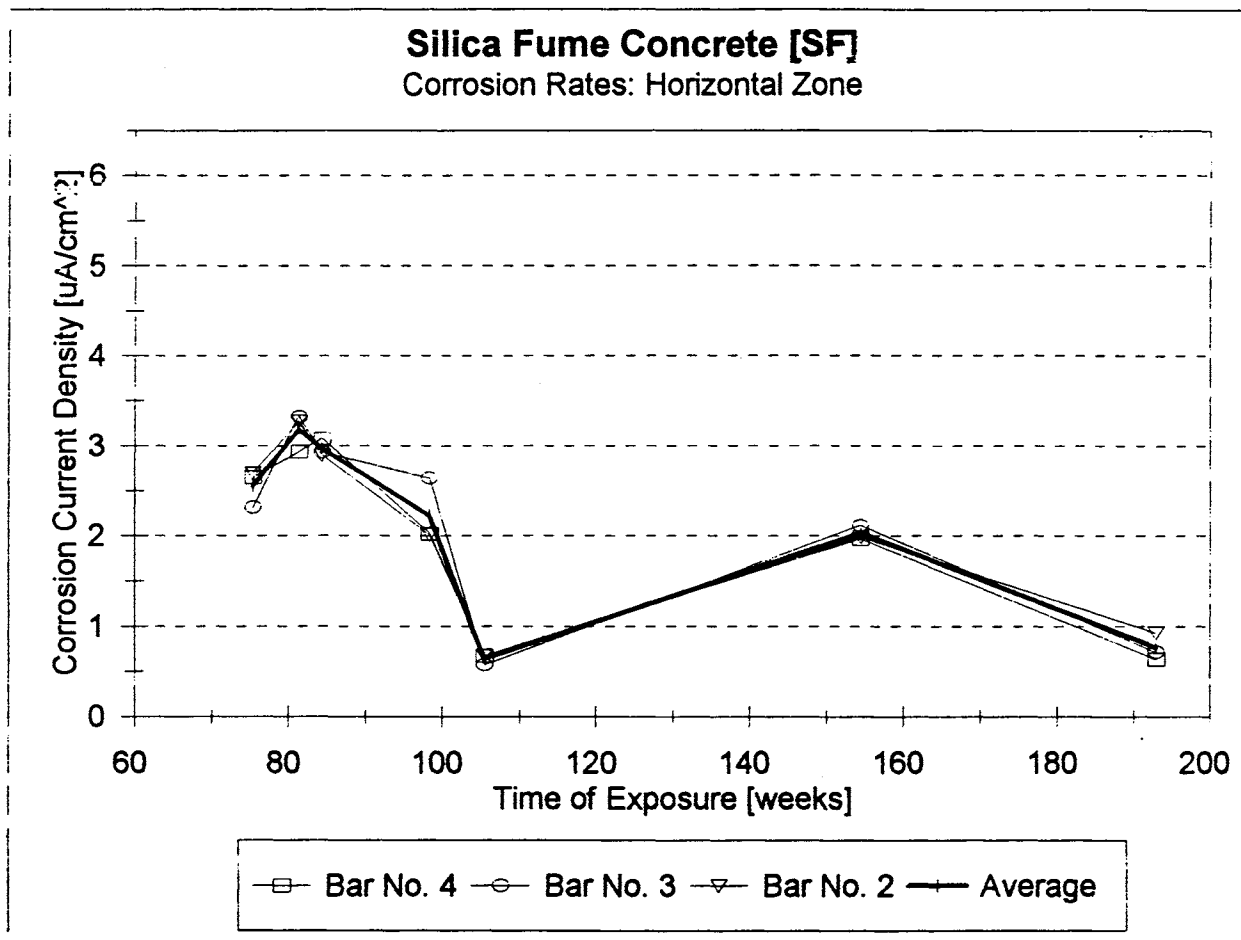


FIGURE 47. Corrosion Rates in the Horizontal Zone, SF Specimen.

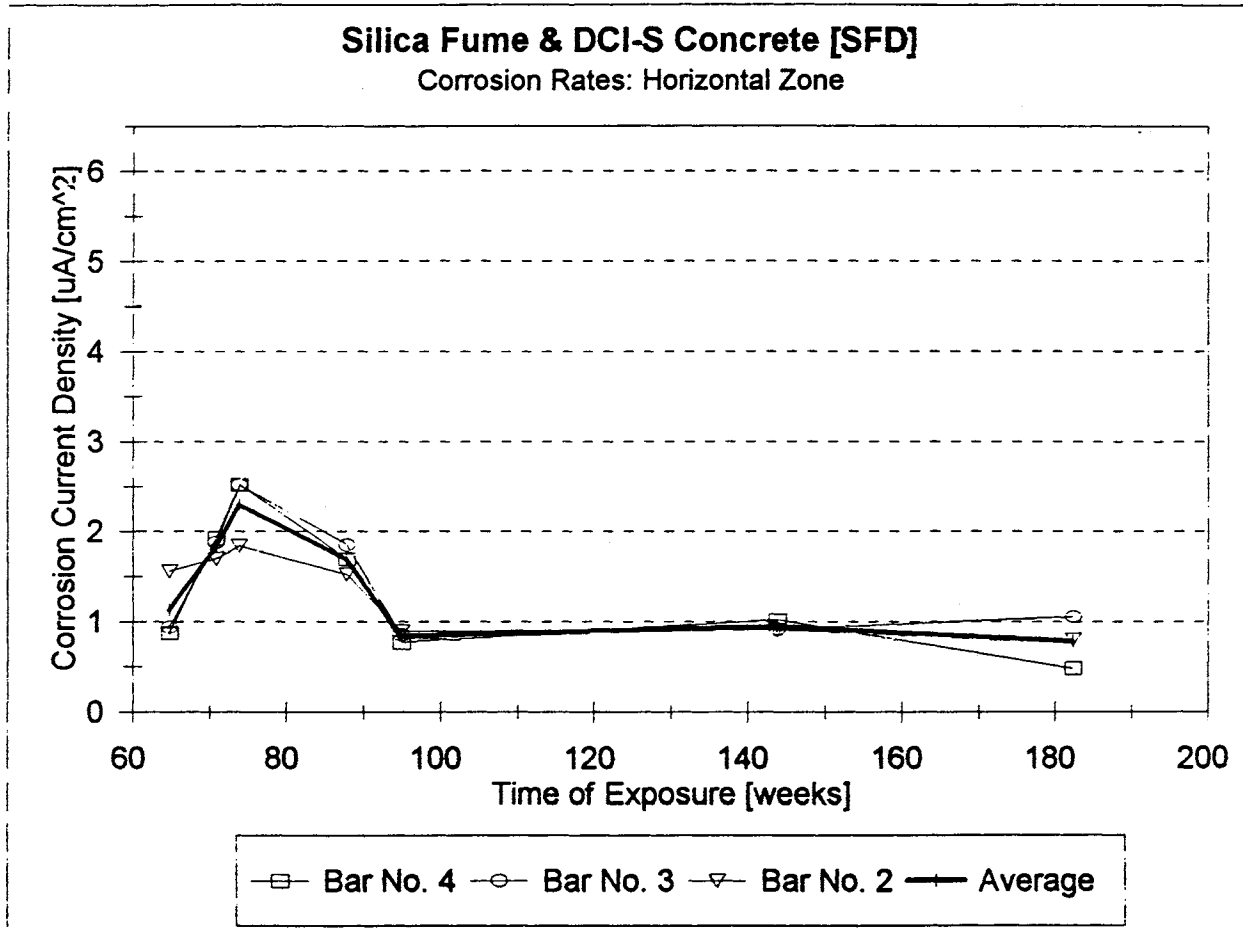


FIGURE 48. Corrosion Rates in the Horizontal Zone, SFD Specimen.

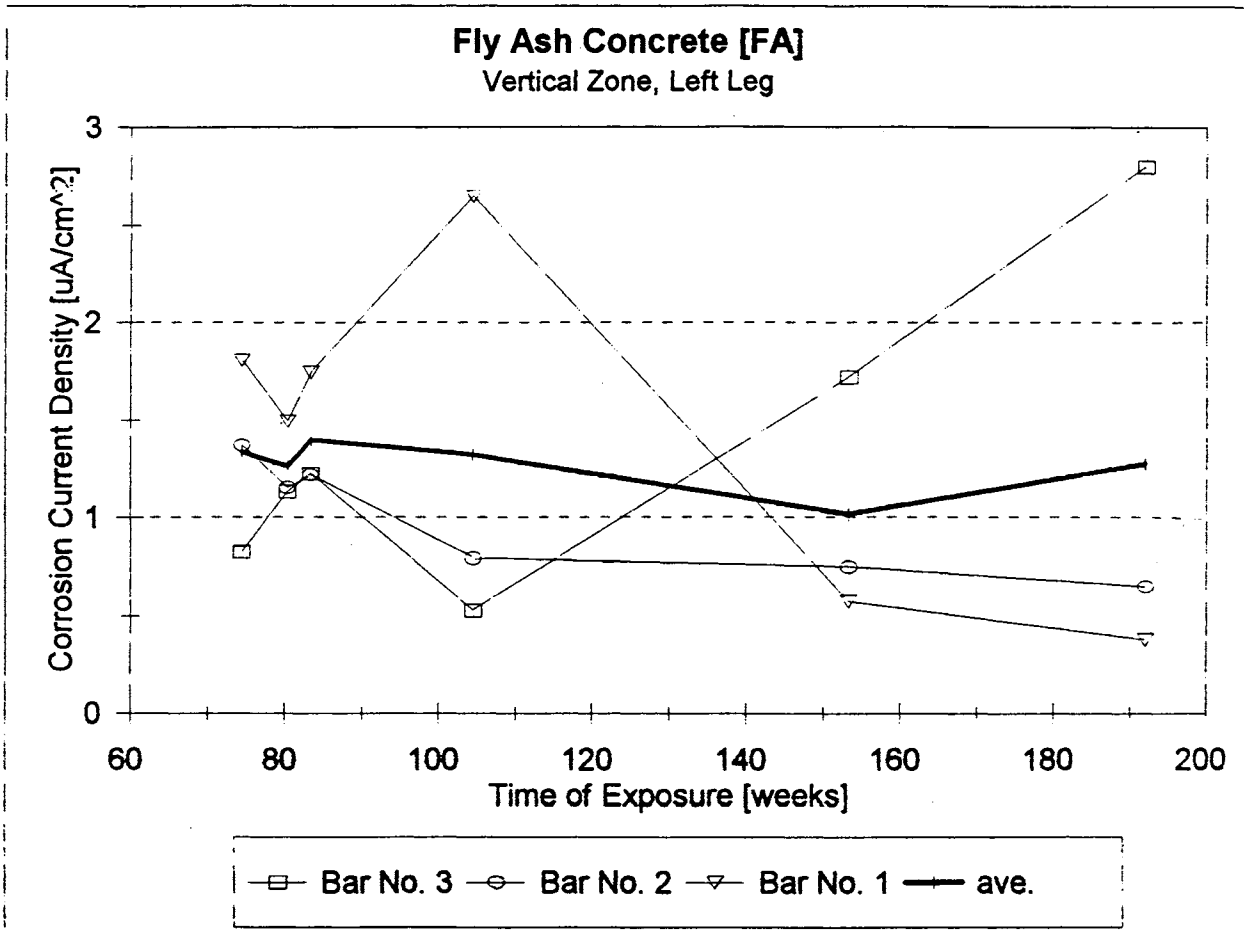


FIGURE 49. Corrosion Rates in the Vertical Zone, Left Leg, FA Specimen.

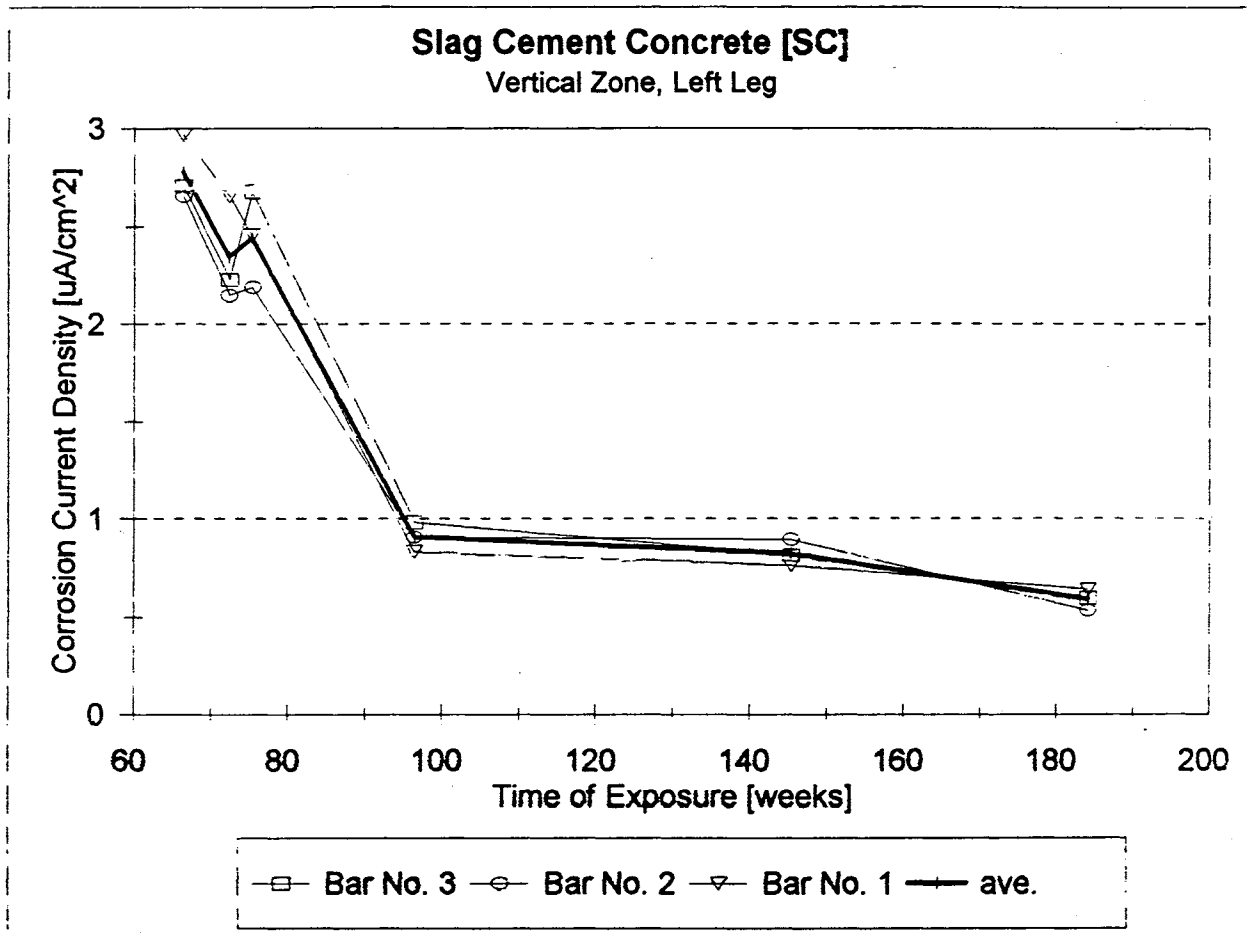


FIGURE 50. Corrosion Rates in the Vertical Zone, Left Leg, SC Specimen.

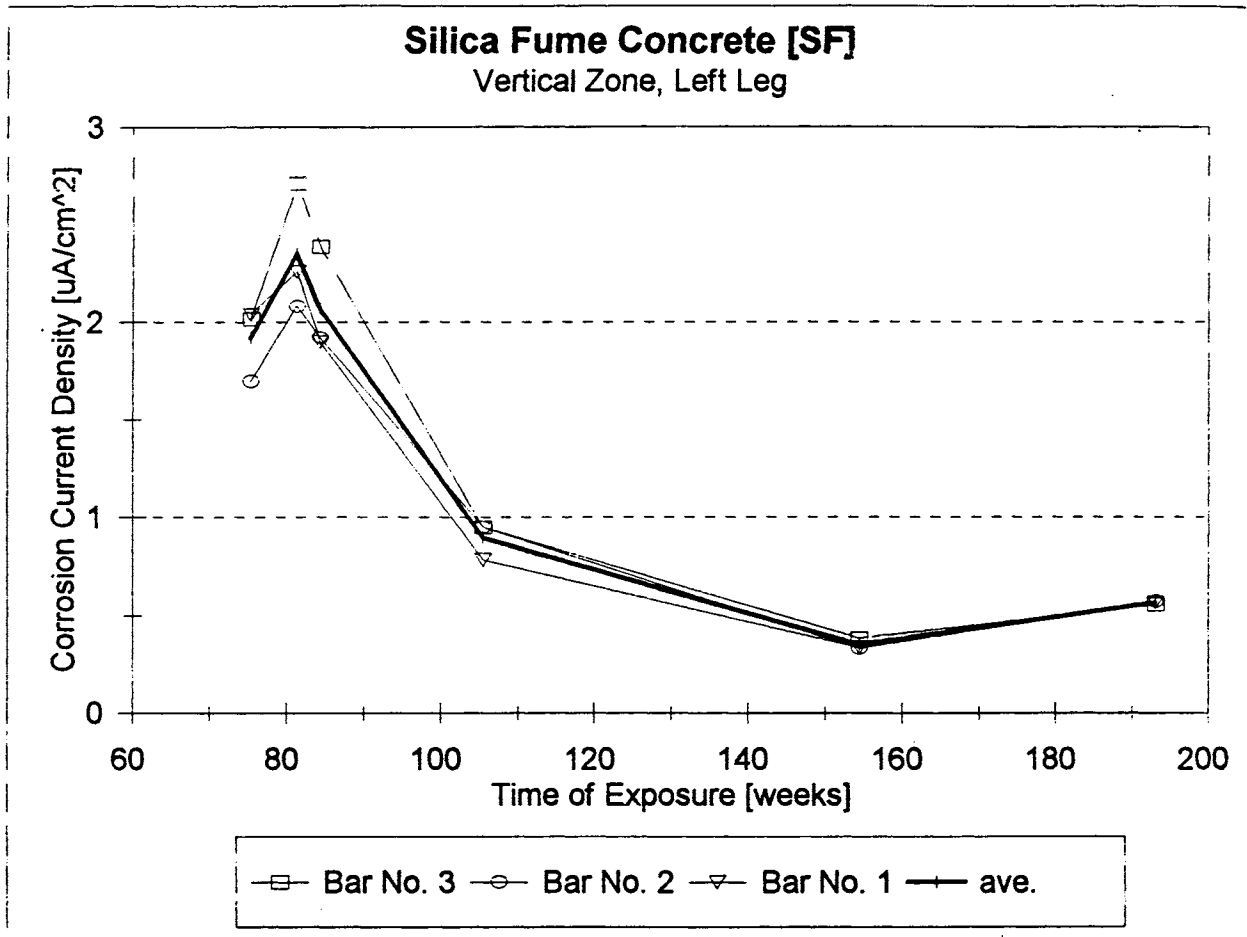


FIGURE 51. Corrosion Rates in the Vertical Zone, Left Leg, SF Specimen.

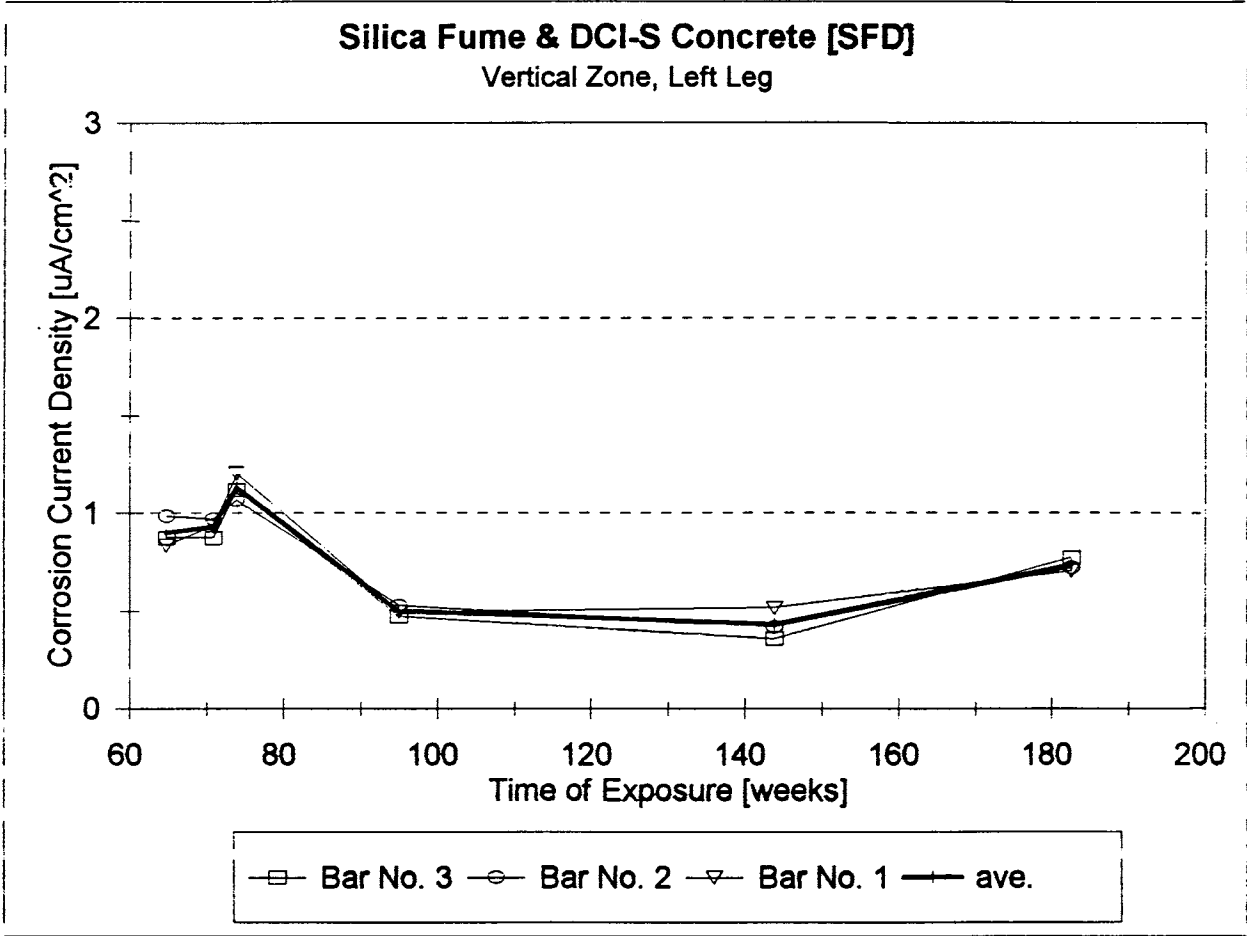


FIGURE 52. Corrosion Rates in the Vertical Zone, Left Leg, SFD Specimen.

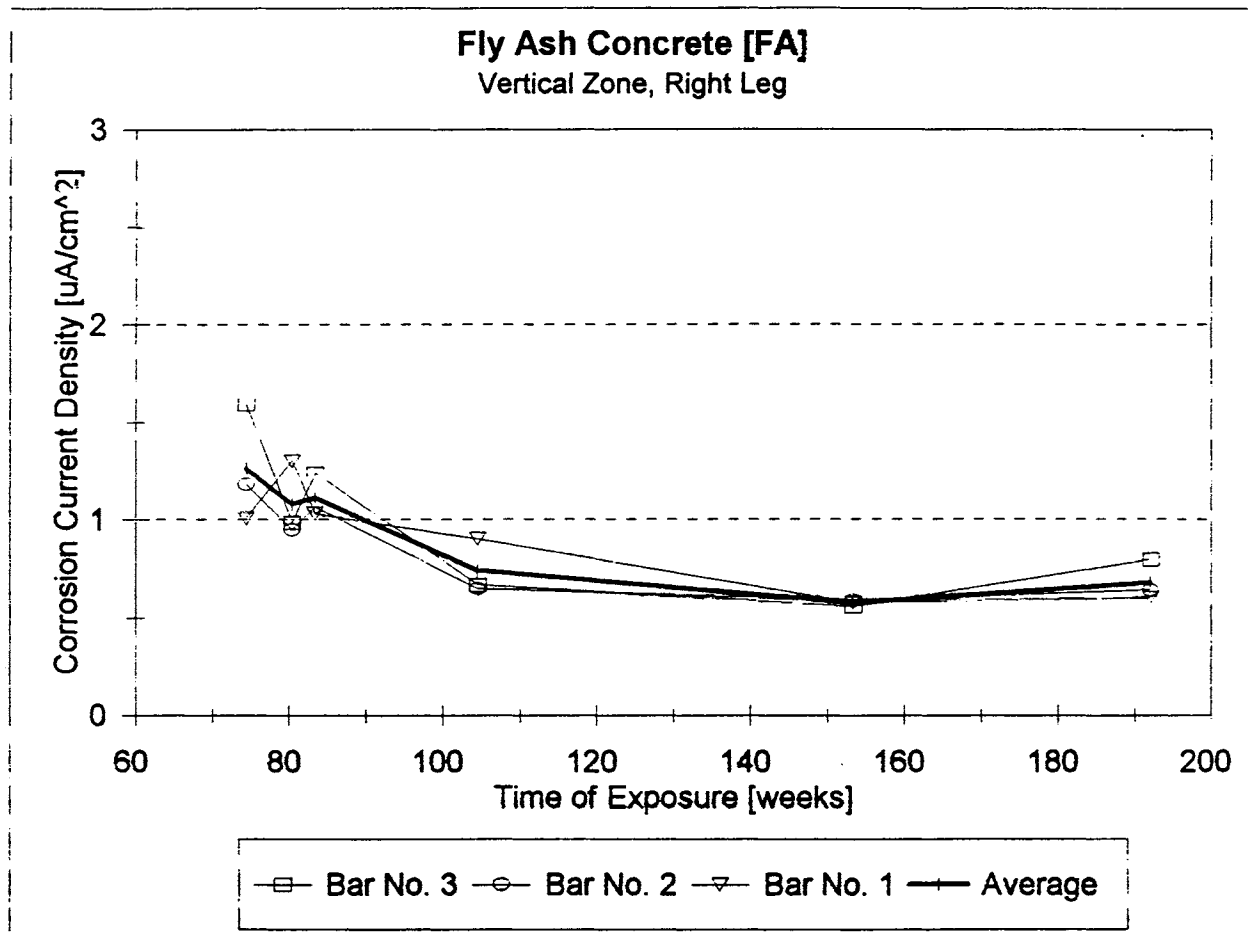


FIGURE 53. Corrosion Rates in the Vertical Zone, Right Leg, FA Specimen.

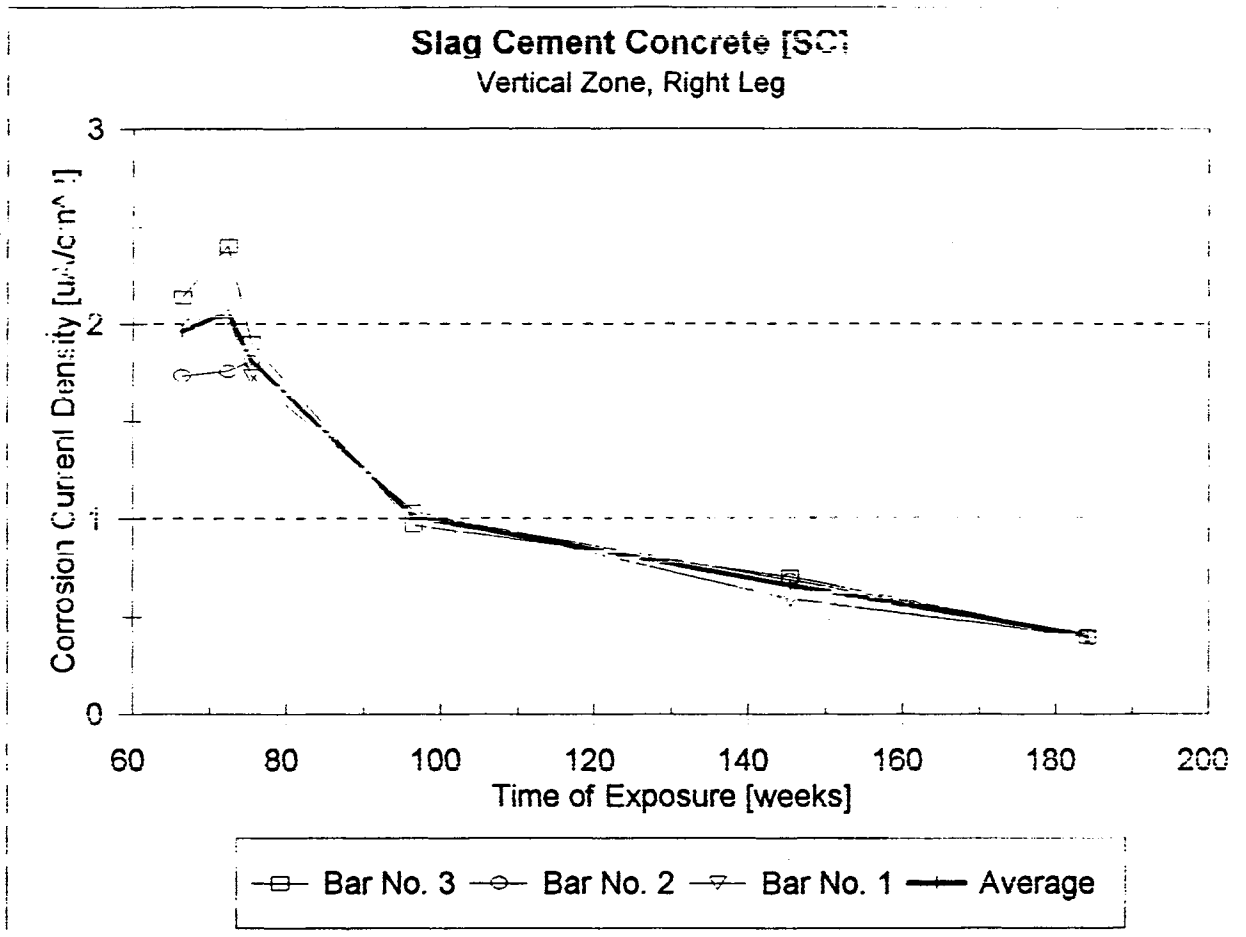


FIGURE 54. Corrosion Rates in the Vertical Zone, Right Leg, SC Specimen.

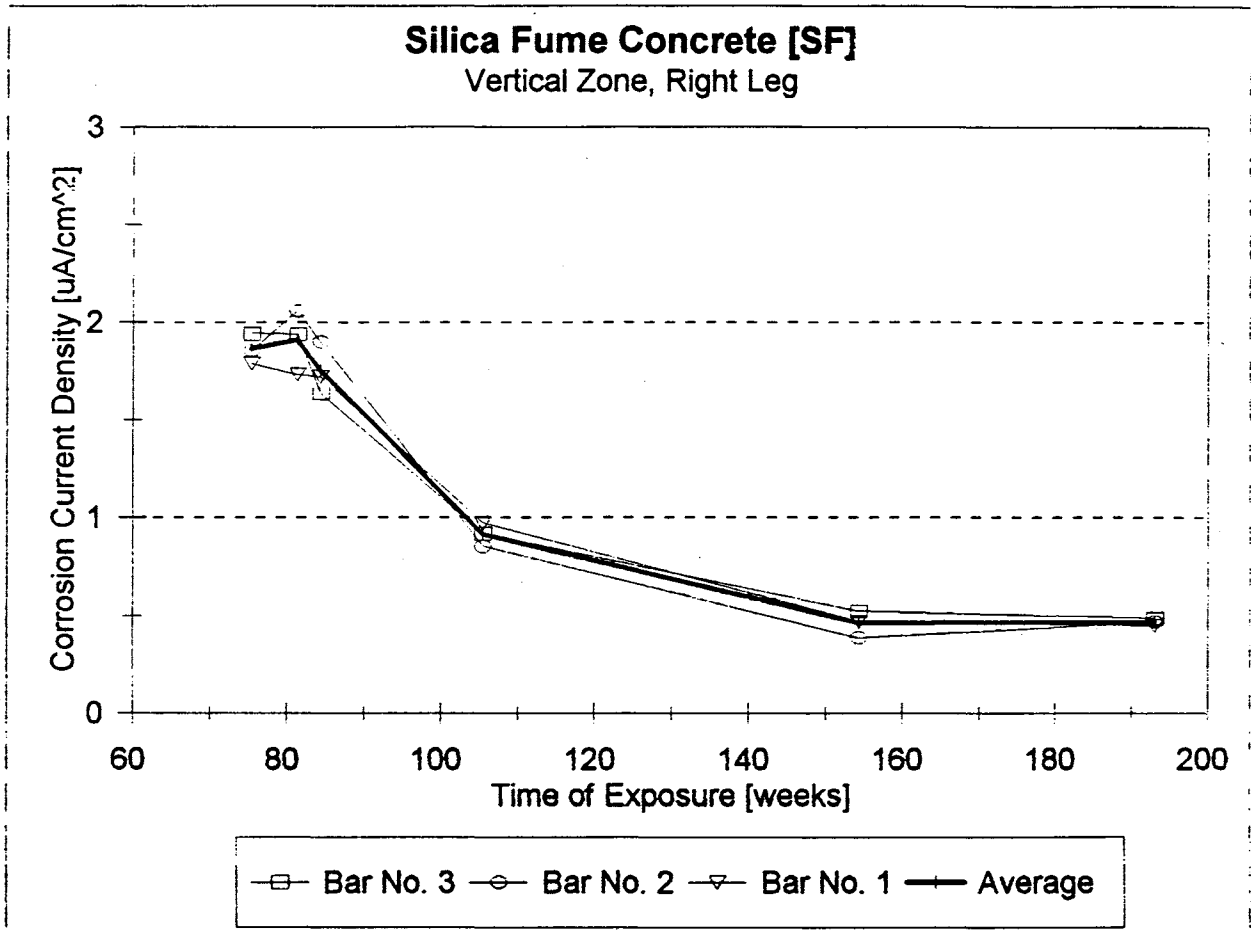


FIGURE 55. Corrosion Rates in the Vertical Zone, Right Leg, SF Specimen.

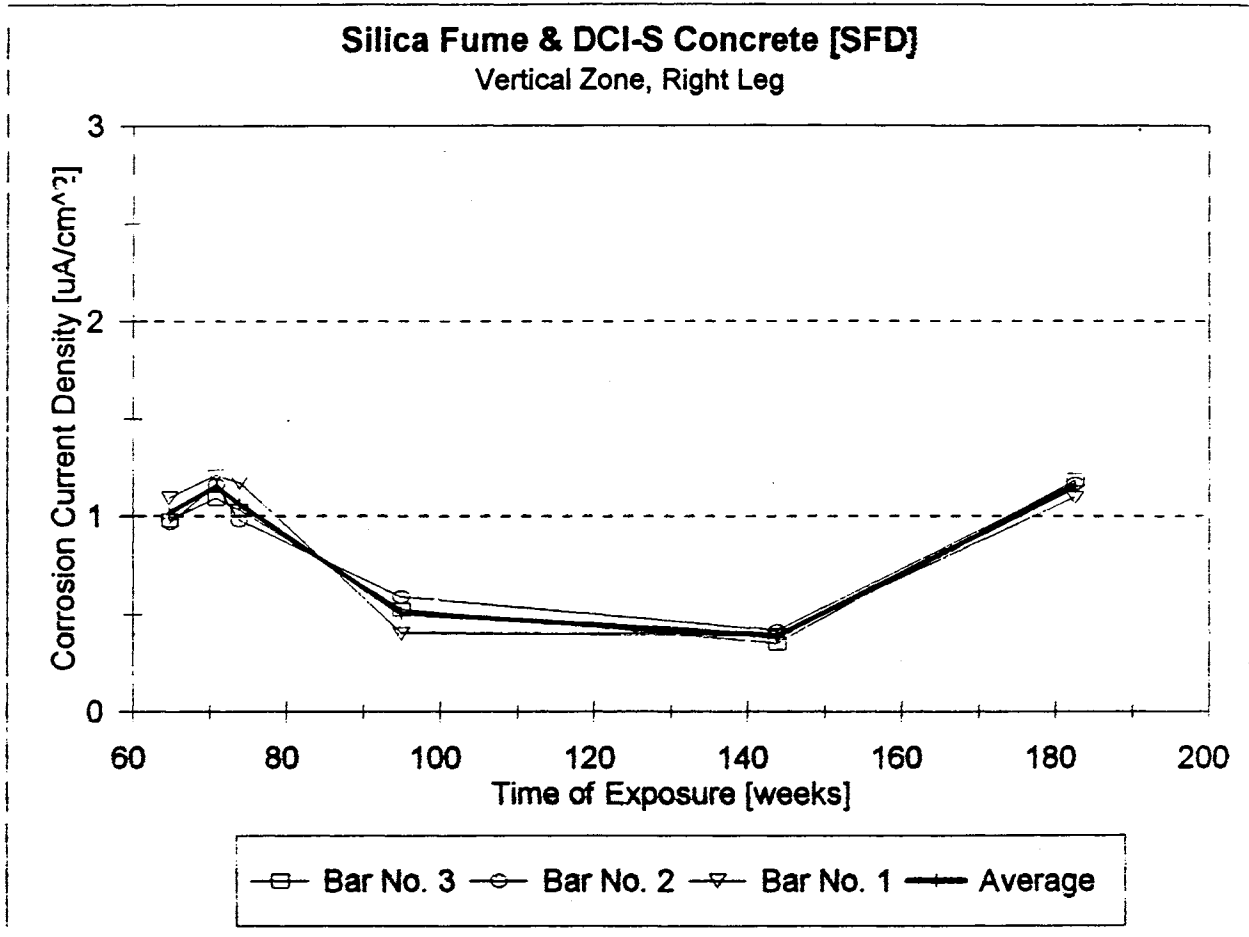


FIGURE 56. Corrosion Rates in the Vertical Zone, Right Leg, SFD Specimen.

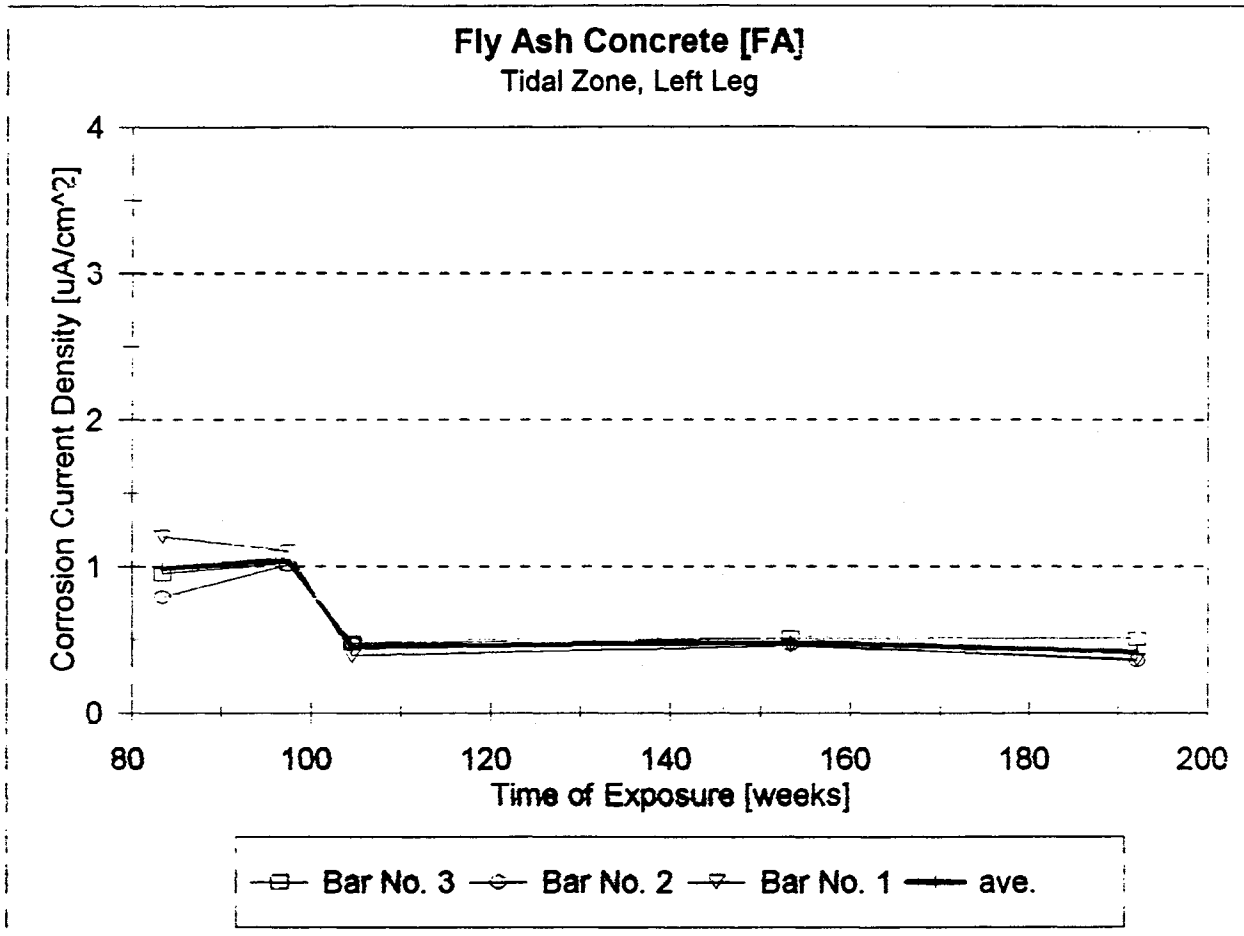


FIGURE 57. Corrosion Rates in the Tidal Zone, Left Leg, FA Specimen.

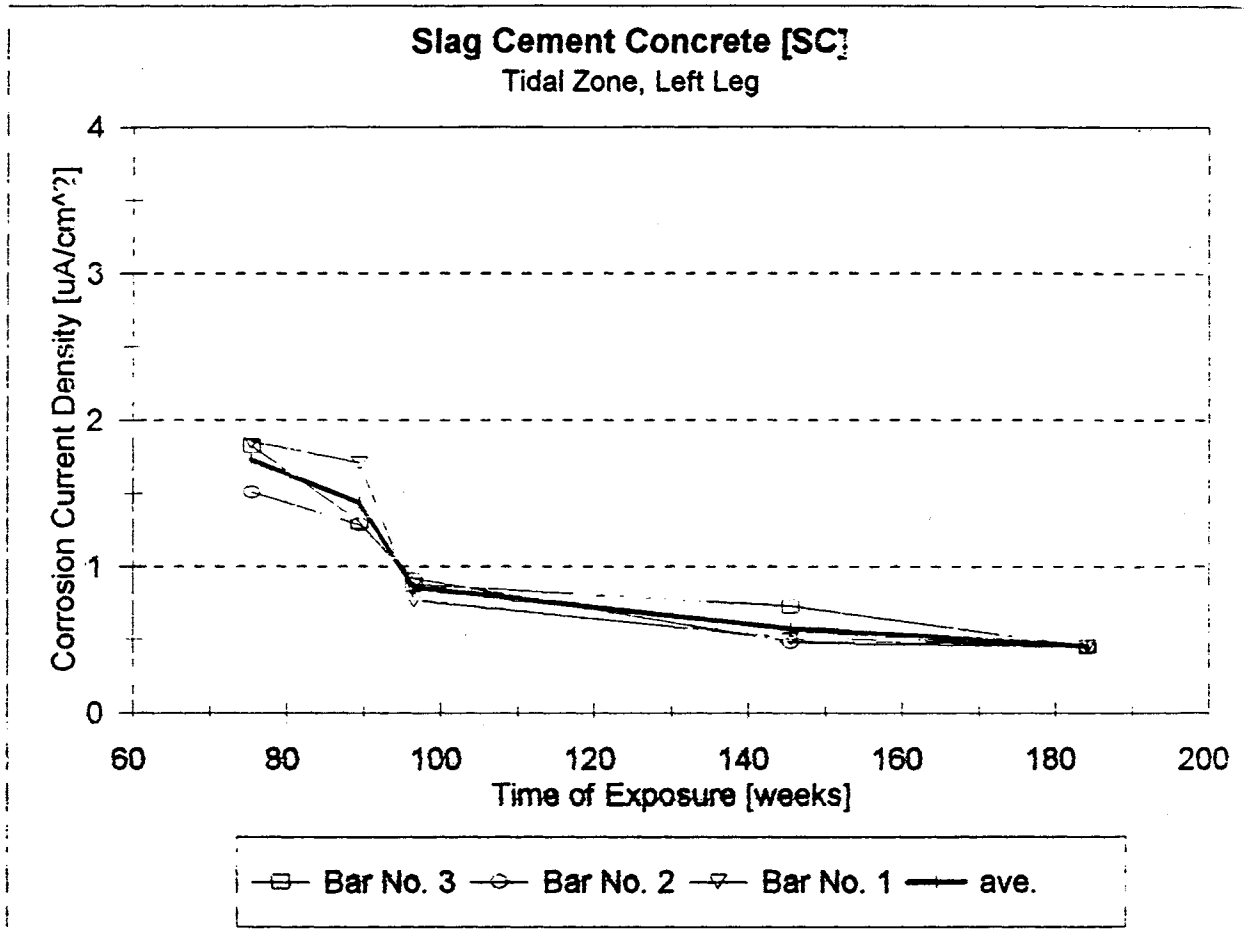


FIGURE 58. Corrosion Rates in the Tidal Zone, Left Leg, SC Specimen.

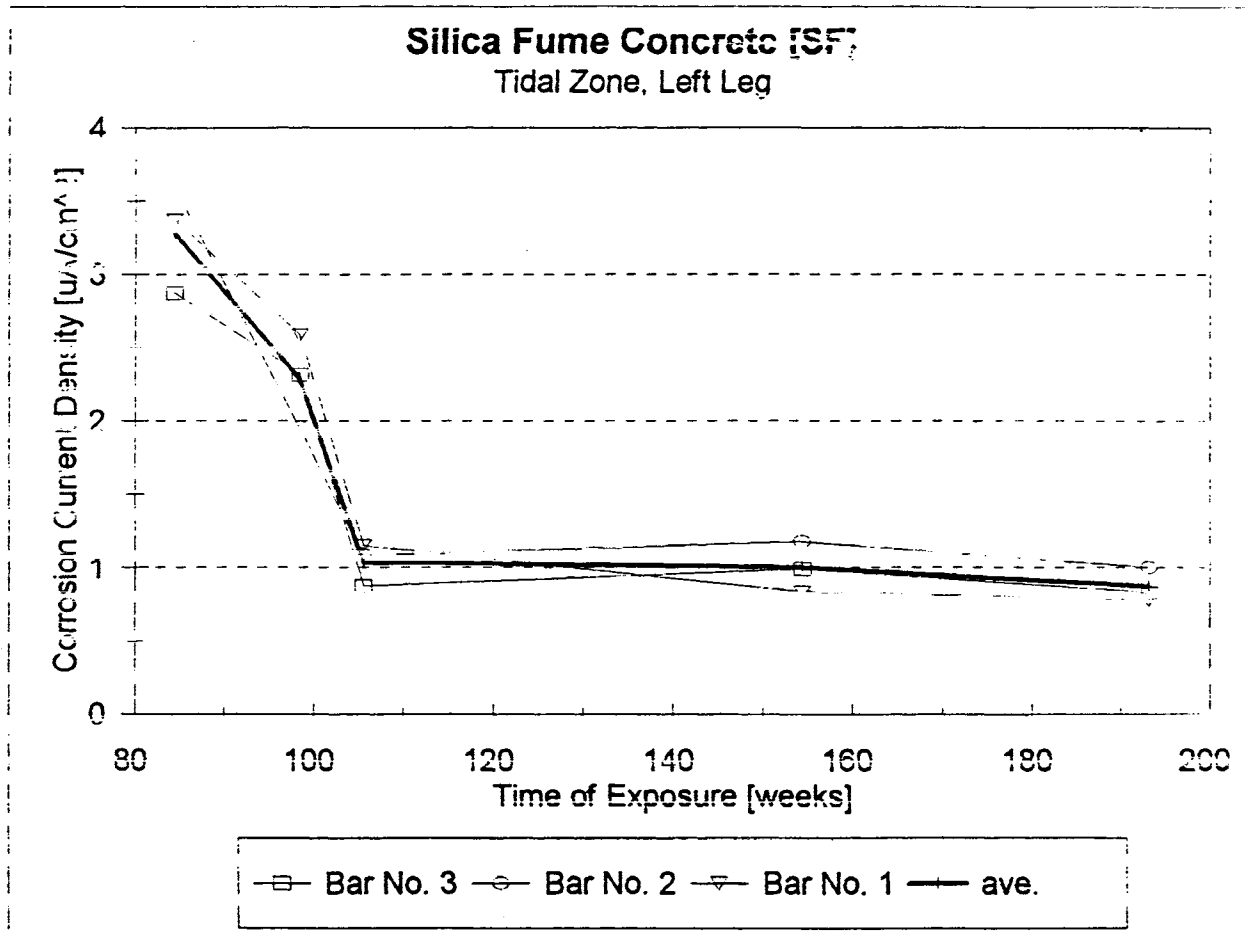


FIGURE 59. Corrosion Rates in the Tidal Zone, Left Leg, SF Specimen.

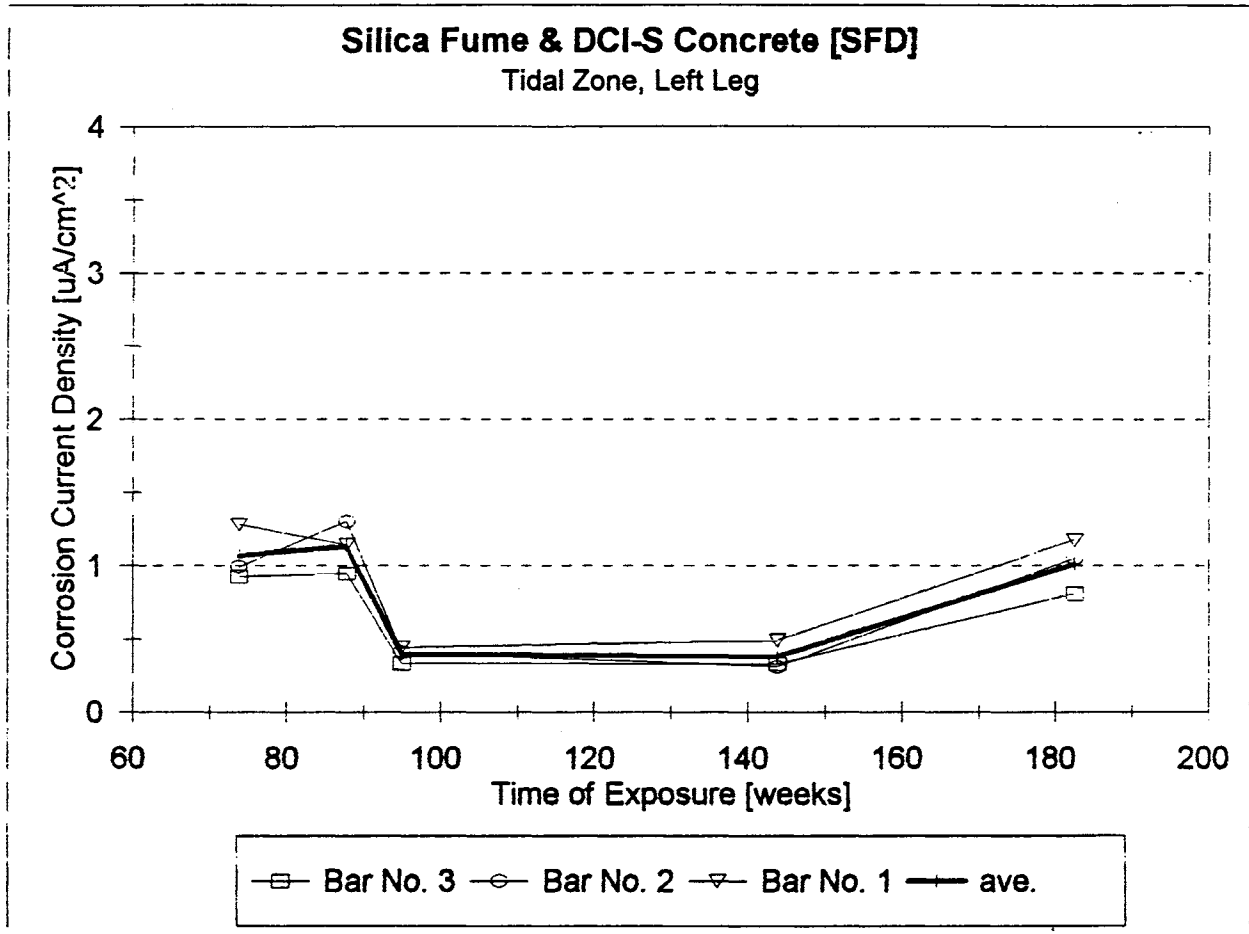


FIGURE 60. Corrosion Rates in the Tidal Zone, Left Leg, SFD Specimen.

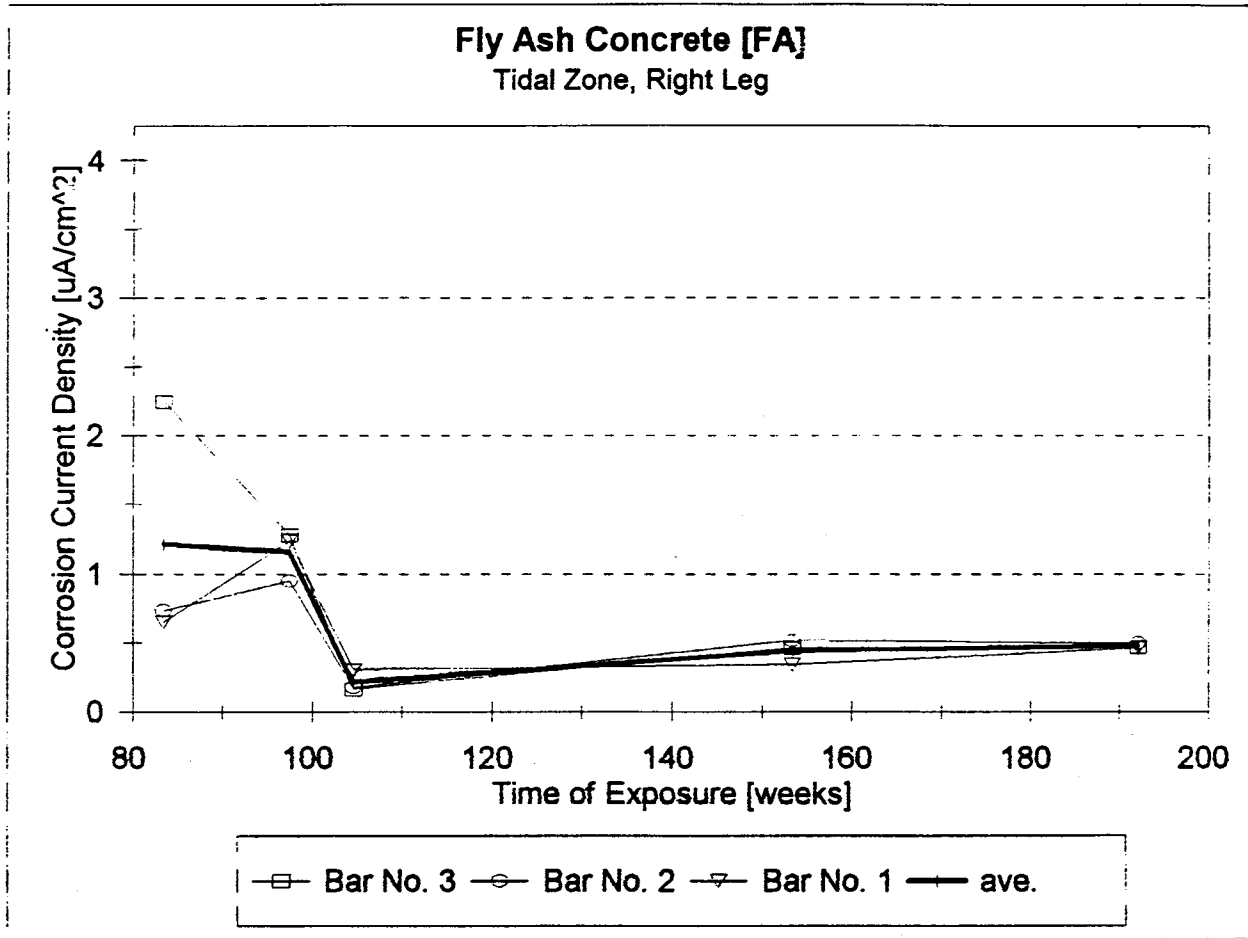


FIGURE 61. Corrosion Rates in the Tidal Zone, Right Leg, FA Specimen.

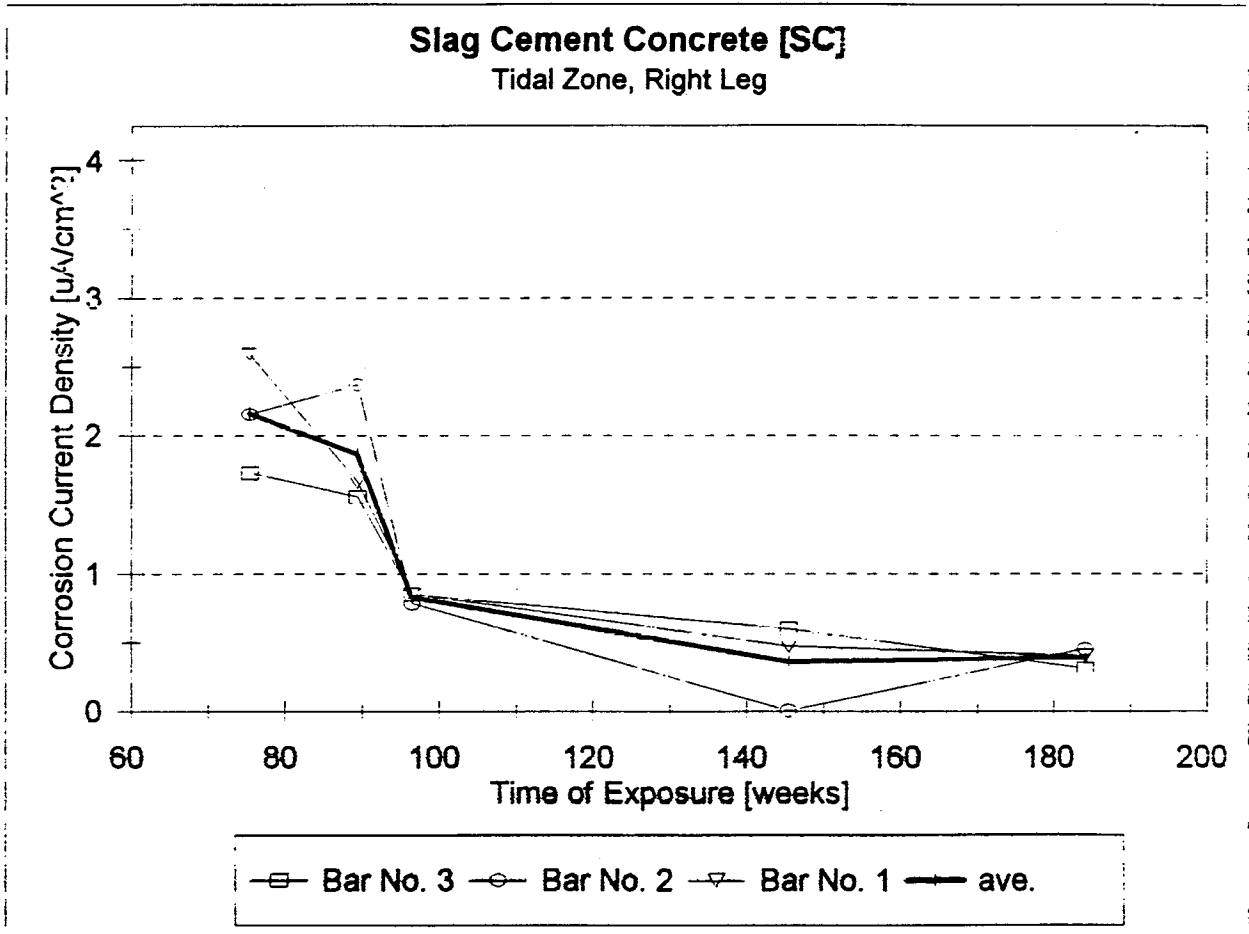


FIGURE 62. Corrosion Rates in the Tidal Zone, Right Leg, SC Specimen.

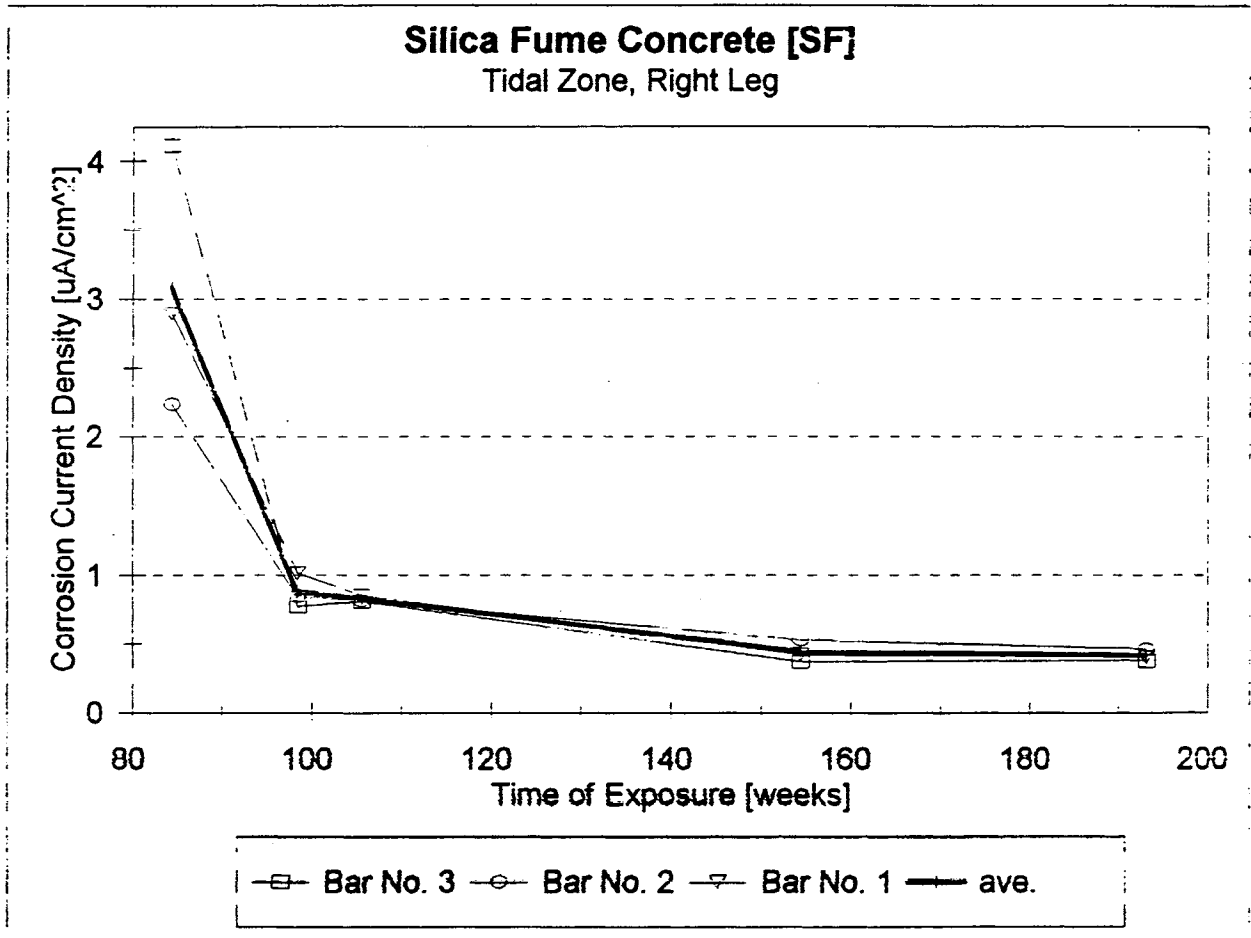


FIGURE 63. Corrosion Rates in the Tidal Zone, Right Leg, SF Specimen.

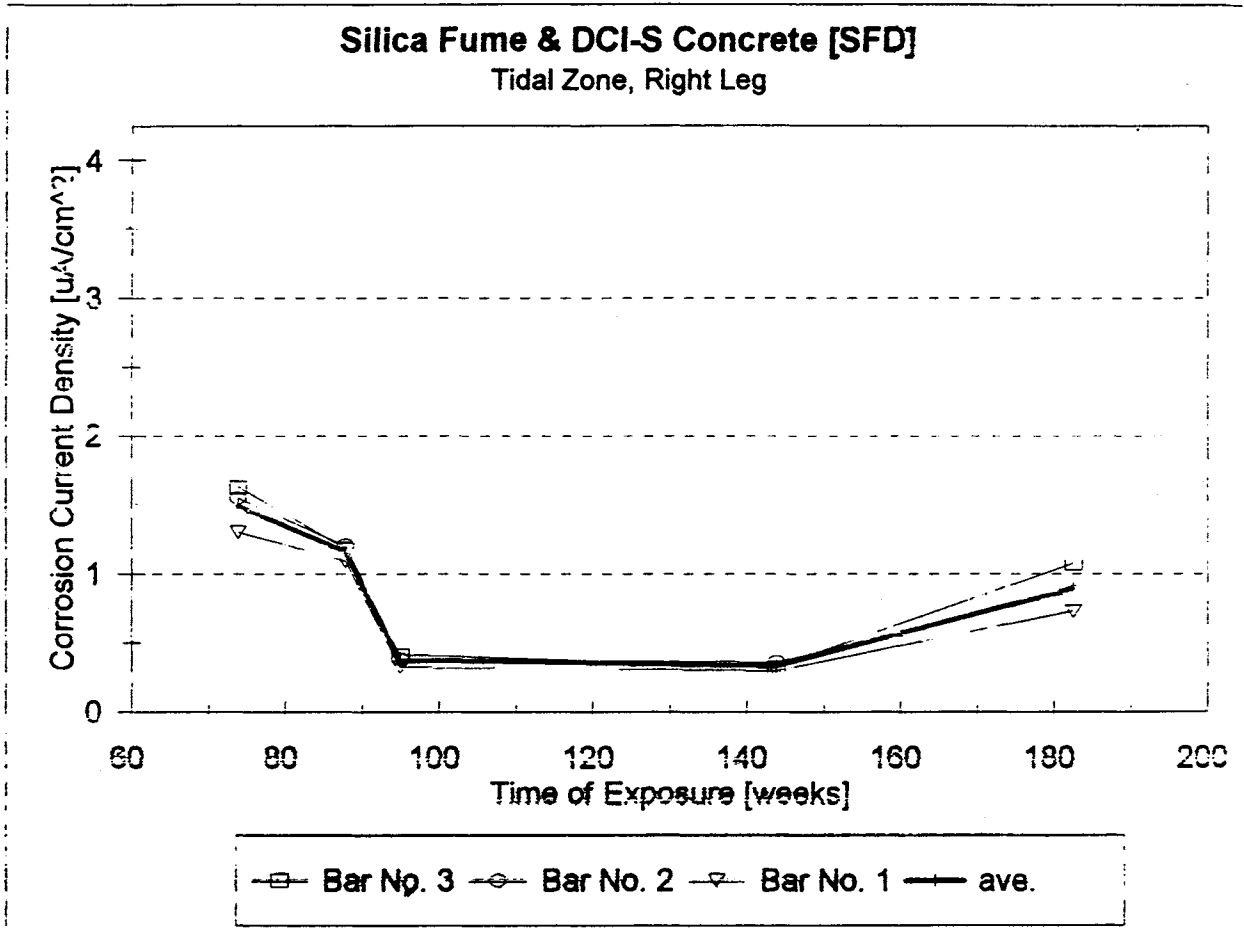


FIGURE 64. Corrosion Rates in the Tidal Zone, Right Leg, SFD Specimen.

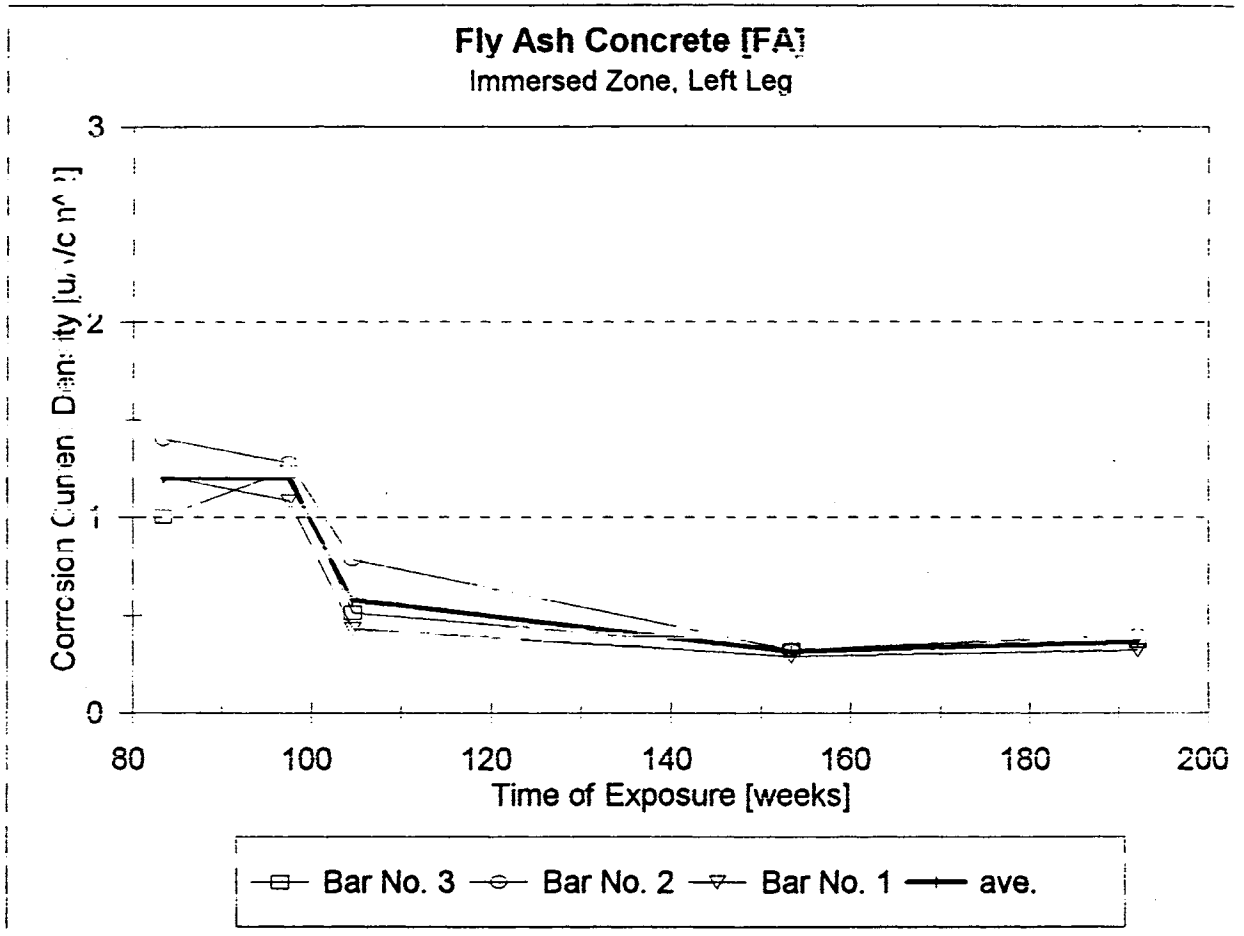


FIGURE 65. Corrosion Rates in the Immersed Zone, Left Leg, FA Specimen.

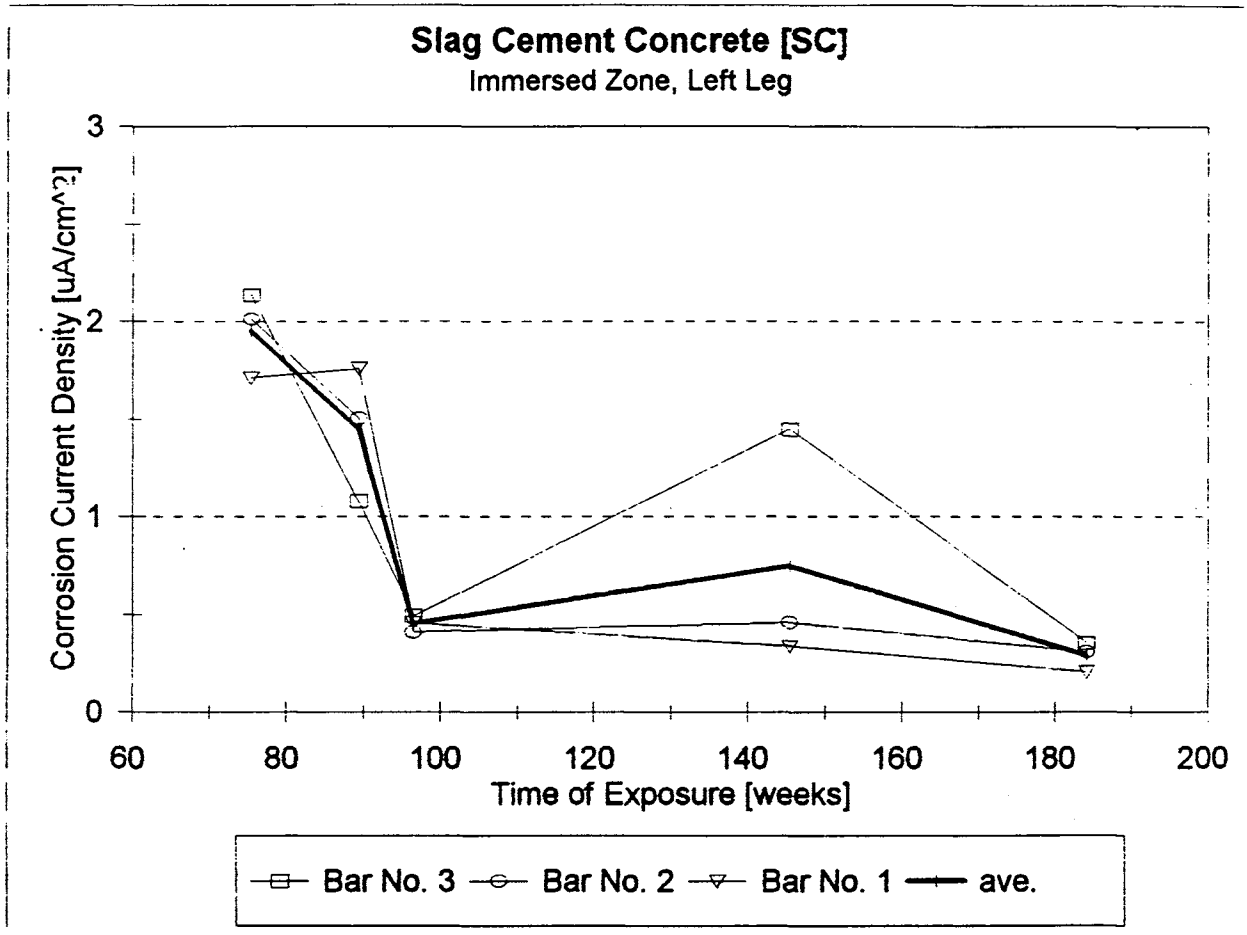


FIGURE 66. Corrosion Rates in the Immersed Zone, Left Leg, SC Specimen.

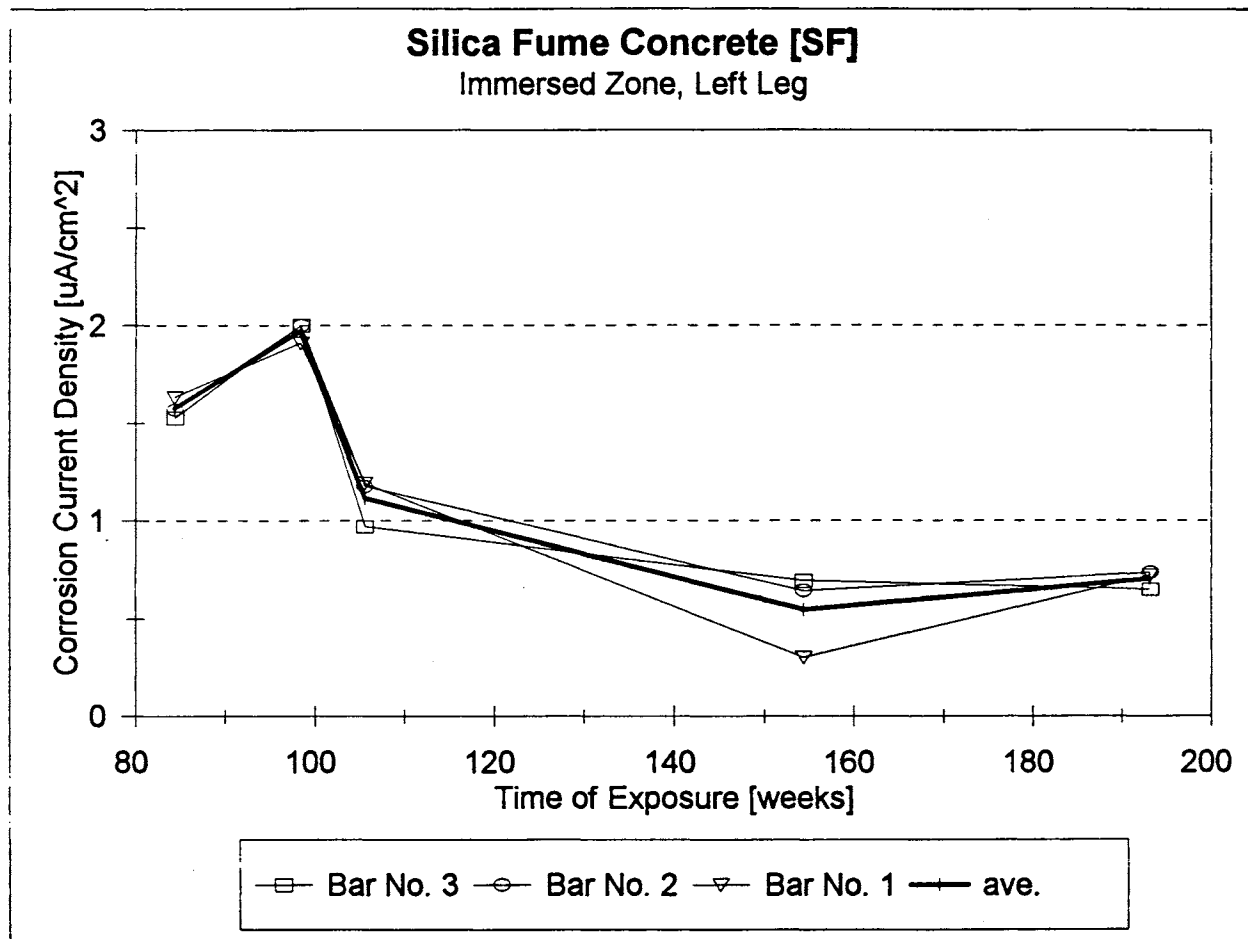


FIGURE 67. Corrosion Rates in the Immersed Zone, Left Leg, SF Specimen.

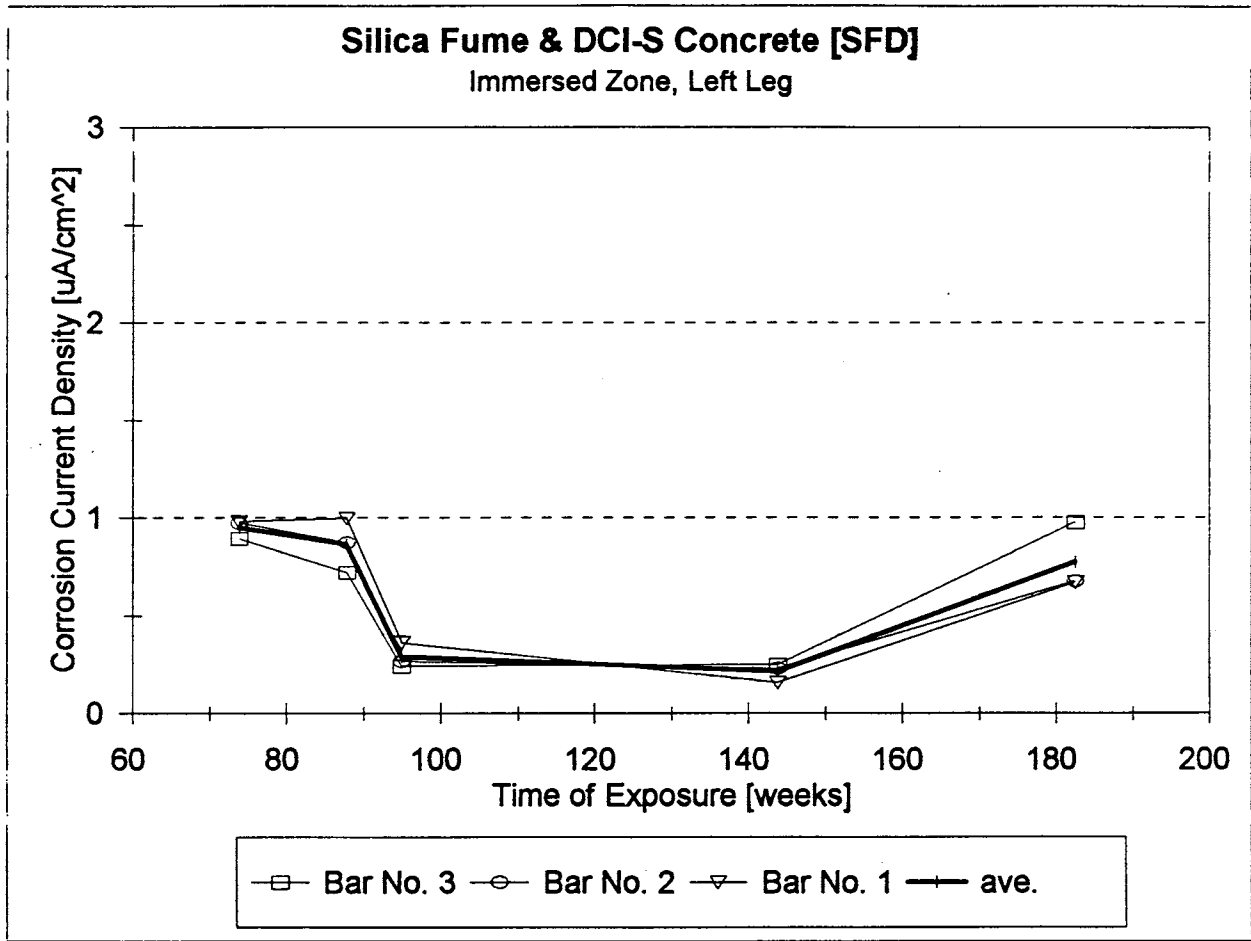


FIGURE 68. Corrosion Rates in the Immersed Zone, Left Leg, SFD Specimen.

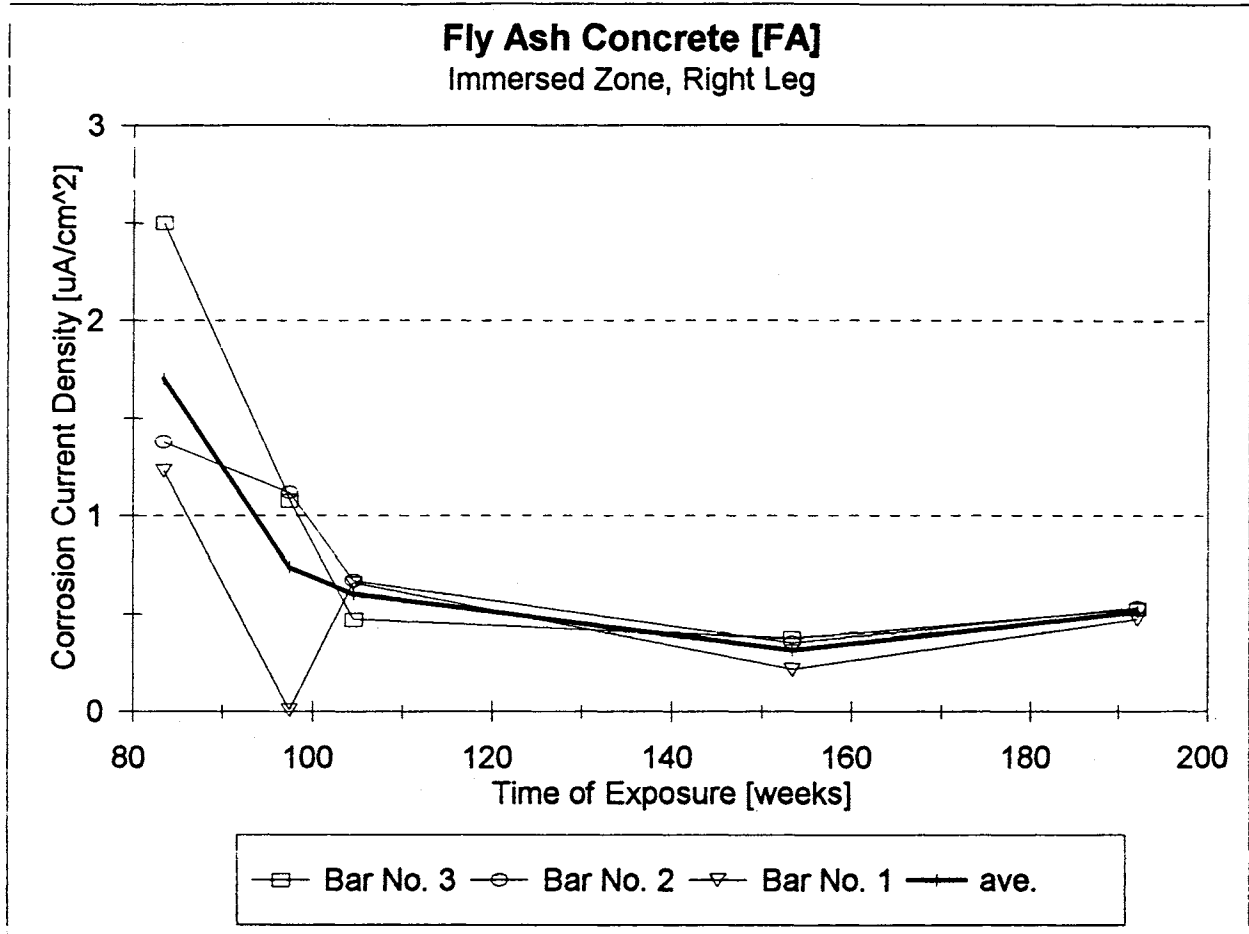


FIGURE 69. Corrosion Rates in the Immersed Zone, Right Leg, FA Specimen.

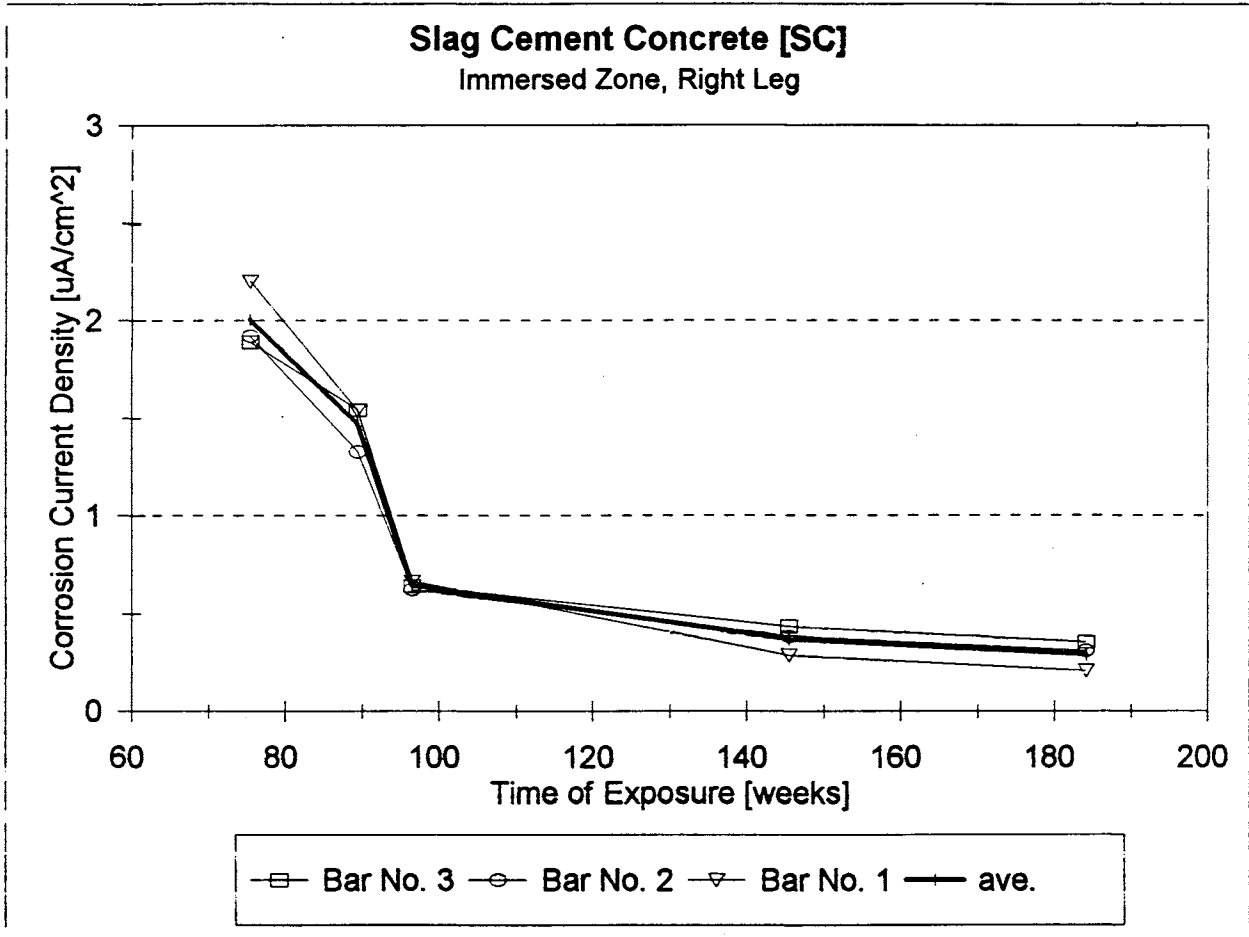


FIGURE 70. Corrosion Rates in the Immersed Zone, Right Leg, SC Specimen.

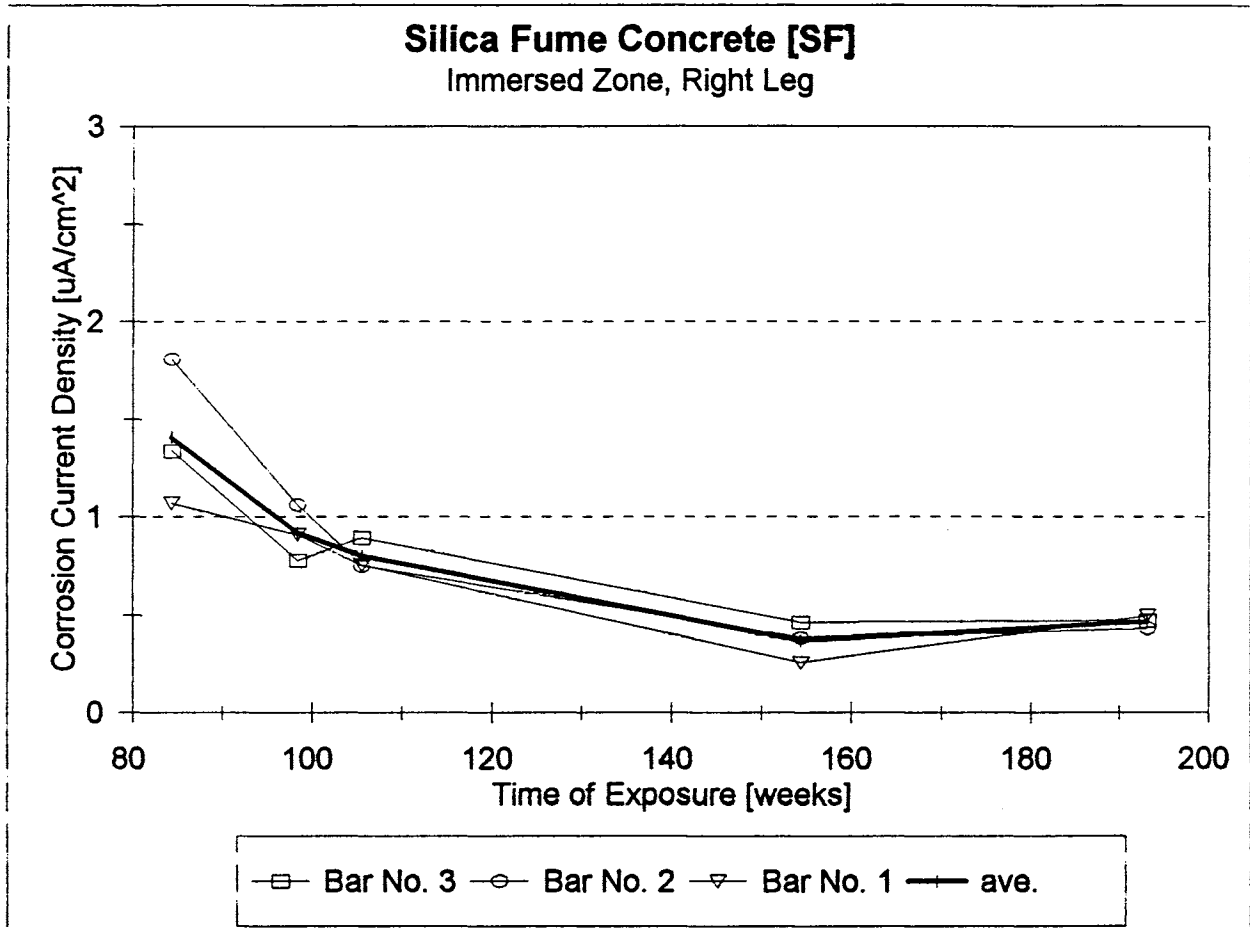


FIGURE 71. Corrosion Rates in the Immersed Zone, Right Leg, SF Specimen.

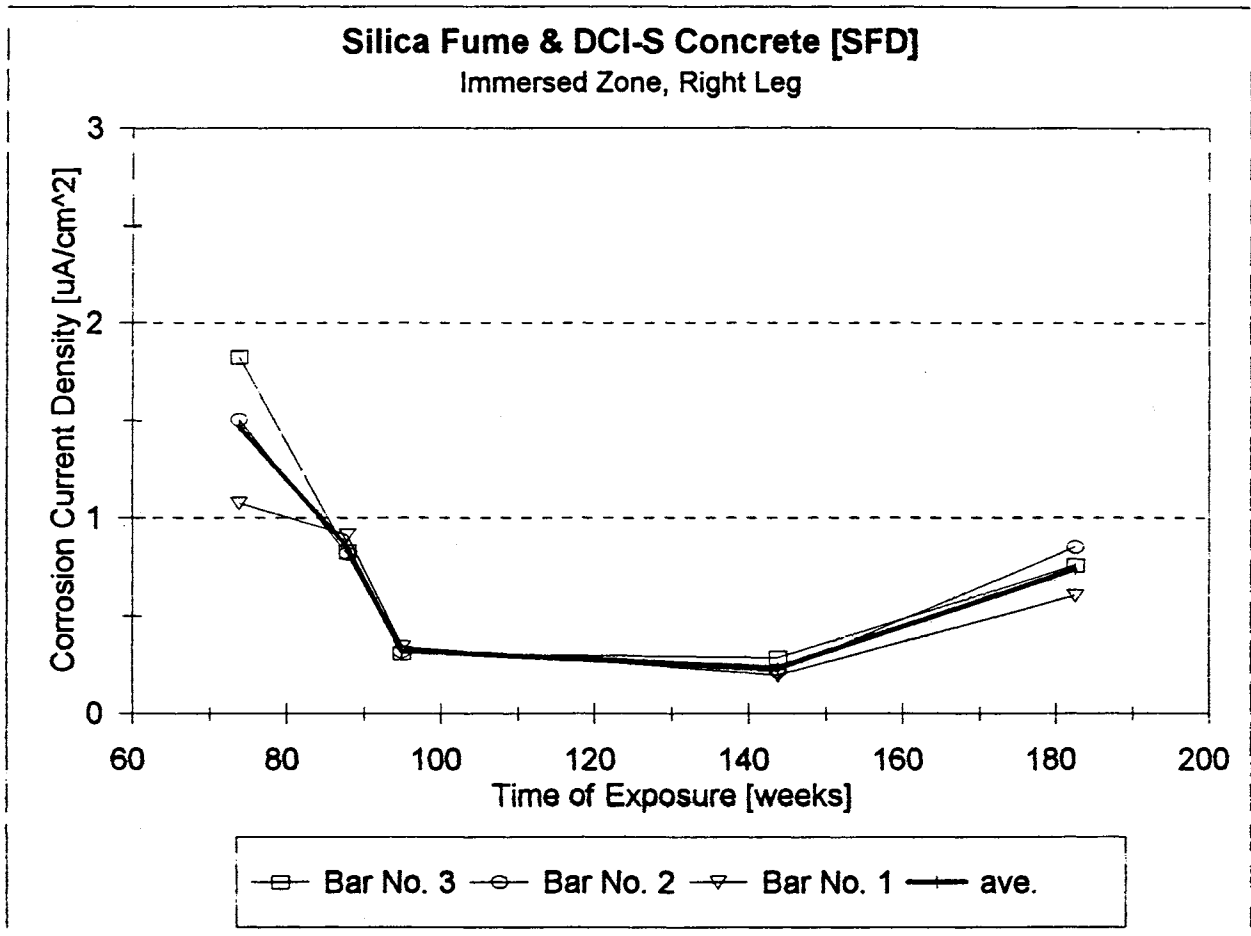


FIGURE 72. Corrosion Rates in the Immersed Zone, Right Leg, SFD Specimen.

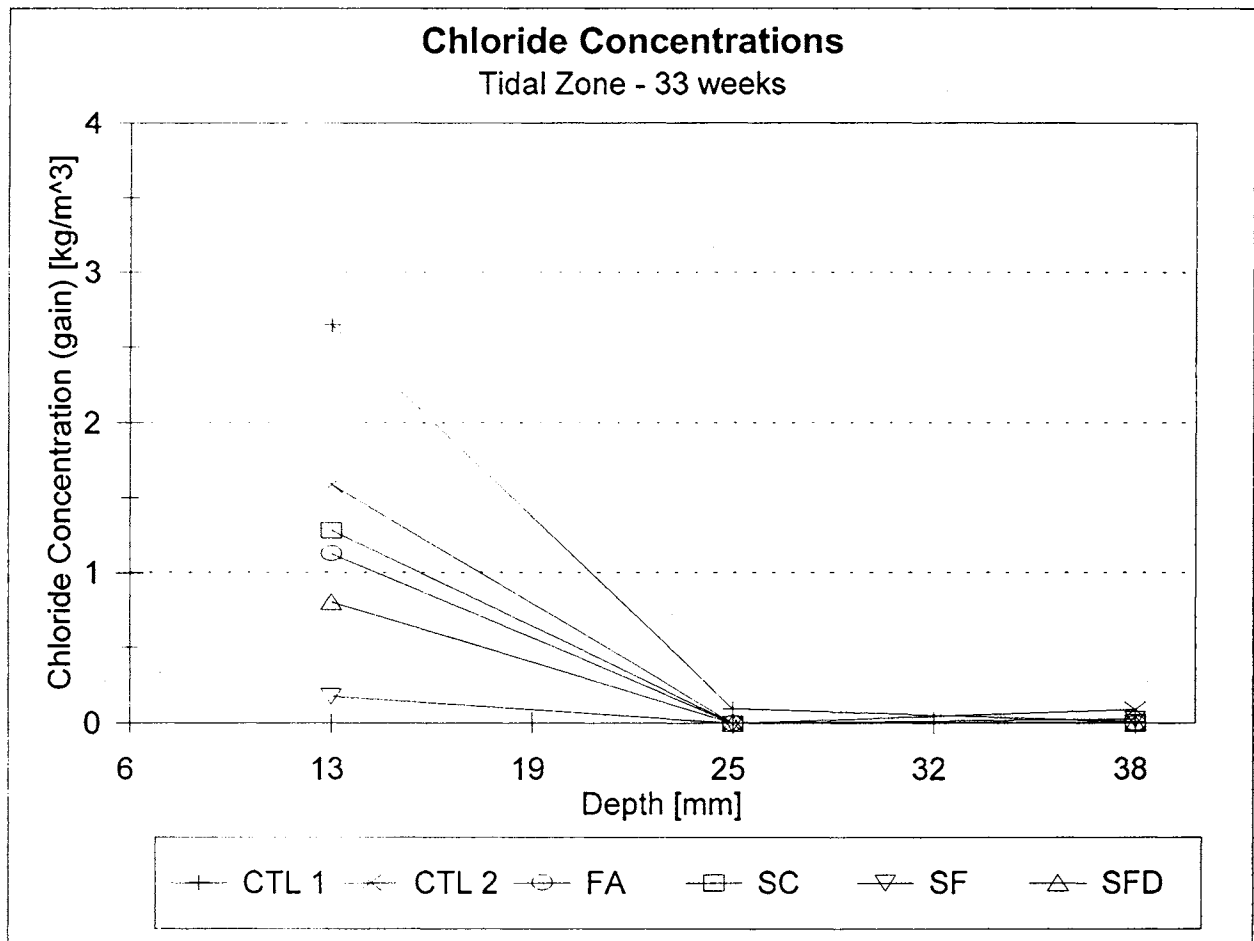


FIGURE 73. Chloride Concentrations at 33 Weeks, Tidal Zone.

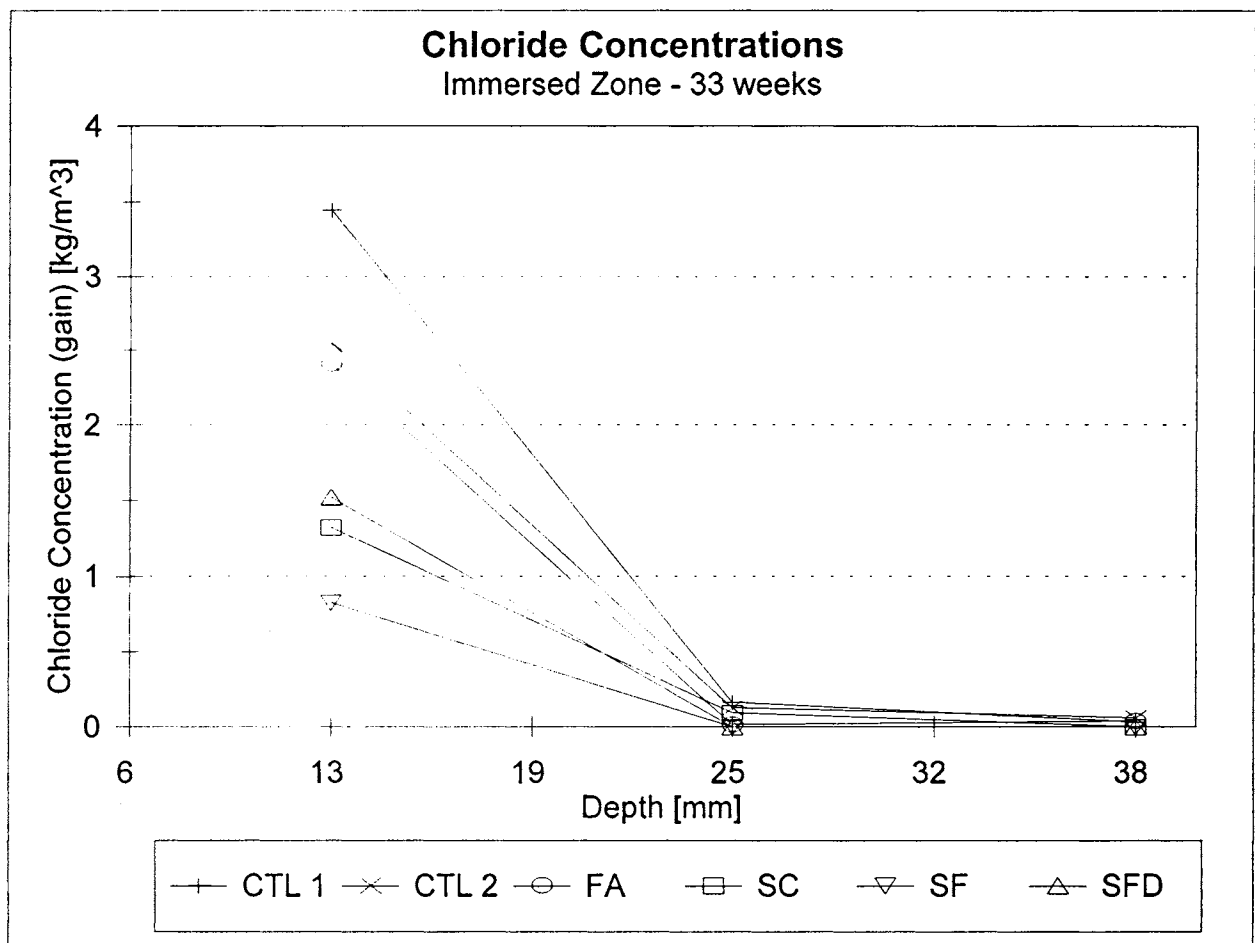


FIGURE 74. Chloride Concentrations at 33 Weeks, Immersed Zone.

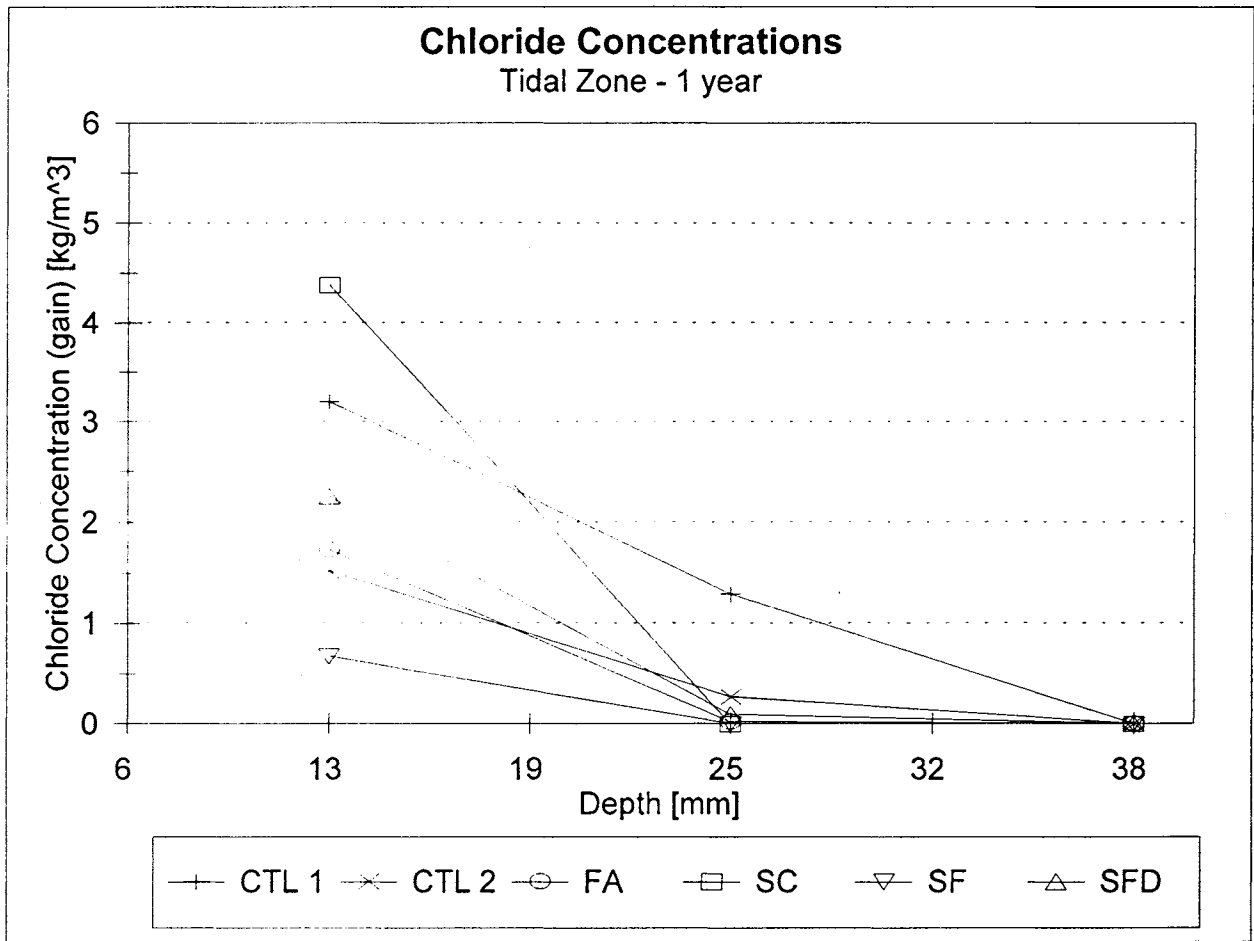


FIGURE 75. Chloride Concentrations at 1 Year, Tidal Zone.

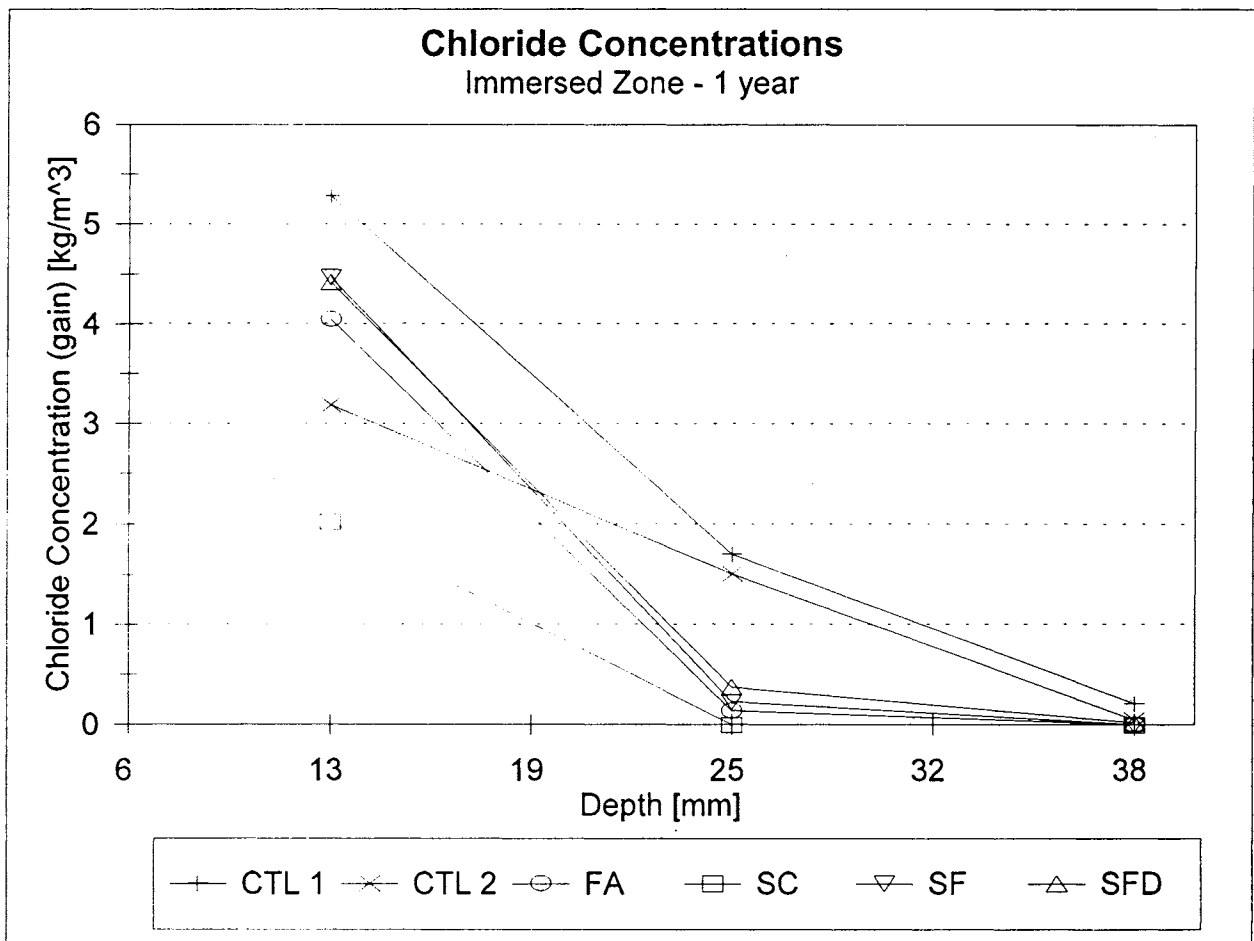


FIGURE 76. Chloride Concentrations at 1 Year, Immersed Zone.

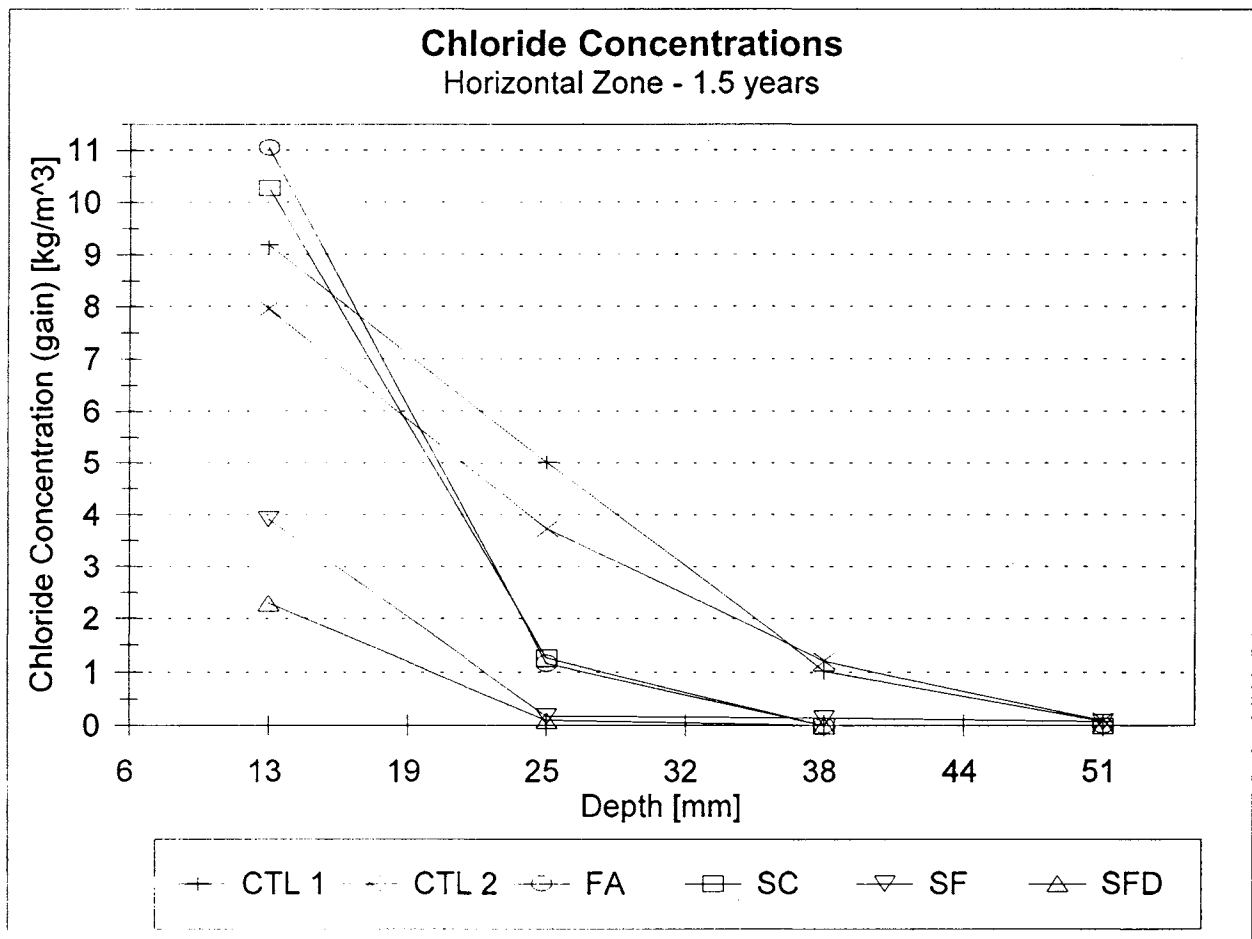


FIGURE 77. Chloride Concentrations at 1.5 Year, Horizontal Zone.

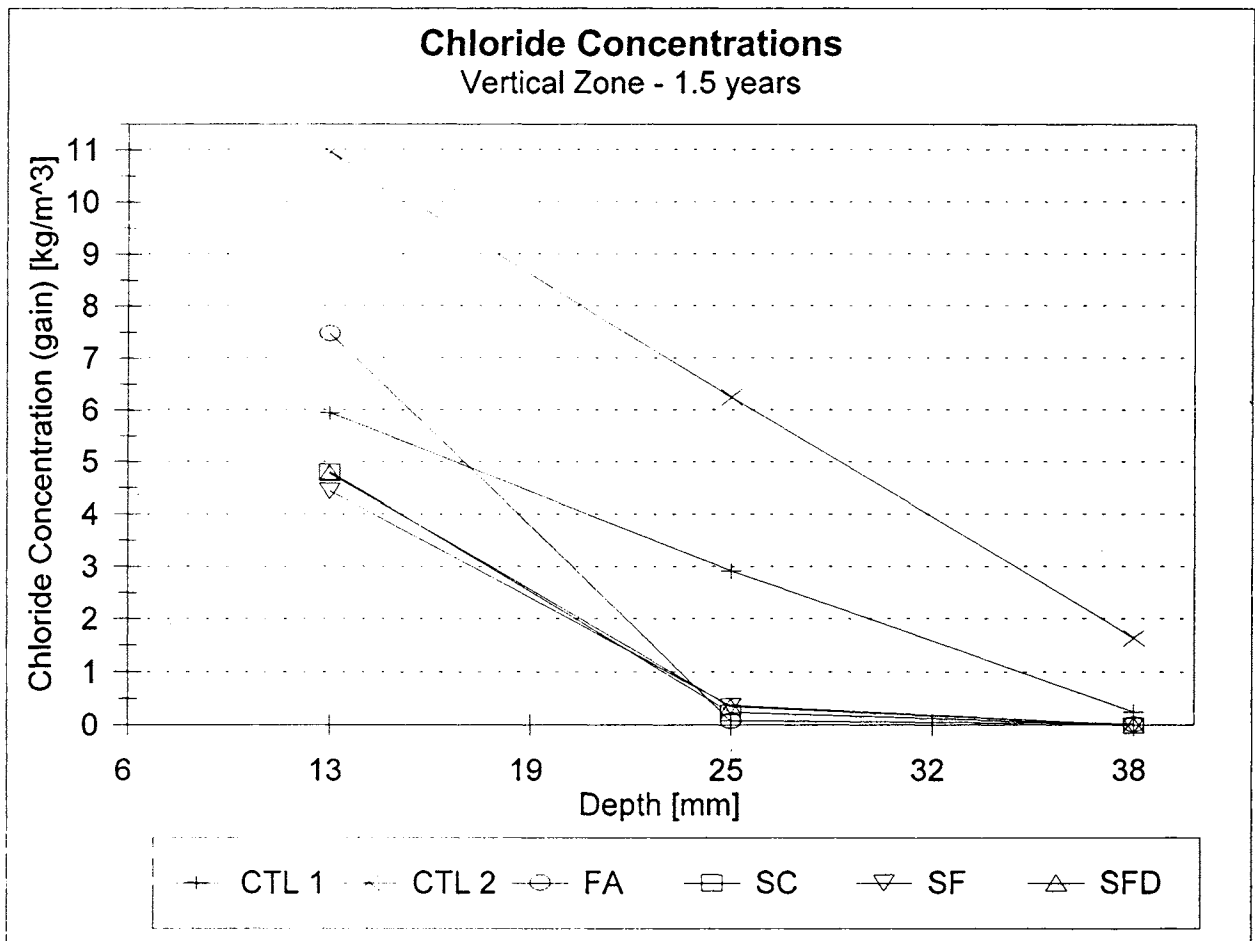


FIGURE 78. Chloride Concentrations at 1.5 Year, Vertical Zone.

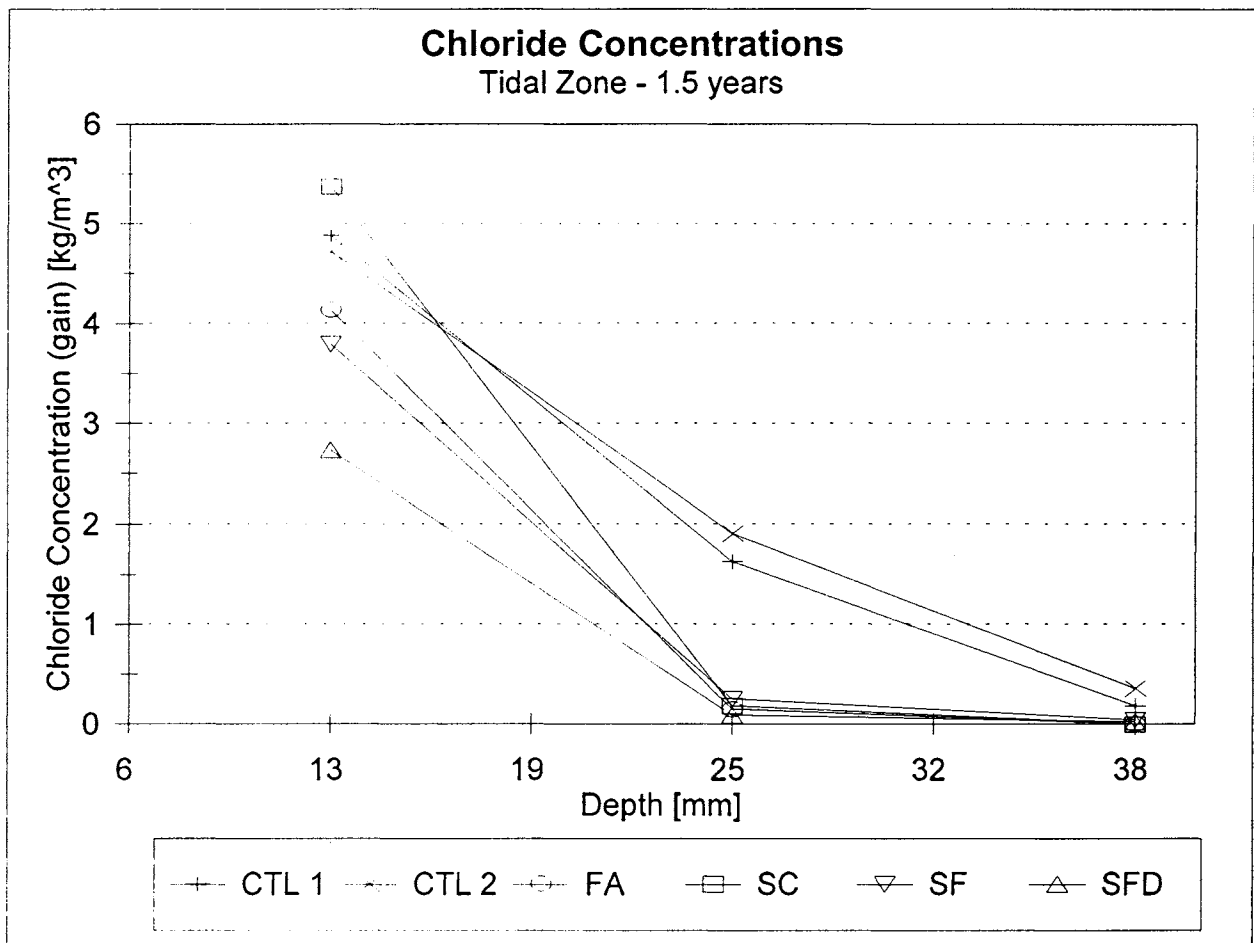


FIGURE 79. Chloride Concentrations at 1.5 Year, Tidal Zone.

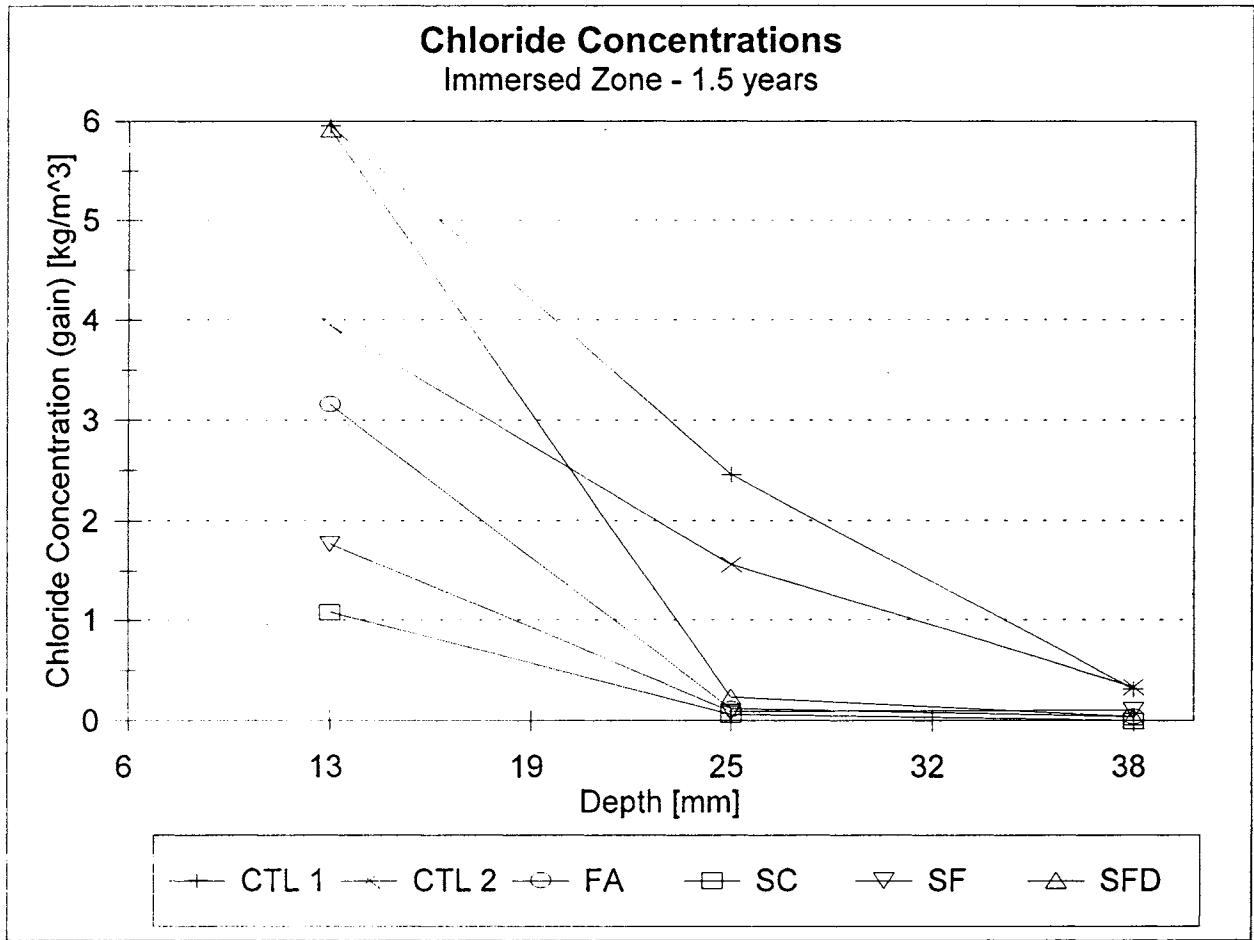


FIGURE 80. Chloride Concentrations at 1.5 Year, Immersed Zone.

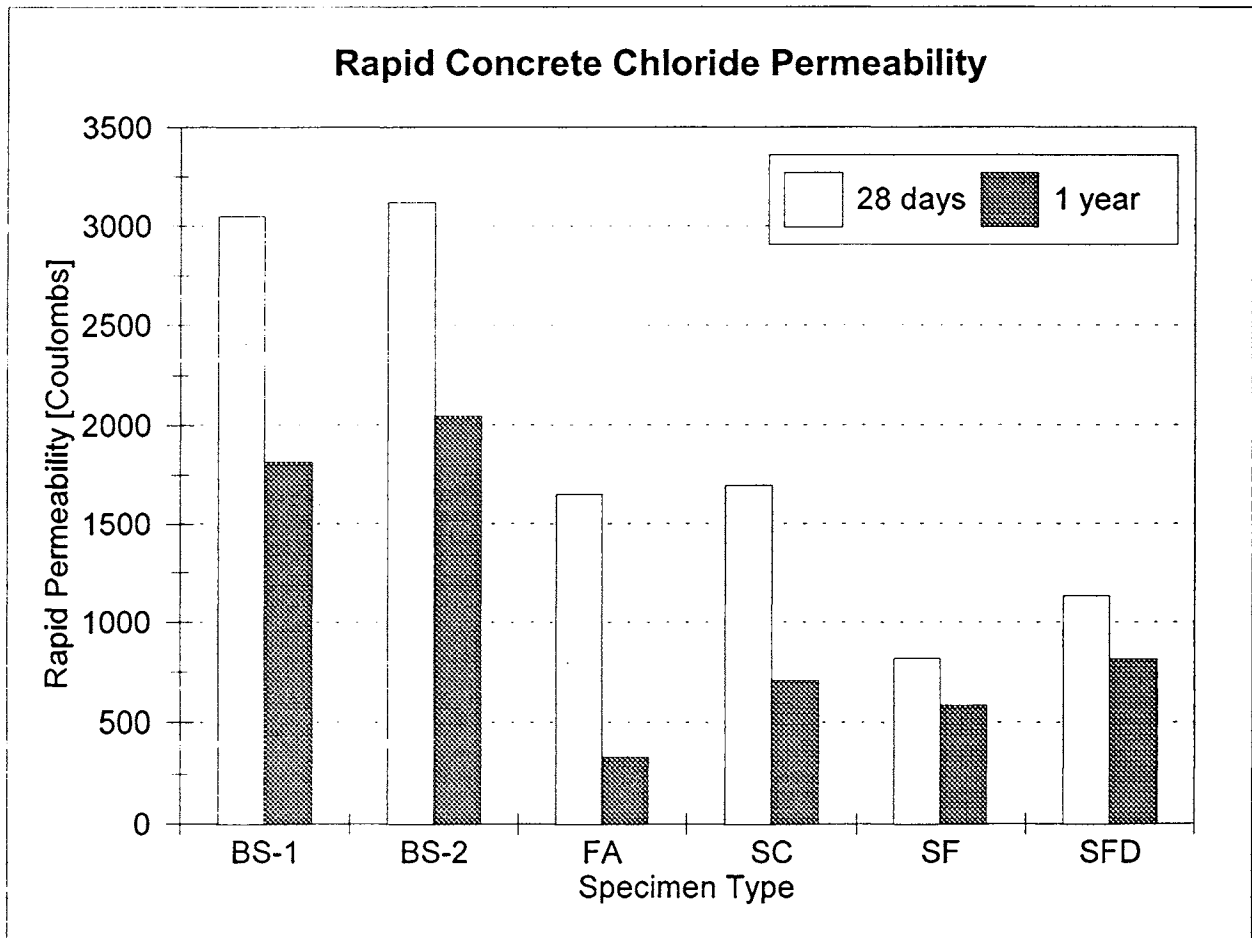


FIGURE 81. Electrical Indication of Concrete's Ability to Resist Chloride Ion Penetration @ 28 days and @ 1 year.

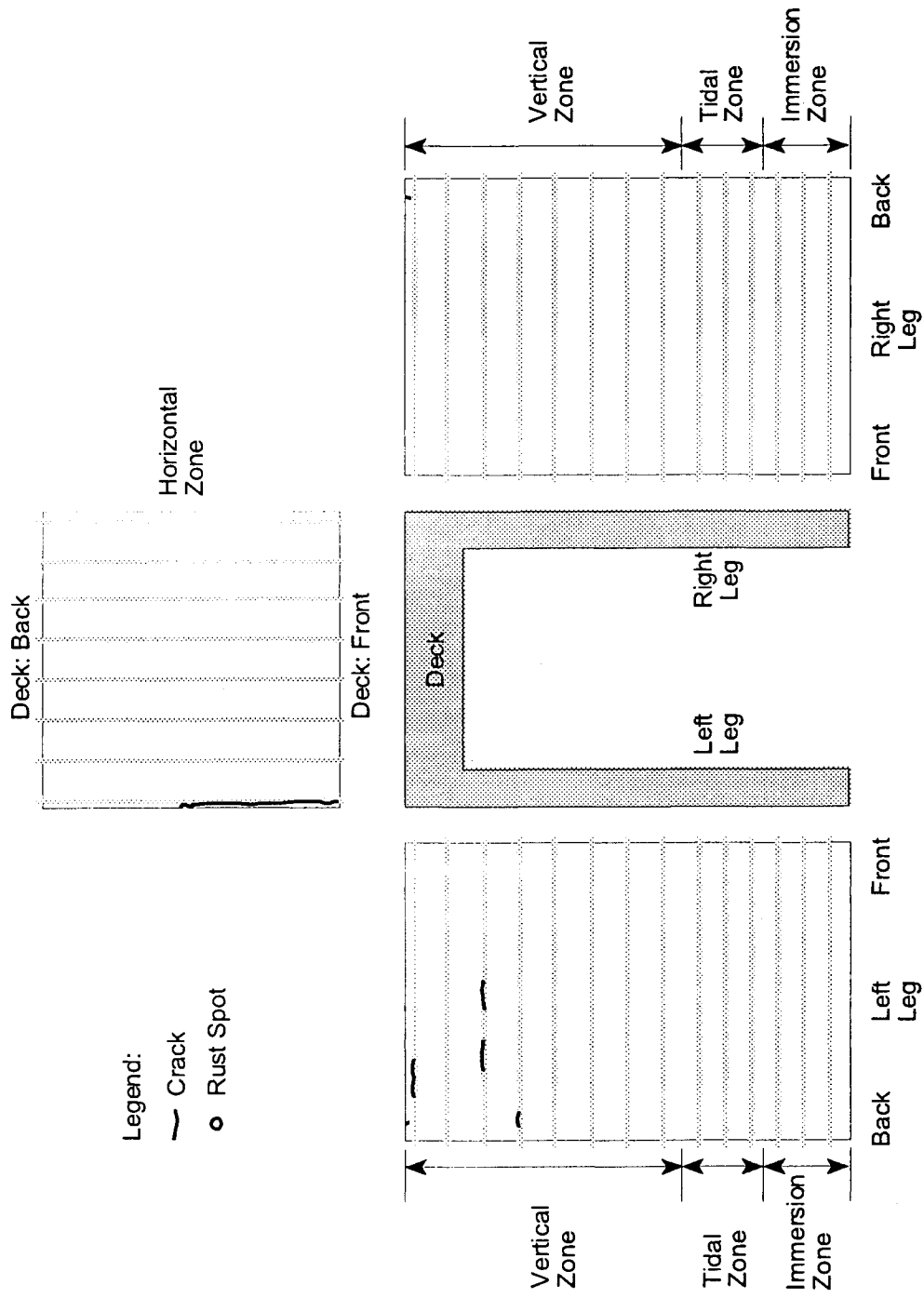


Figure 82. Visual Observations: October 1996. Cracking and Rust Spots in the BS-1 Specimen.

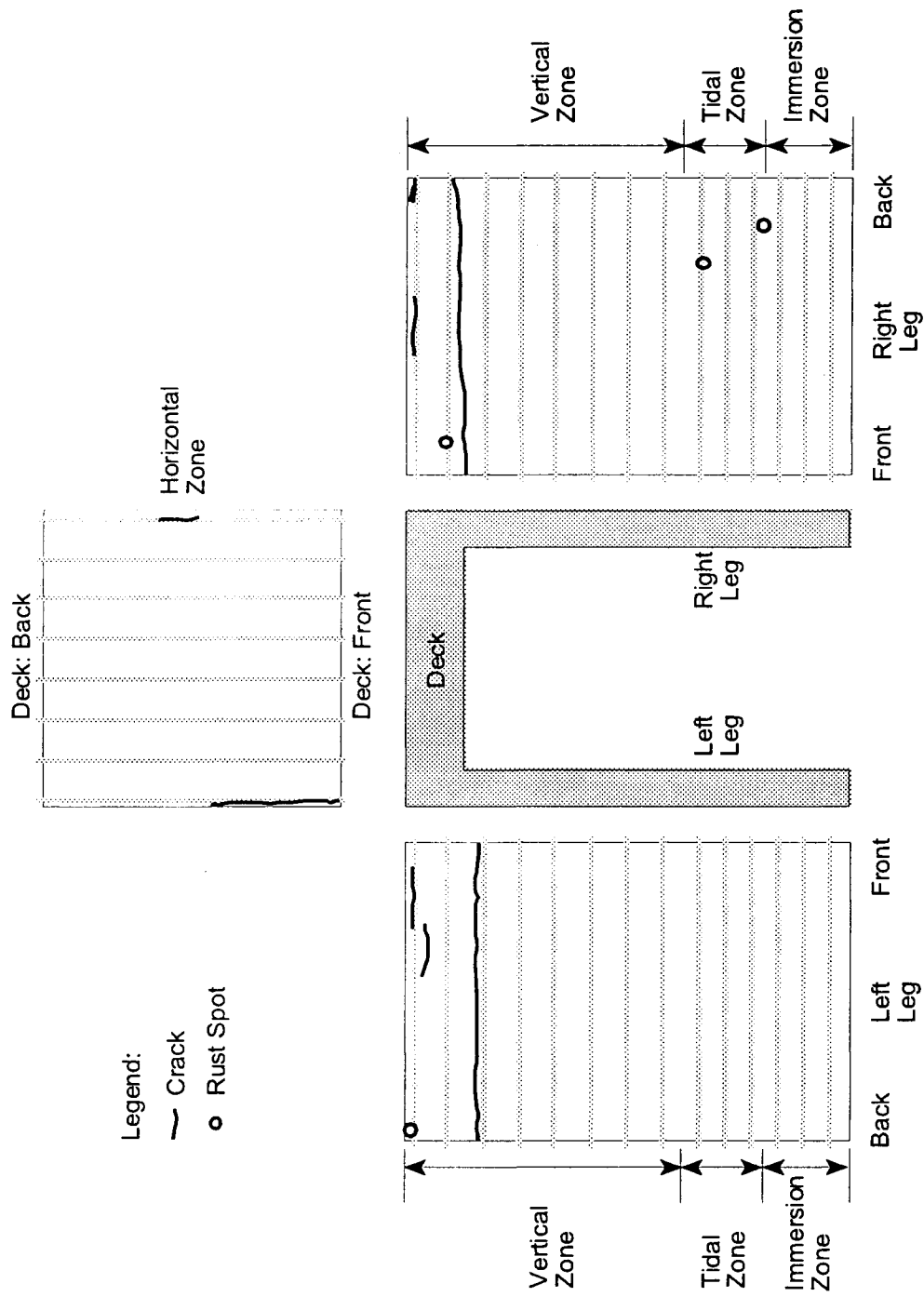


Figure 83. Visual Observations: October 1996. Cracking and Rust Spots in the BS-2 Specimen.

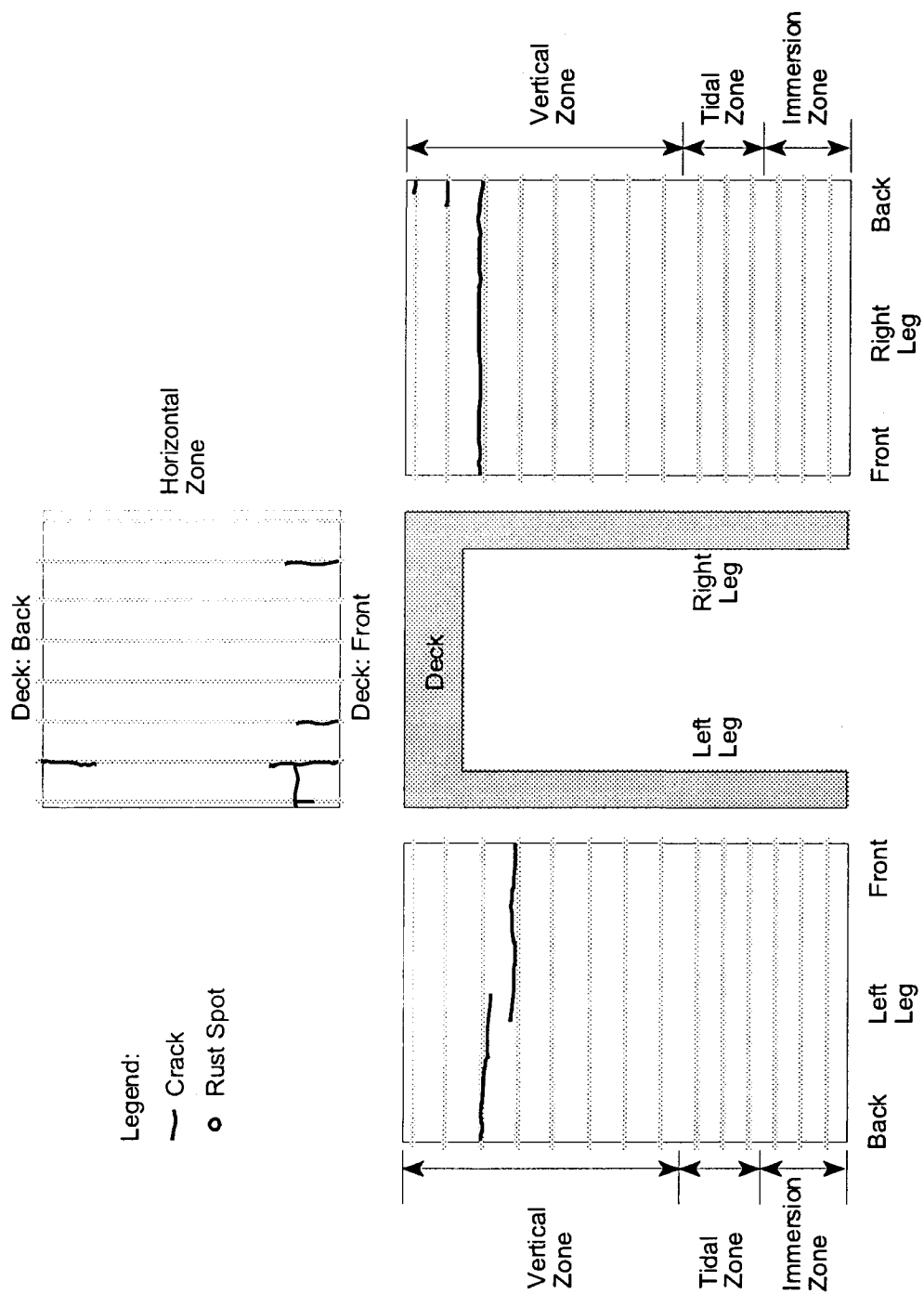


Figure 84. Visual Observations: October 1996. Cracking and Rust Spots in the FA Specimen.

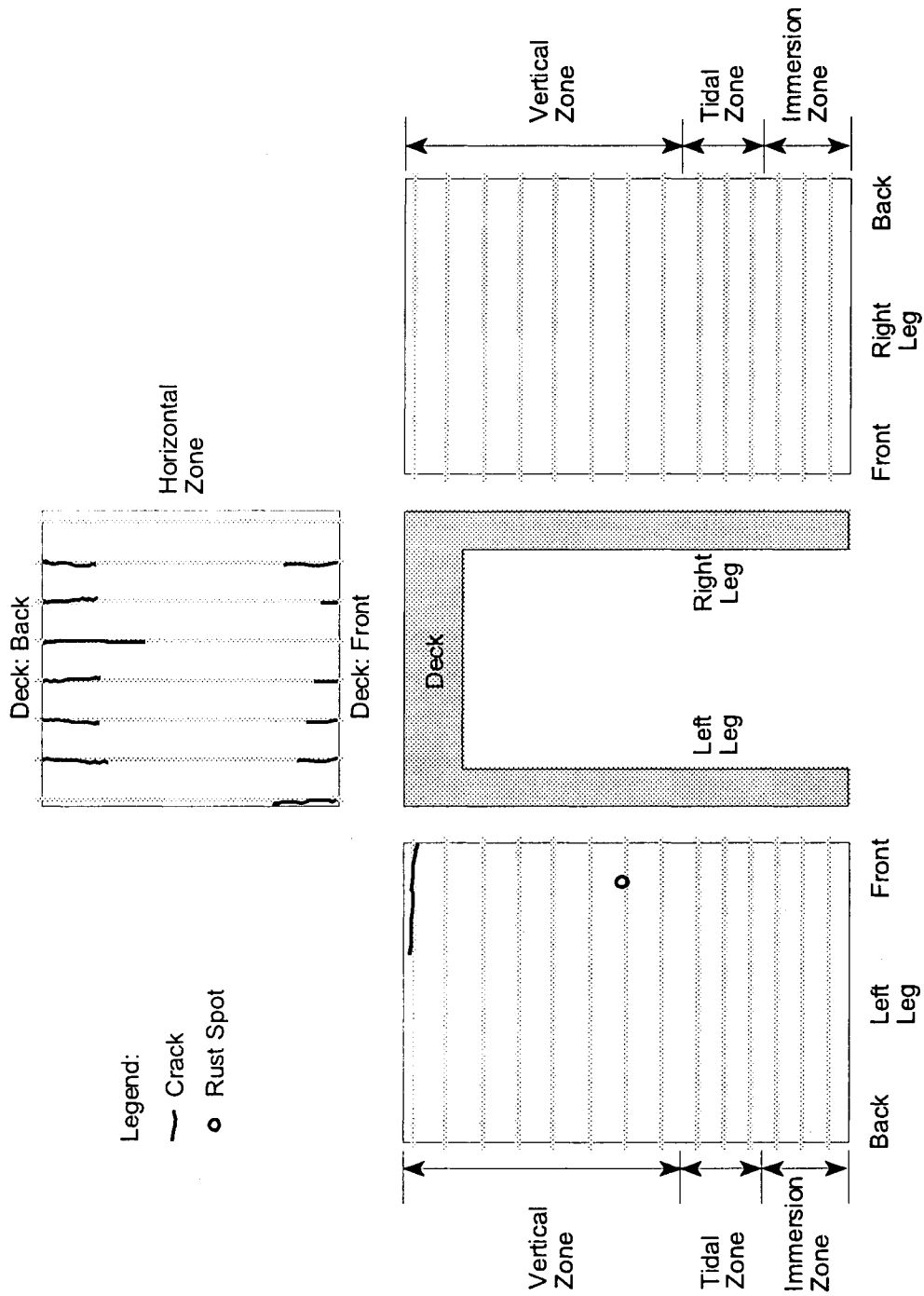


Figure 85. Visual Observations: October 1996. Cracking and Rust Spots in the SC Specimen.

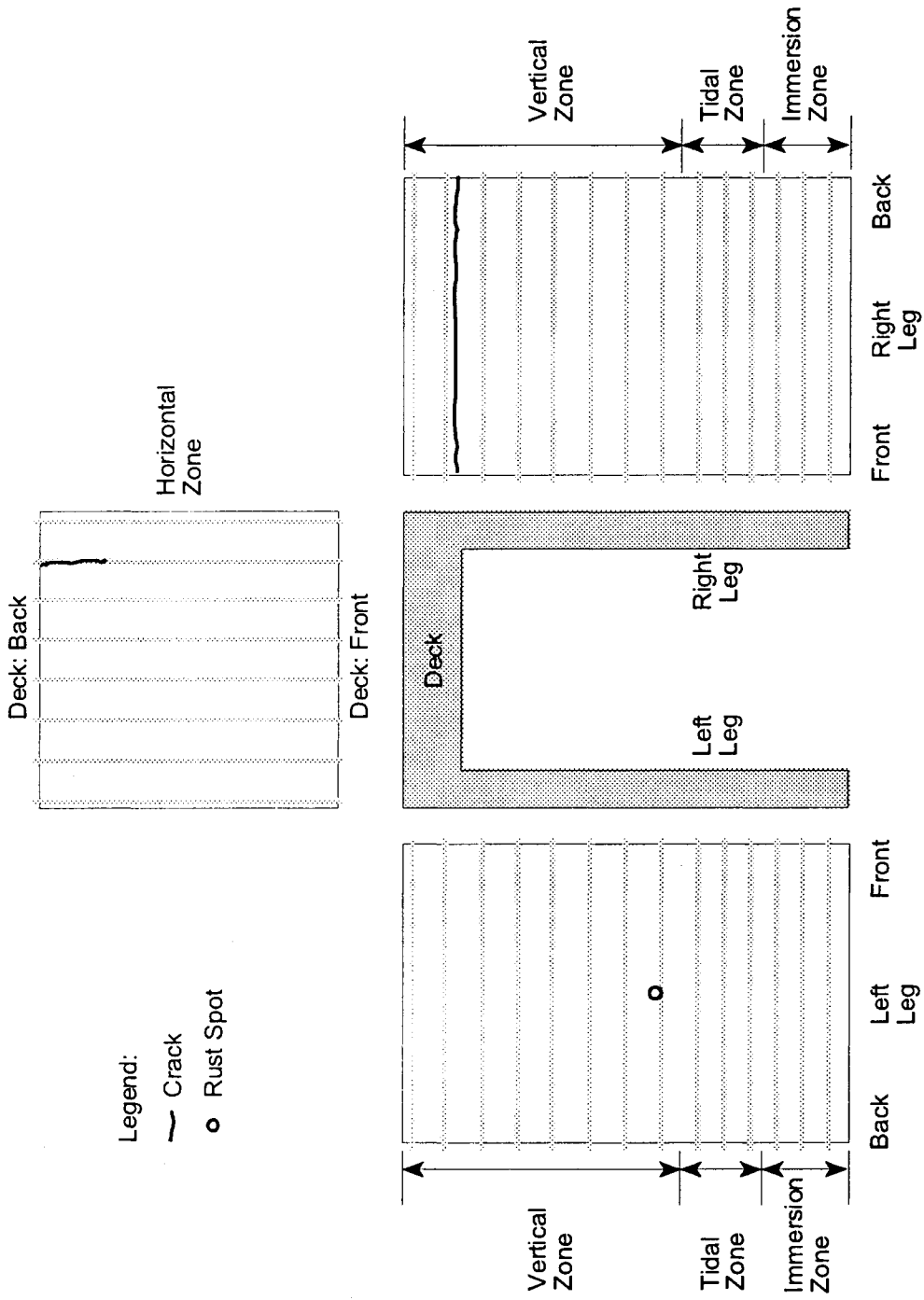


Figure 86. Visual Observations: October 1996. Cracking and Rust Spots in the SF Specimen.

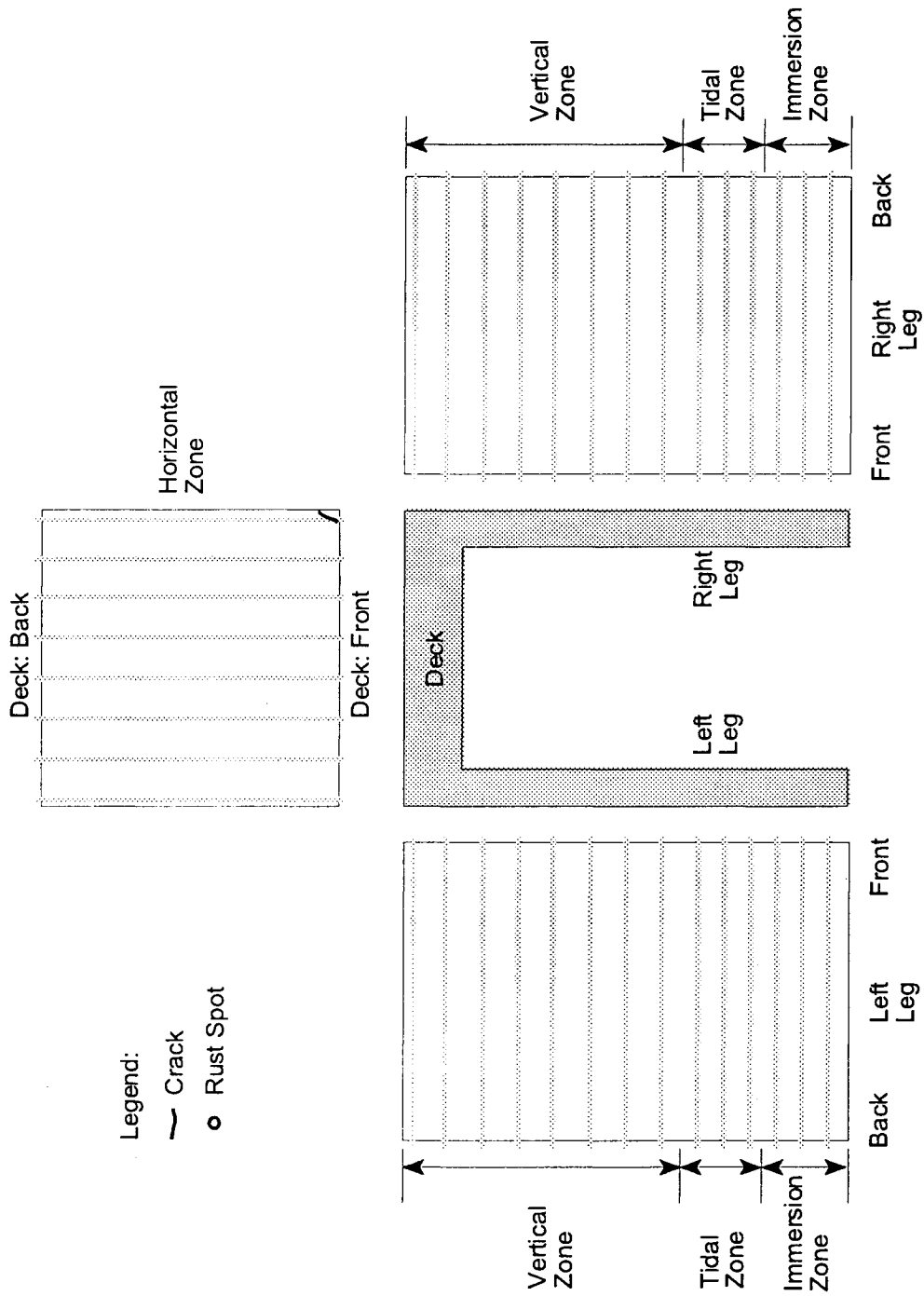


Figure 87. Visual Observations: October 1996. Cracking and Rust Spots in the SFD Specimen.

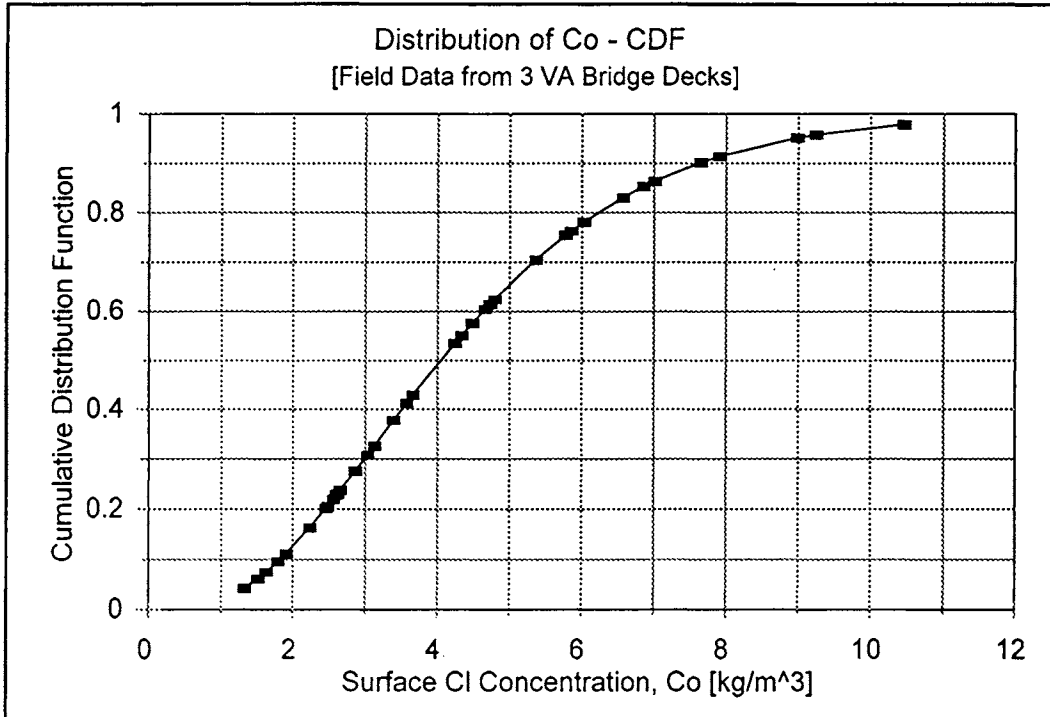


FIGURE 88. Cumulative Distribution Function (CDF) of Surface Chloride Concentration, Gamma Distribution, ($\alpha = 3.56$, $\beta = 1.25$).

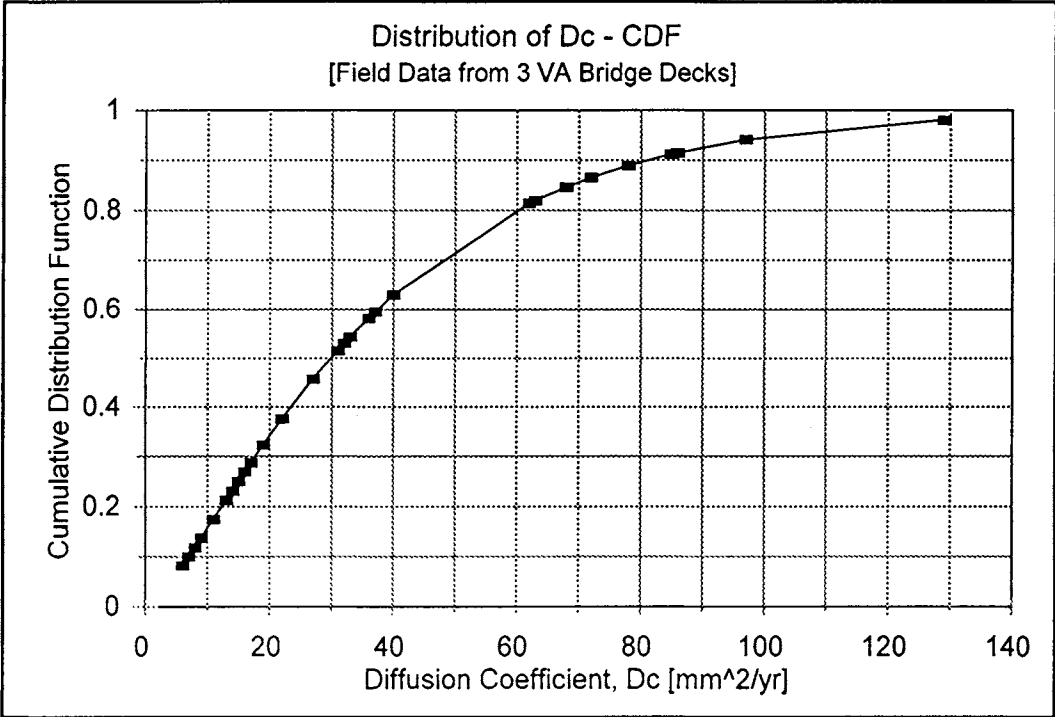


FIGURE 89. Cumulative Distribution Function (CDF) of Diffusion Coefficient, Gamma Distribution, ($\alpha = 1.42$, $\beta = 27.1$).

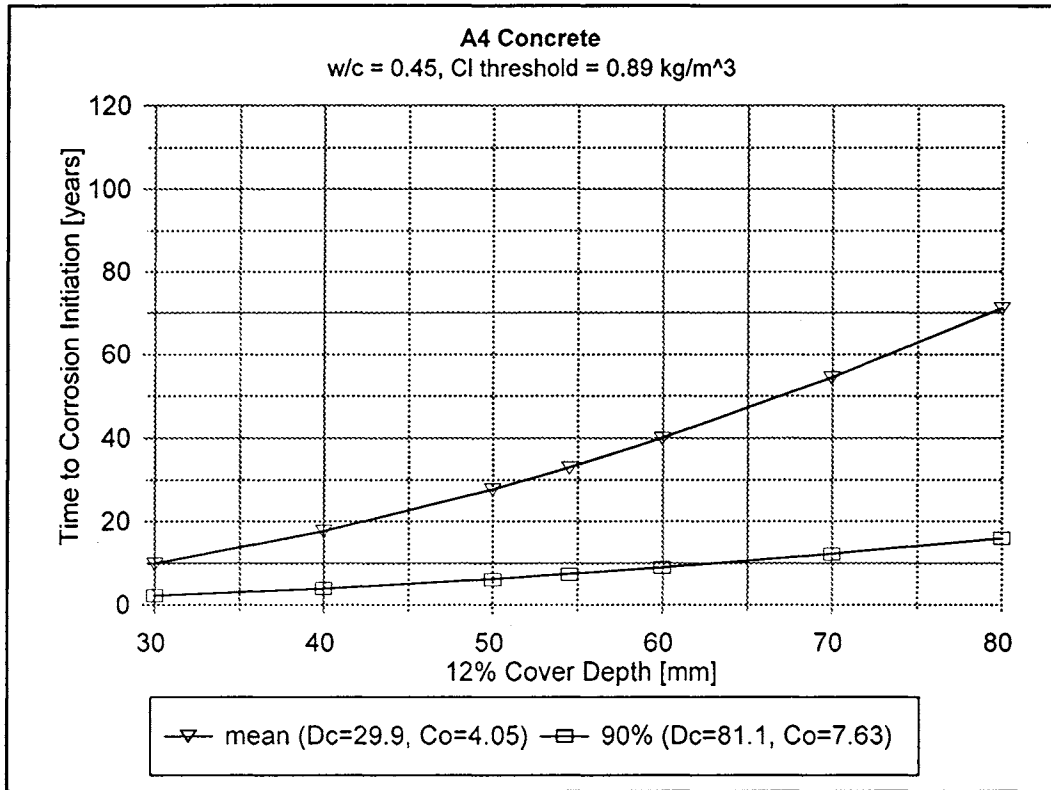


FIGURE 90. Predicted Time to Corrosion Initiation for A4 Concrete, w/c = 0.45, Chloride Threshold = 0.89 kg/m³.

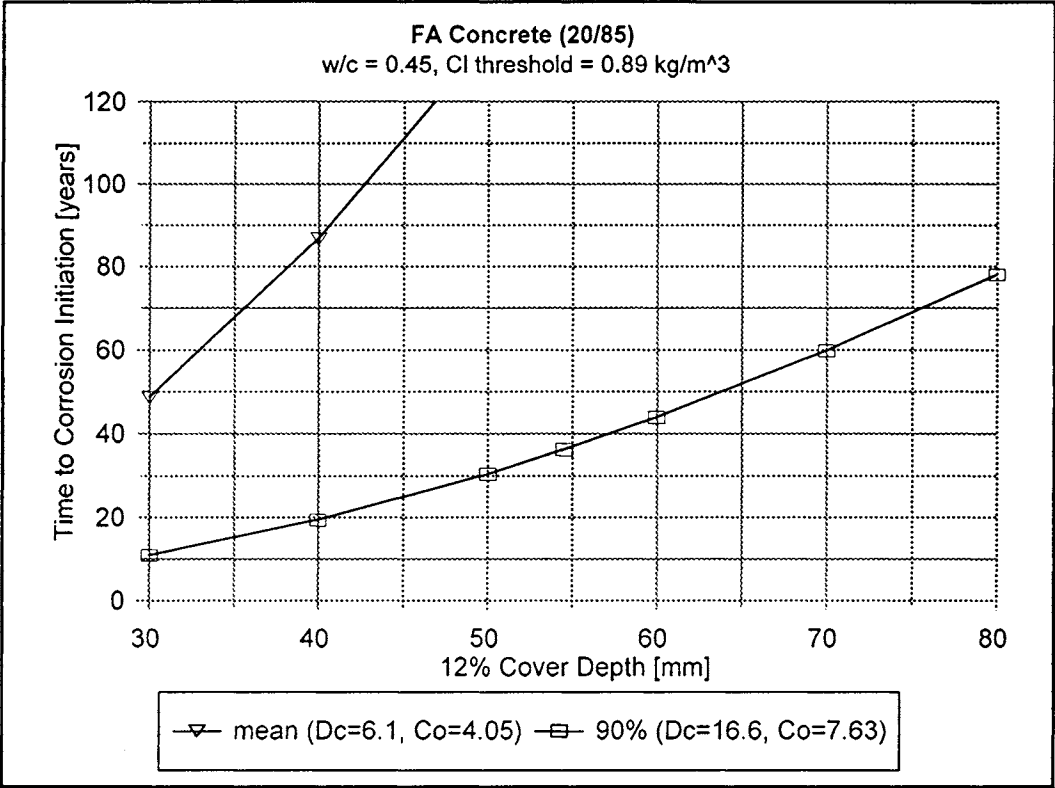


FIGURE 91. Predicted Time to Corrosion Initiation for FA Concrete (20/85), w/cm = 0.45, Chloride Threshold = 0.89 kg/m³.

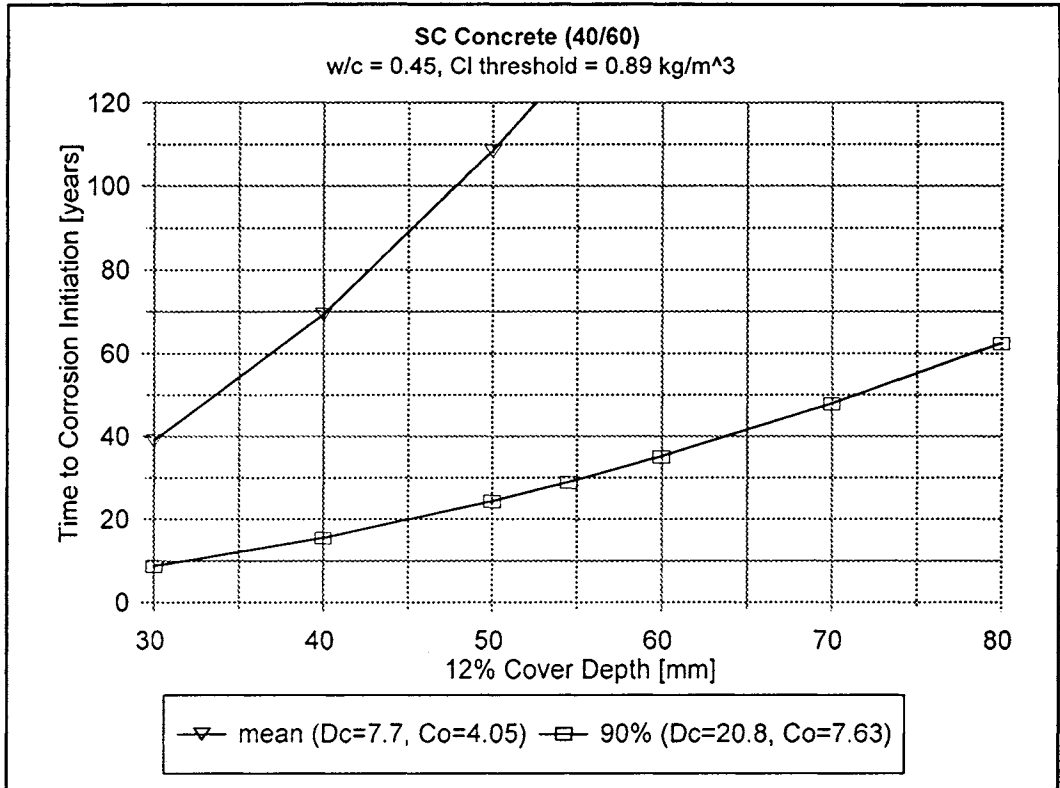


FIGURE 92. Predicted Time to Corrosion Initiation for SC Concrete (40/60), w/cm = 0.45, Chloride Threshold = 0.89 kg/m³.

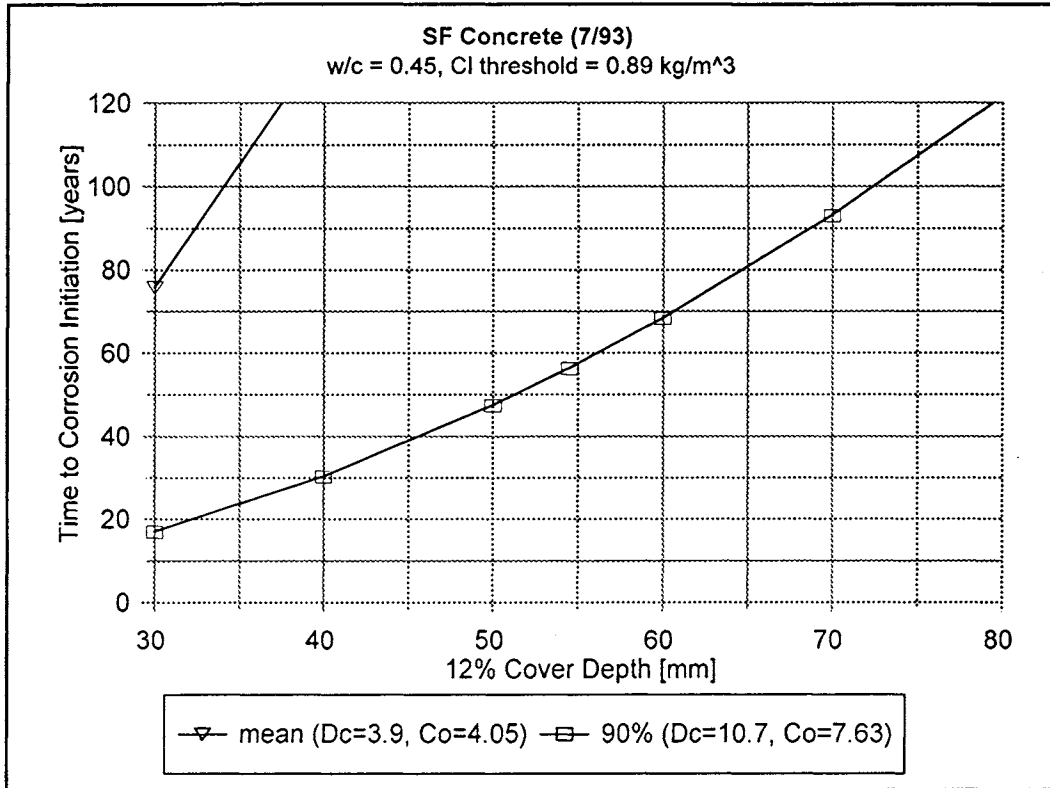


FIGURE 93. Predicted Time to Corrosion Initiation for SF Concrete (7/93), w/cm = 0.45, Chloride Threshold = 0.89 kg/m³.

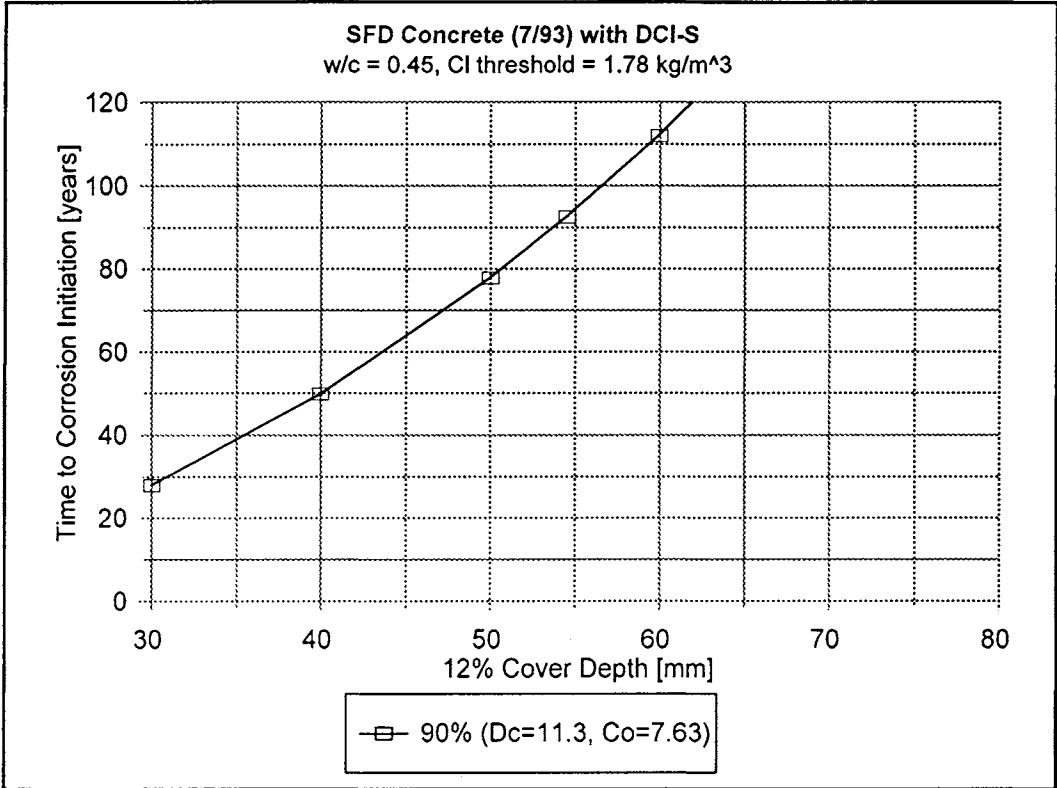


FIGURE 94. Predicted Time to Corrosion Initiation for SFD Concrete (7/93), w/cm = 0.45, Chloride Threshold = 1.78 kg/m³.

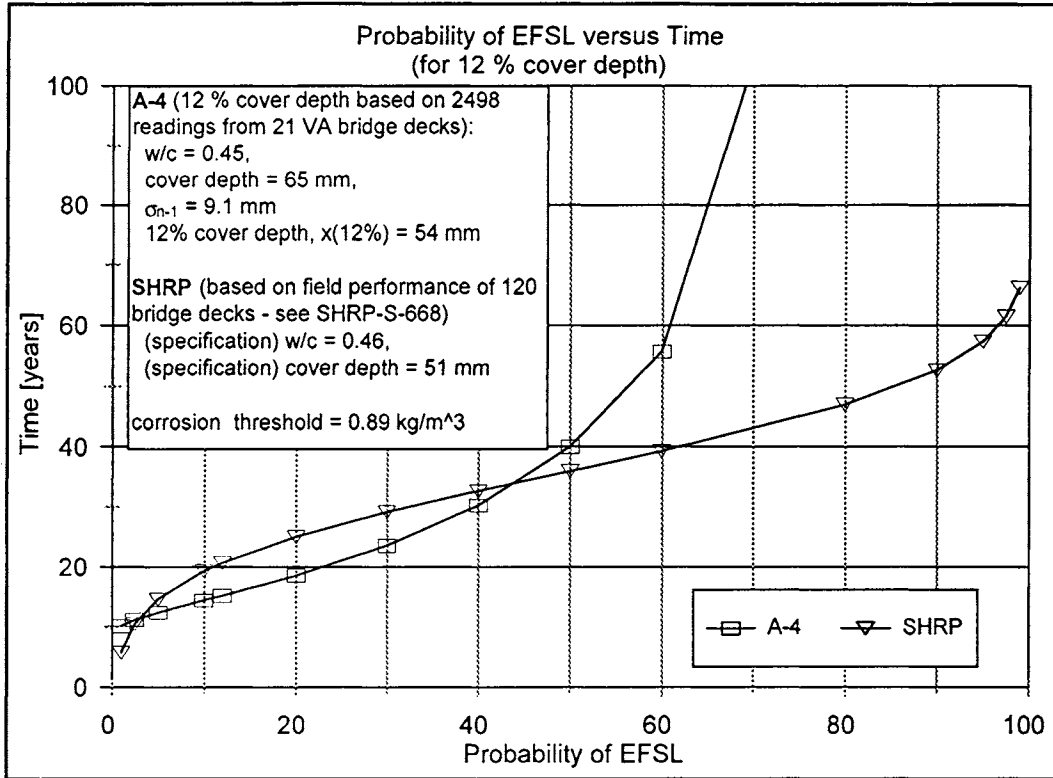


FIGURE 95. Probability of End of Functional Service Life for A4 Concrete: Comparison Between Field Performance (SHRP) and Predictions from Field Data (A-4).

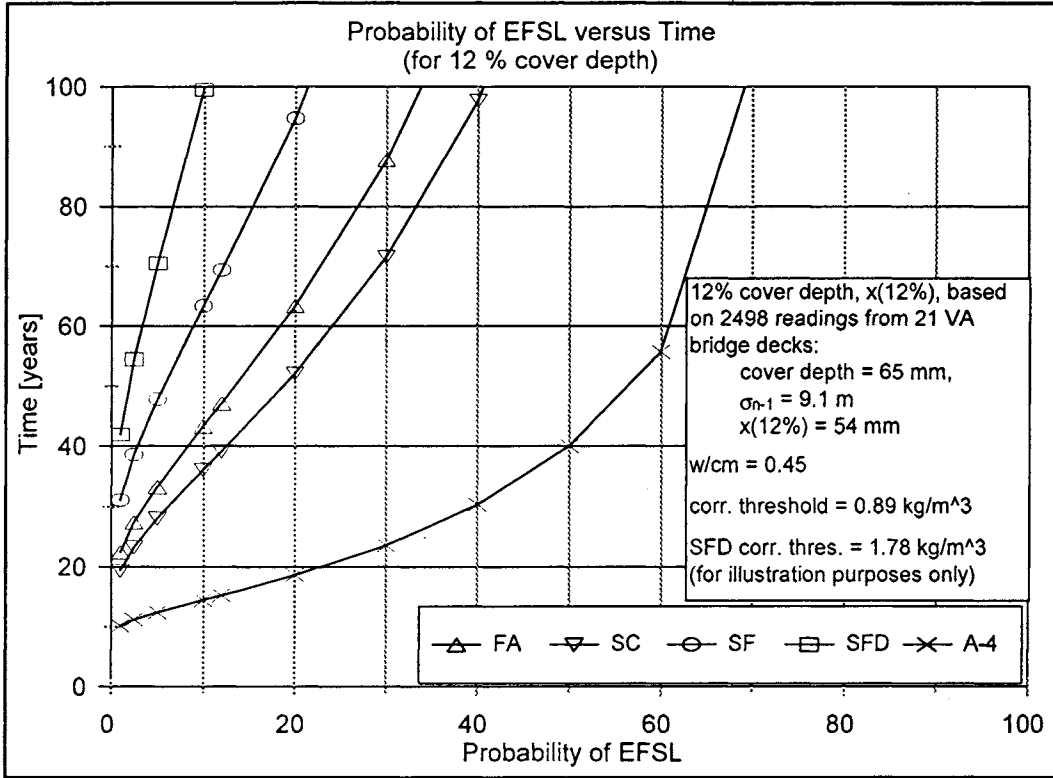


FIGURE 96. Probability of End of Functional Service Life for LP Concretes versus A4 Concrete: Predictions from Laboratory and Field Data.

APPENDIX

Average Corrosion Potentials for the Deck and Left and Right Legs of Specimens

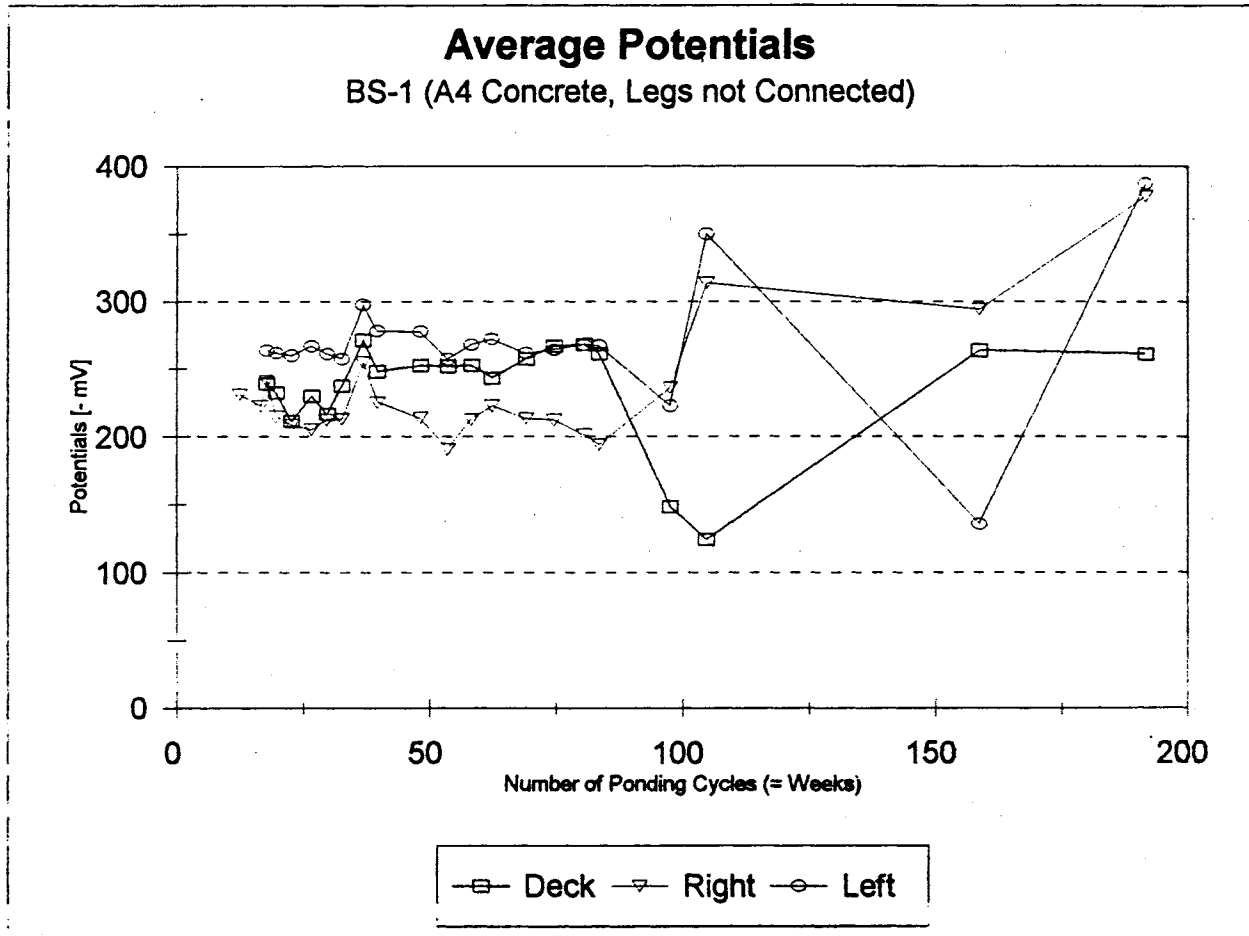


Figure A1. Average Potentials for BS-1 Specimen

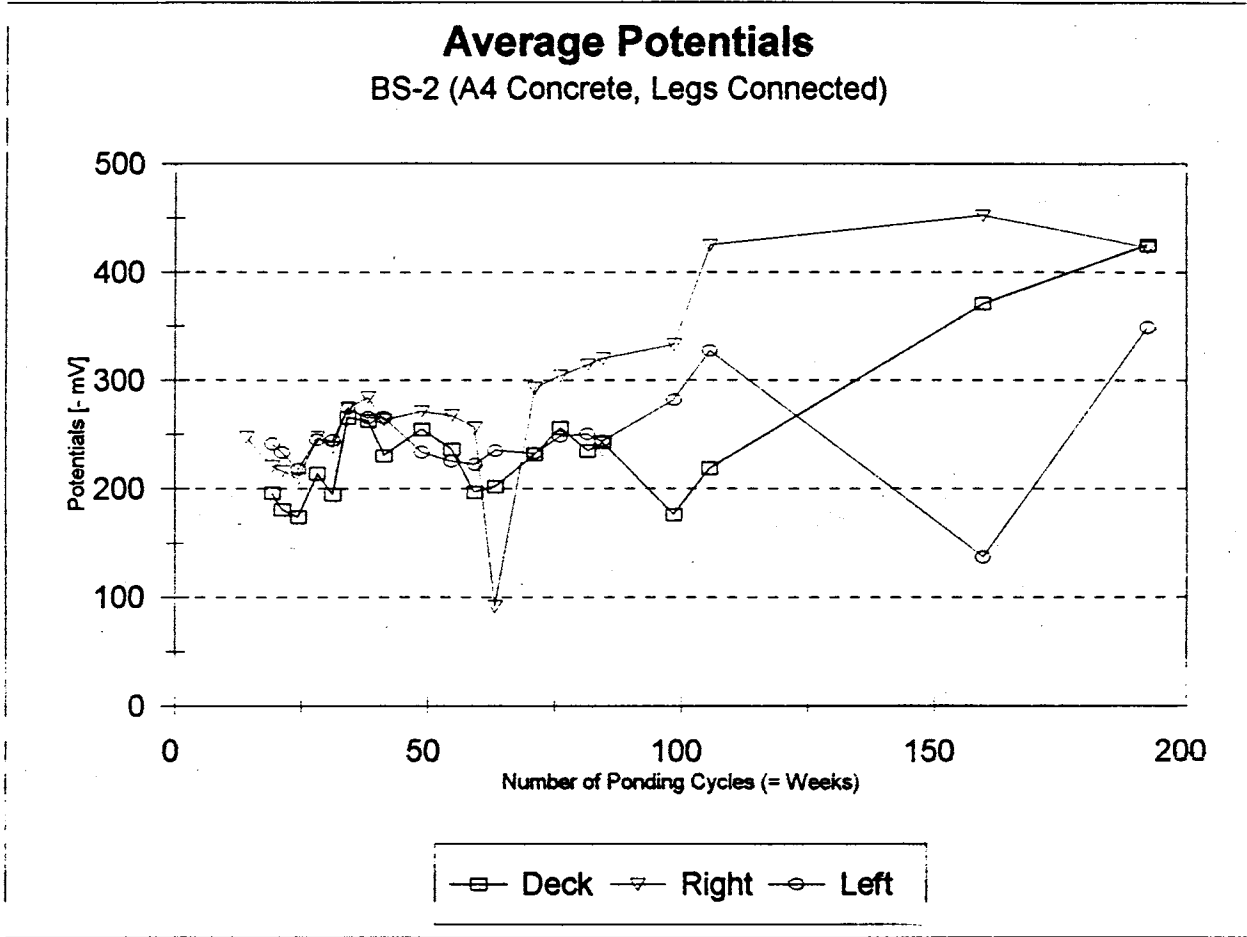


Figure A2. Average Potentials for BS-2 Specimen

Average Potentials BS-3 (Fly Ash, L. Leg Connected)

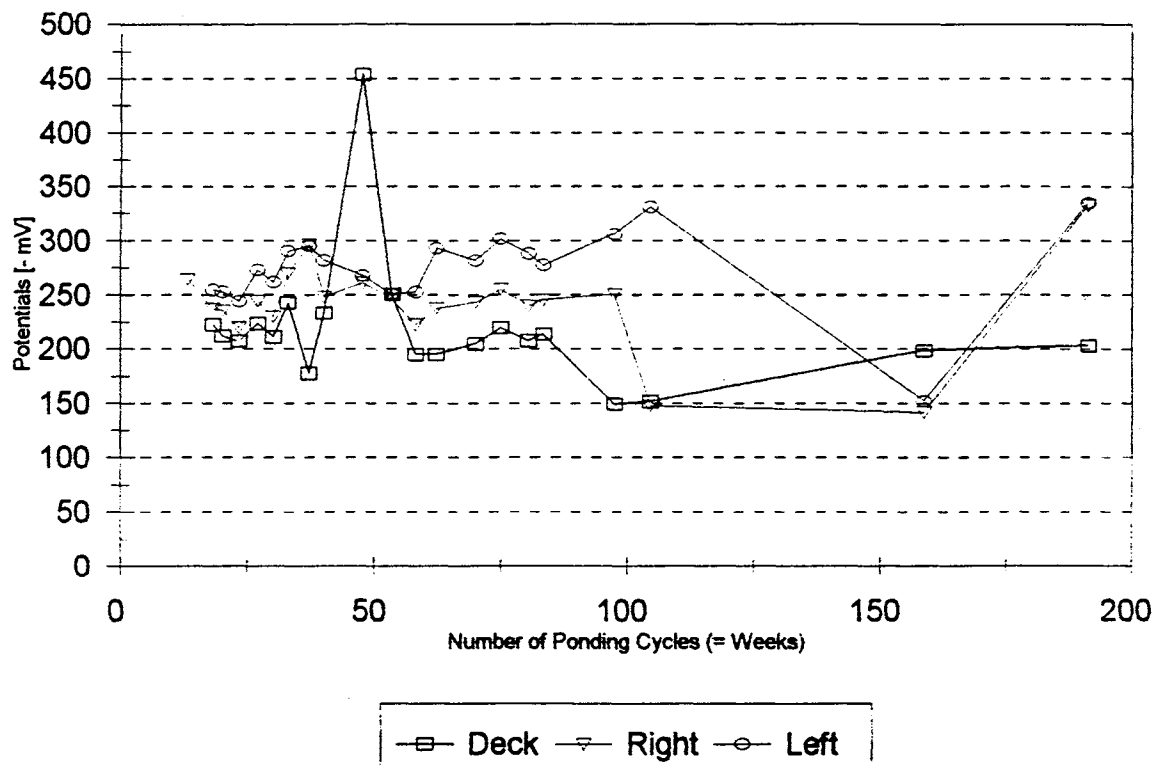


Figure A3. Average Potentials for BS-3 Specimen

Average Potentials BS-4 (Slag, L. Leg Connected)

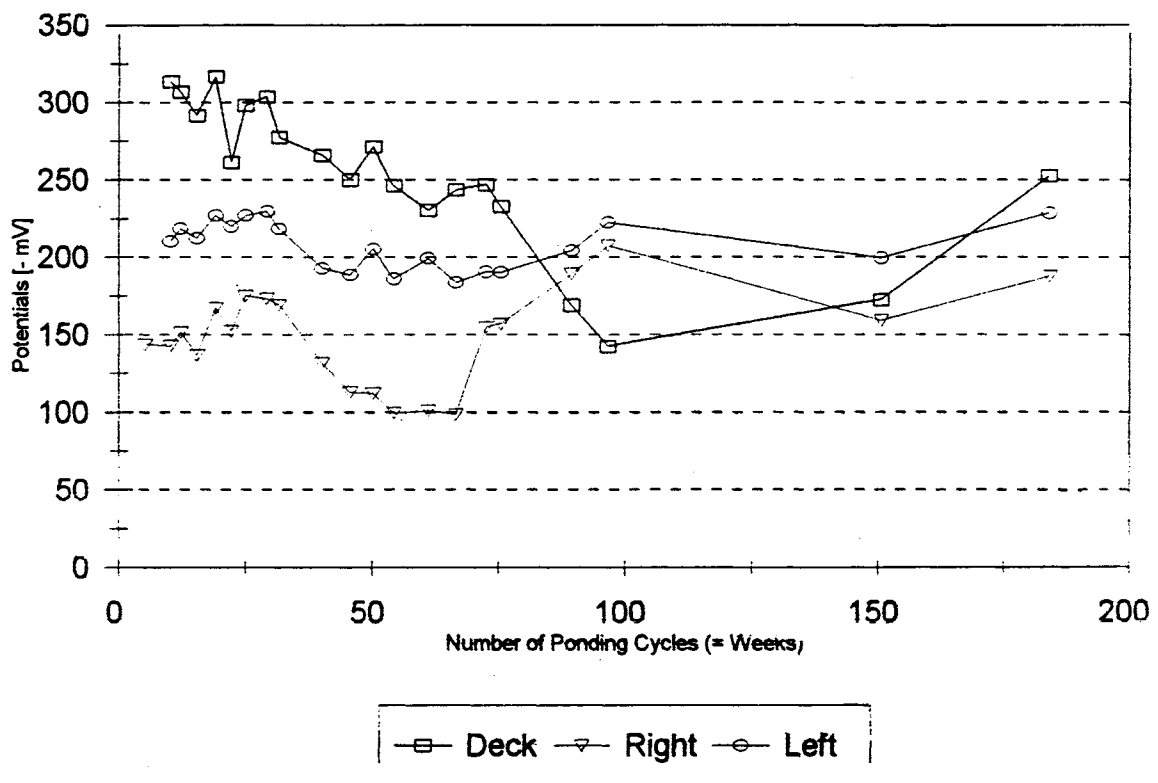


Figure A4. Average Potentials for BS-4 Specimen

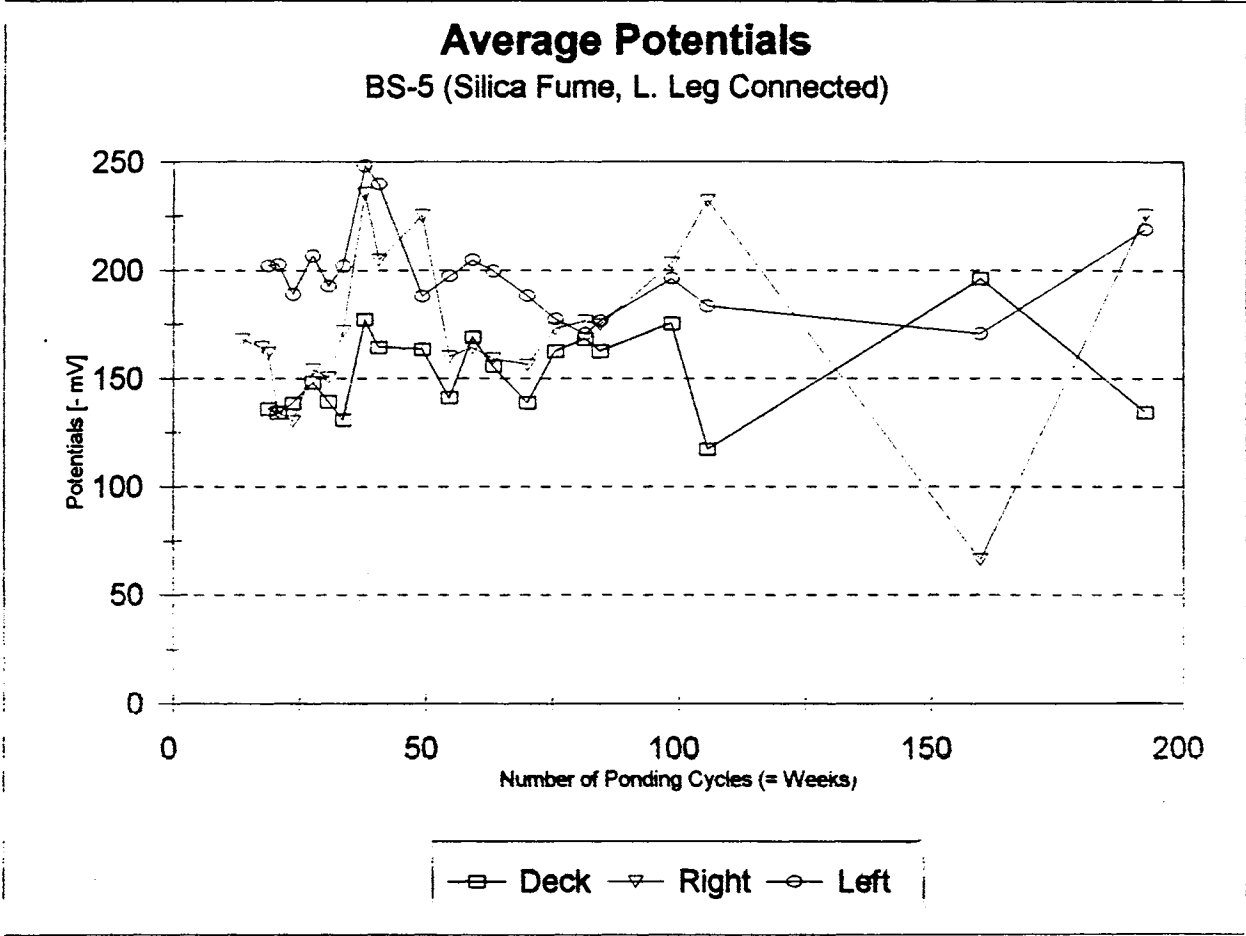


Figure A5. Average Potentials for BS-5 Specimen

Average Potentials BS-7 (S.F. & DCI-S, L. Leg Connected)

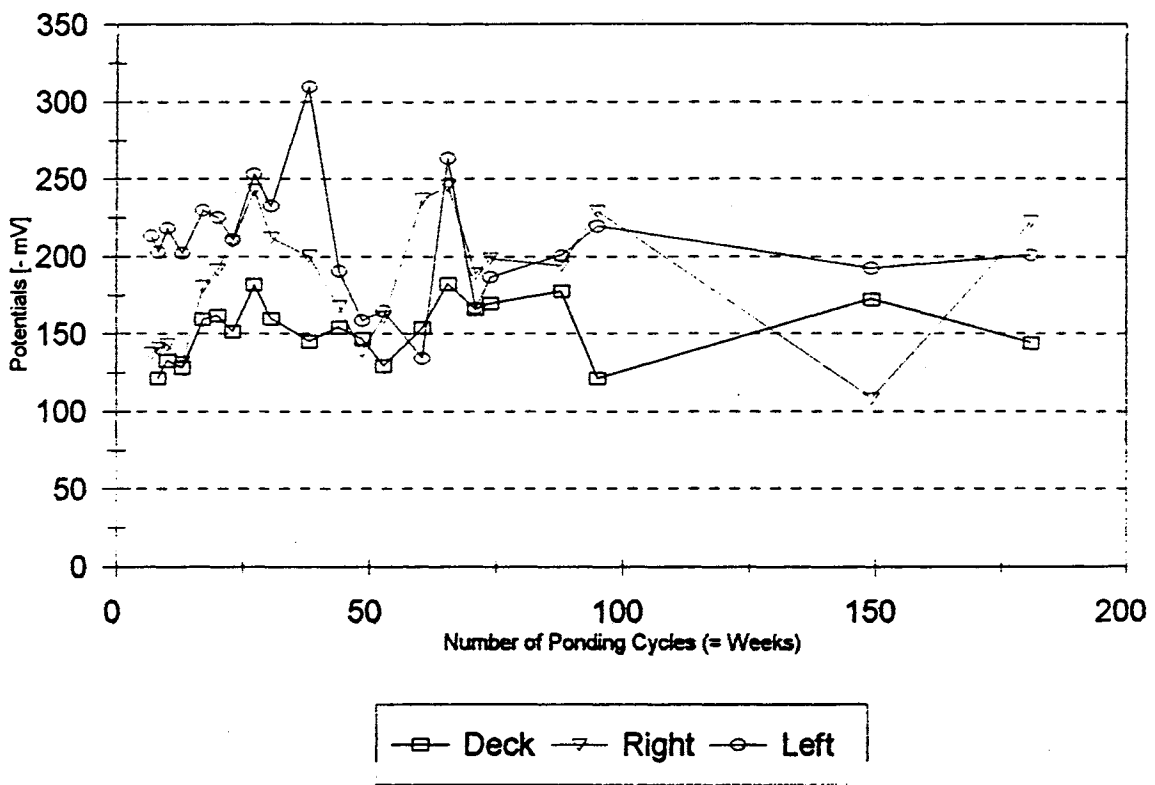


Figure A6. Average Potentials for BS-7 Specimen